Electronic Theses and Dissertations   Fogler Library

12-2001

Magmatic Enclaves and Evidence for Magma Mixing in the Oak Point Granite, Deer Isle, Maine, USA

Ben Johnston

Follow this and additional works at: http://digitalcommons.library.umaine.edu/etd

Part of the Geology Commons, and the Tectonics and Structure Commons

MAGMATIC ENCLAVES AND EVIDENCE FOR MAGMA

MIXING IN THE OAK POINT GRANITE,

DEER ISLE, MAINE, U.S.A.

By

Ben Johnston

B.S. University of Cincinnati, 1998

A THESIS

Submitted in Partial Fulfillment of the

Requirements for the Degree of

Master of Science

(in Geological Sciences)

The Graduate School

The University of Maine

December, 2001

Advisory Committee:

Daniel R. Lux, Professor of Geological Sciences, Advisor

David Gibson, Professor of Geological Sciences, University of Maine at Farmington

Martin G. Yates, Associate Scientist, Geological Sciences

MAGMATIC ENCLAVES AND EVIDENCE FOR MAGMA

MIXING IN THE OAK POINT GRANITE,

DEER ISLE, MAINE, U.S.A.

By Ben Johnston

Thesis Advisor: Dr. Daniel R. Lux

The Coastal Maine Magmatic Province (CMMP) consists of over 100 post tectonic plutons with ages varying from Silurian to Carboniferous. Predominately, plutons are either felsic or mafic with little intermediate material. Several plutons within the CMMP show evidence for direct interaction of contemporaneous mafic and felsic magmas. These are classified as Mafic and Silicic Layered Intrusions (MASLI), a specific group of plutons with characteristics indicative of mafic magma replenishment into silicic magma chambers. While the Maine coast contains several MASLI type plutons, other plutons in the CMMP contain less definitive, more cryptic evidence that suggests interaction of mafic and silicic magmas during petrogenesis. One such pluton is the Oak Point Granite, Deer Isle, Maine.

The Oak Point Granite (371± 2 Ma) is a coarse-grained, seriate, red-orange to salmon, hornblende-bearing, rapakivi granite. Evidence for MASLI type processes and

mafic replenishment includes composite dikes and magmatic enclaves of variable composition. Magmatic enclaves are widely distributed throughout the pluton, varying in abundance at each outcrop.

Three types of enclaves are present in the Oak Point Granite: medium-grain felsic, medium-grained dioritic, and fine-grained dioritic. All three groups of enclaves are more fine-grained than the host granite. Of the three, the fine-grain dioritic variety is the most abundant. These have relatively planar, disk shapes. Thickness can range from 5 cm to 60 cm but are most commonly 6-20 cm. Long dimensions are typically 10 to 25 cm, although some exceed 1 m. Field relations show that the enclaves and foliation defined by aligned feldspars have similar orientations, suggesting either magmatic flow or crystal settling within the magma chamber.

Field and petrographic investigations conclude that the enclaves formed as a contemporaneous magma with the Oak Point Granite. The fine-grained textures and acicular apatite suggest quenching against the host granite. Inclusions of feldspar megacrysts derived from the Oak Point Granite, variations in textures and zoning of feldspars and relic clinopyroxene cores within some hornblende are consistent with the hypothesis that the enclaves are hybrids between silicic and mafic magmas.

Enclaves, aplites, composite dikes and granite samples were analyzed for major and many trace elements. Bivariant variation diagrams produced highly correlated linear trends for major elements (excluding K_2O). This relationship is interpreted to reflect magma mixing. Interpretation of the data concludes that the mafic component of the composite dikes chemically represents a mafic injection during petrogenesis. This parental magma fractionated producing a residual magma that subsequently mixed with

the granitic host. The resultant magma is the origin of the magmatic enclaves. Feldspar megacrysts were incorporated into the enclave magma during this mixing event. The aplite dikes, the felsic component of the composite dikes and the felsic enclaves have similar compositions and are interpreted to represent the felsic end member.

AKNOWLEDGMENTS

TABLE OF CONTENTS

Chapter

LIST OF TABLES

LIST OF FIGURES

Chapter 1

INTRODUCTION

An issue of considerable debate among geologists is the dynamics of granitic magma chambers (see Sparks and Marsh Discussion and Reply, 1990). Direct observation of magma chamber processes is not possible, therefore geologists must rely either on quenched samples from active magma chambers, i.e. volcanic rock, or the limited exposure of "frozen" magma chambers, i.e. plutons. The diverse composition, mineralogy, and texture variations of igneous rocks observed in the latter permit numerous interpretations of petrogenetic processes.

Many studies conclude that shallow crustal, granitoid magma chambers are static, closed systems (Marsh, 1989; Spera, 2000). Internal chamber processes such as wall rock assimilation, fractional crystallization, and the chemical composition of the melt source region determine the mineralogical and chemical composition of the magma. Furthermore, these authors suggest that crystallization of the magma chamber begins at the chamber margins and slowly and systematically migrates inward along a "solidification front" (Marsh, 1989). These studies imply that granitic magmas are extremely viscous, crystal-rich bodies, in which processes such as crystal setting or chamber convection are impossible.

Other researchers have reached very different conclusions about the nature of processes within crustal granitoid magma chambers (Huppert et al., 1984; Singer et al., 1995; Wiebe, 1996). Mineral textures, chemical compositions, and isotopic data from volcanic feldspars (Singer et al., 1995), as well as detailed field relations and chemical

1

analysis of plutons suggest crustal chambers are dynamic, open systems (Wiebe, 1993). Though crystal nucleation may occur along pluton margins, these authors believe that the crystals do not remain there, but are free to move about the magma chamber in response to magmatic currents. Convection currents, driven by thermal and compositional gradients (Huppert et al., 1984) keep crystals suspended in the crystal poor granitic liquid (Wiebe and Collins, 1998). Once convection currents cease, the crystals settle and accumulate on the chamber floor.

Many similar studies suggest that magma chambers are repeatedly injected by new, fresh magma, of variable composition (Wiebe, 1996; Knesel et al., 1999). Under some circumstances, the two magmas can thoroughly mix to form new, hybrid magmas. In other cases, a double diffusive boundary can develop at the magma interface permitting exchange of matter and energy between the magmas. The degree of mixing depends on factors such as density contrast, viscosity ratio, as well as the relative volume of the magmas involved (Huppert et al., 1984; Wiebe, 1996).

1.1. Statement of Problem

The purpose of this study is to evaluate the plausibility of these two conflicting views of magma chamber processes and dynamics. Furthermore, this study investigates features common in many granitic bodies throughout the world that suggests interaction of mafic magma during petrogenesis.

Several Silurian plutons in the Coastal Maine Magmatic Province (CMMP) show distinctive characteristics of bimodal petrogenesis, and some are classic examples of Mafic and Silicic Layered Intrusions, or MASLI plutons, such as Isle au Haut (Chapman

2

and Rhodes, 1992), Cadillac Mountain (Wiebe, 1994), and Pleasant Bay (Wiebe, 1993). Contacts between the contrasting magmas are observed at outcrop localities. However, younger plutons in the CMMP show minor evidence, but lack the diagnostic structures and textures definitive of a MASLI pluton. These plutons may contain more prominent MASLI characteristics at depth, however at current erosion levels such features are absent.

The Deer Isle Pluton (Stewart, 1956) exhibits feldspar foliation, rapakivi feldspars, magmatic enclaves, and composite dikes, suggesting magma chamber dynamics and mafic input during petrogenesis. Previous studies have investigated magmatic enclaves commonly found within granitic bodies and found them to be chemically related to mafic injections, as well as evidence for magma hybridization. This study utilizes field, petrographic, and chemical data of magmatic enclaves and other samples from the Oak Point Granite to assess the role of mafic magma interaction during petrogenesis of the Oak Point Granite.

1.2. MASLI Plutons

Wiebe (1996) defined MASLI plutons as having distinct physical characteristics that provide evidence for the intrusion of mafic magma into felsic magma chambers during their petrogenesis. Definitive characteristics of MASLI plutons include alternating mafic and felsic compositional layers, silicic pipes and diapirs, feldspar and cumulate mineral lamination, hybrid rocks and magmatic enclaves (Wiebe, 1996). These plutons are typically basin shaped, and reflect shallow crustal level emplacement (Wiebe, 1996).

Series of alternating stratigraphic compositional layers in MASLI plutons are interpreted to record repeated injections of mafic magma into the felsic host magma (Wiebe, 1996). Upon injection, the dense mafic magma settles and is chilled against a relatively cool, semi-rigid, crystal-rich floor of the granitic magma chamber (Wiebe, 1993). Heat transfer from the mafic unit may induce convection currents in the overlying magma. The upper contact of the mafic unit compositionally grades into dioritic to leucocratic granitic layers. The transition from the mafic into felsic layers may occur over a few meters (Wiebe, 1993). Field relations and chemical data indicate that these mafic and felsic layers are cumulates and are often foliated (Wiebe, 1993; Wiebe et al., 2000). Each stratigraphic sequence is bound at the top by the next overlying chilled mafic layer. Figure 1.1 shows a schematic diagram of such a sequence.

The mafic layers have fine-grained chilled basaltic textures near the contact and have medium-grained sub-ophitic cumulate textures away from contacts (Chapman and Rhodes, 1992; Wiebe, 1993; Wiebe, 1994). Common minerals present in mafic layers include olivine, pyroxene, plagioclase and hornblende. Typical accessory minerals are magnetite, biotite, sphene and apatite (Wiebe, 1993; Wiebe et al., 1997; Chapman and Rhodes, 1992). Hornblende and biotite abundance increases near dioritic margins, reflecting dehydration of the dioritic layer (Wiebe, 1993). Plagioclase laths typically show normal zoning (Chapman and Rhodes, 1992; Wiebe, 1993; Wiebe et al., 1997). Compositions of mafic layers are slightly evolved due to fractional crystallization and contamination with the granitic chamber (Wiebe, 1993).

Overlying felsic layers compositionally grade from diorite to highly evolved granite (Chapman and Rhodes, 1992; Wiebe, 1994). The layers are medium to coarse-
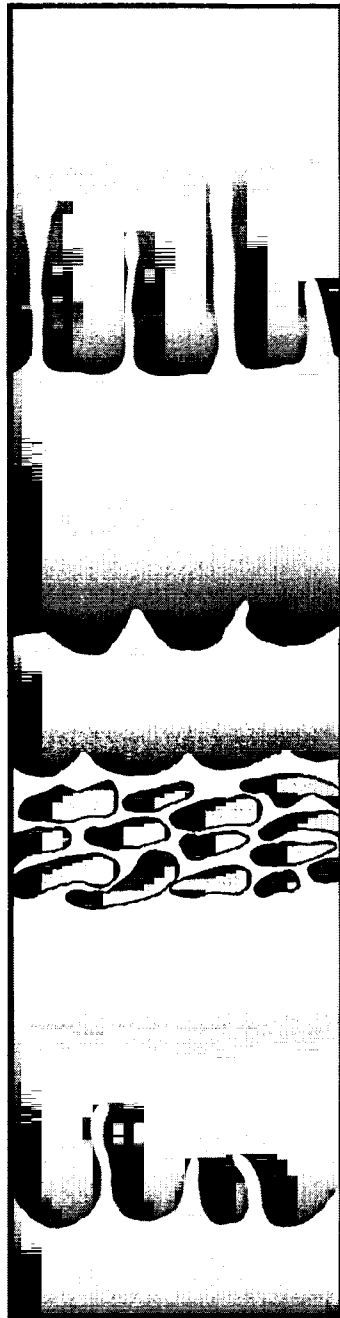
Pipes and diapirs, some pass completely
through the mafic layers, some widen
with increasing stratigraphic height

Increase in Ba, and Zr; decrease in CaO, MgO with
increasing height between mafic layers

Sharp and chilled basal contacts

Elongated pillows and enclaves parallel to
mafic layers, some showing molding around others

Gradation from gabbroic to granitic layers,
cumulate foliation is often present

Irregular forms of pipes and diapirs, indicating
semi-liquid, non convecting mafic layer

Lobes similar to load cast, result from differential
settling of mafic layers

Felsic   Intermediate   Mafic

Figure 1.1: Sketch of a MASLI sequence (after descriptions and figures by
Chapman and Marshall, 1992; Wiebe, 1993; and Wiebe, 1996).

grained and are dominated by plagioclase and hornblende. Plagioclase can exceed 55 modal percent (Wiebe, 1993). Feldspars occur in a wide range of composition (Wiebe et al., 2000). Quartz is typically rare, but increases in abundance in more evolved layers (Wiebe, 1993). Dioritic layers are structurally homogeneous but tabular feldspars may define a faint foliation (Chapman and Rhodes, 1992; Wiebe, 1993). Evidence for hybridization exists in the dioritic layers, such as alkali feldspar cores in plagioclase, pyroxene cores in hornblende, strongly zoned and resorbed plagioclase, rapakivi feldspars and armored xenocrysts.

Granitic and dioritic pipes and diapirs often develop between mafic lobes and migrate into overlying chilled mafic units (Chapman and Rhodes, 1992; Wiebe, 1993). Lengths of pipes and diapirs can vary from a few centimeters to several meters. Diameters are typically several centimeters and often widen with increasing height (Chapman and Rhodes, 1992). Pipes and diapirs are depleted in elements that are enriched in the felsic layers (i.e. K_2O, Ba), suggesting they originated from intercumulus fluids of the incompletely solidified lower felsic unit (Chapman and Rhodes, 1992; Wiebe, 1994). These features are nearly perpendicular to the MASLI layering and show the original orientation of the magma chamber floor (Wiebe, 1993).

Basaltic dikes in MASLI plutons are interpreted to be important in magma chamber petrogenesis. Textures, mineralogy and chemistry of the basaltic dikes are similar to gabbroic layers, suggesting a similar origin and a source as the gabbroic layers (Wiebe, 1993). Basaltic dikes may have wavy to irregular non-matching walls and may dissipate into pillows or magmatic enclaves (Wiebe, 1993; Wiebe et al., 1997). These features indicate that the chamber was only partially solidified during the dike intrusion.

High MgO, incompatible elements, and primitive compositions suggest that the mafic dikes represent parental liquids for the mafic layers (Wiebe, 1993).

Felsic dikes also occur in MASLI plutons, however they are less common than basaltic dikes (Wiebe, 1993). These have fine-grained textures dominated by plagioclase, alkali feldspar and quartz and have low color index (Wiebe, 1993). Cross cutting relations indicate that the basaltic dikes may come before or after the granitic dikes. Compositions of felsic dikes are similar to the granitic material in composite dikes (Wiebe et al., 1997). Granitic dikes are likely to have fed the active chamber.

Composite dikes contain both felsic and mafic rocks and are associated with MASLI plutons (Snyder et al., 1997). They often cut cumulate layers and may be feeders to the MASLI magma chamber. There are two groups of composite dikes, based on whether the mafic or felsic unit is in contact with the host rock (Snyder et al. 1997).

- Composite dikes with mafic margins contain a felsic core. The mafic unit is chilled against the host rock but not necessarily chilled against the felsic core. The mafic-felsic contact often parallels the strike and may be gradational to sharp (Snyder et al., 1997; Wiebe et al., 2000). The absence of felsic diapiric structures suggests the mafic unit was significantly solidified before it came in contact with the felsic unit (Snyder et al., 1997). The mafic component is typically fine-grained and consists mostly of tabular plagioclase and hornblende. Relic pyroxene and xenocrystic quartz and feldspars are common in mafic units (Wiebe et al., 2000). Silicic cores have a fine-grained matrix of quartz and feldspar (Wiebe et al., 2000). Phenocrysts are sodium-rich plagioclase and quartz (Wiebe et al., 2000).

The other type of composite dikes has silicic margins. The felsic component contains numerous basaltic pillows. These pillows are elliptical to round, dark gray and homogeneous, and they are often plastically deformed around other pillows (Vogel and Wilband, 1978; Taylor et al., 1980). Elongated pillows are parallel along strike of the dike walls (Wiebe, 1973; Snyder et al., 1997). Pillows margins with the felsic unit are sharp, crenulated and have convex outward lobes (Taylor et al., 1980; Snyder et al., 1997).

1.3. Enclaves

Lacroix (1890) introduced the term "enclave" to describe fragments of foreign rocks enclosed in homogeneous igneous rock (Didier and Barbarin, 1991). They can consist of one individual crystal or an aggregate of crystals. As with the granitic host, enclaves have diverse characteristics, implications, and origins. As enclaves are included within a plutonic rock, they may be older or contemporaneous with the host. Because of the diverse mineralogy, composition and texture of enclaves, Didier and Barbarin (1991) proposed a nomenclature for four major types of enclaves: surmicaceous, schlieren, xenolith and magmatic.

Surmicaceous enclaves, or mica-rich inclusions (Chen et al., 1989) have elongated, sub-rounded disk shapes. Contacts of the enclave with the host granitoid are sharp. Textures are foliated metamorphic (schistose to gneissic) and some show evidence of folding (Chen et al., 1989; Montel et al., 1991). Surmicaceous enclaves range in size from 2-8 cm long, and 1-2 cm thick (Montel et al., 1991). Studies report mineralogical assemblages of surmicaceous enclaves to include biotite, plagioclase, cordierite, garnet,

muscovite, andalusite, sillimanite ± quartz (Chen et al., 1989; Didier and Barbarin, 1991; Montel et al., 1991). A possible origin of surmicaceous enclaves is fragments of deep country rocks not exposed at the surface that was carried up by the ascending magma (Chen et al., 1989; Montel et al., 1991).

Xenoliths are rock fragments or single crystals (xenocrysts) from the country rock, incorporated into the magma chamber either during magma ascent or emplacement. Xenoliths are angular and exhibit sharp contacts with the host granite (Didier and Barbarin, 1991). Evidence for thermal (or contact) metamorphism and recrystallization textures exists along the enclave-host contact. Xenoliths are typically found near the intrusion margins (Didier and Barbarin, 1991; Maury and Didier, 1991).

Schlieren enclaves are lenticular to elongated or oblate in shape (Didier and Barbarin, 1991). They have gradual contacts, planar orientations, and may lie in magmatic foliation (Lefort, 1991; Platevoet and Bonin, 1991). Common minerals include biotite, tourmaline, and muscovite, and they may be enriched in accessory phase minerals (Barbey, 1991; Le Fort, 1991; Platevoet and Bonin, 1991). Schlieren are typically associated near pluton margins, and are more common in anatectic granites rather than high-level intrusions (Didier and Barbarin, 1991). Schlieren enclaves are suspected to originate from the disruption of other enclaves or mineral cumulates, by either convection currents or magmatic flow regimes (Didier and Barbarin, 1991).

Magmatic enclaves occur in many igneous systems and are ubiquitous in MASLI plutons (Didier and Barbarin, 1991; Wiebe et al., 1997). These are the most common and abundant of enclaves found in granitoid rocks. Other names for this type of enclave include microgranitoid, or microgranular enclaves. These enclaves are widely distributed

9

throughout a pluton and can vary in abundance at local outcrops (Vernon, 1984; Wiebe et al., 1997). Sizes can range from a few centimeters to several meters and their shapes vary from elongated-ovoid disks to irregular and round masses (Vernon, 1984; Wiebe et al., 1997). Contacts with the host granite are sharp and may be crenulated or irregular. Grain size is consistently finer than the host, and enclaves often show chilled margins (Vernon, 1984). They have equigranular textures and often contain megacrysts derived from the host (Barbarin, 1988; Pitcher, 1991). These megacrysts are sometimes situated across the enclave-host contact (Barbarin, 1988; Didier and Barbarin, 1991).

The composition of magmatic enclaves can be either felsic or mafic, with respects to the granitic host but most commonly are intermediate in composition (Vernon, 1984; Wiebe et al., 1997). Common mineral assemblages include plagioclase, biotite, hornblende and alkali feldspar. Plagioclase grains show complex zoning histories (Vernon, 1990). Quartz is either absent or present in small amounts and is typically interstitial or poikilitic (Vernon, 1990). Acicular apatite is common in most enclaves. Mafic magmatic enclaves are rich in hornblende and biotite and may contain clinopyroxene either as individual crystals or in cores of hornblende. Felsic magmatic enclaves have minerals similar to the host but differ in modal proportions (Wiebe and Adams, 1997). These felsic enclaves typically occur at the top of high level intrusions and may be the result of disrupted chilled pluton margins (Didier, 1991; Wiebe and Adams, 1997).

Some proposed origins of magmatic enclaves are 1). Xenoliths from local country rocks, 2.) Re-crystallized rock fragments reincorporated into the host, or 3.) Deep xenoliths brought up during ascent (Chen et al., 1989). However, most studies suggest

that the magmatic enclaves are the product of hybridization between two distinct magmas (Vernon, 1984; Didier and Barbarin, 1991; Wiebe, 1996).

Rounded shapes and cuspate margins indicate that the granite and the magmatic enclaves were contemporaneous liquids. Fine-equigranular textures, apatite needles, and chilled margins reflect rapid cooling and quenching of the enclave in the granitic host (Vernon, 1984). Evidence for hybridization in enclaves includes armoured quartz grains, megacrysts derived from the host, pyroxene cores in hornblende, rapakivi feldspars, and strongly zoned plagioclase (Vernon, 1990). In MASLI plutons enclave size and abundance decrease with distance upward from the gabbroic layers (Wiebe and Collins, 1998). Chemical analyses of enclaves with MASLI host rocks further support that enclaves are a product of hybridization between mafic and felsic end members (Wiebe et al., 1997).

Preferred orientations of magmatic enclaves can give insight to magma chamber processes. Alignment of elongated and flattened enclaves is commonly attributed to magmatic flow. Alignment of enclaves with prominent flow foliation in the granite supports this suggestion. Lack of plastic deformation in either the enclave or the host granite suggests both were liquid during flow (Vernon, 1984; Vernon, 1990). Alternatively, alignment of the enclaves with gabbroic layering suggests deposition (Wiebe et al., 1997; Wiebe and Collins, 1998). Molding of enclaves around other enclaves and large feldspars further supports magma chamber deposition and compaction while in a liquid state.

1.4. Experimental Models

Numerical and analogue experimental studies have been conducted in order to understand the interaction of two magmas of contrasting properties (Huppert and Turner, 1981; Huppert et al., 1982; Huppert et al., 1984; Campbell and Turner, 1985; Snyder and Tait, 1995; Snyder and Tait, 1998a). The results suggest that the degree of mixing and/or mingling of two magmas depend on composition, crystal content, viscosity, density, temperature contrasts, and relative volumes of the fluids (Huppert et al., 1984; Sparks and Marshall, 1986; Fernandez and Barbarin, 1991; Snyder and Tait, 1998b).

Huppert et al. (1984) performed a series of experiments using aqueous fluids to understand the effect of viscosity during magma interaction. In their study, the host fluid was of higher viscosity, cooler temperature, and larger volume. The injected fluid was low in viscosity, higher temperature and a smaller volume. The viscosity ratio of the fluids is defined as the host fluid divided by the injected fluid (Huppert et al., 1984). These experiments serve as an analog to the situation where a mafic magma injects into a felsic chamber.

Several experiments were conducted in which the viscosity ratio was varied between high and low ratio extremes. Three additional experiments were conducted with intermediate viscosity ratio values (Huppert et al., 1984). In all experiments, the injected dense fluid settled at the base of the tank, and a sharp interface developed between the two fluids. Convection currents developed as cooling proceeded and heat was transferred between the two fluids (Huppert and Turner, 1981).

In the experiment where the viscosity ratio was greatest, mushroom shaped plumes with long, thin stalks rose from the residual fluid in the lower layer through the

upper layer forming a third layer on top (Huppert et al., 1984). Crystals nucleated within the ascending plumes, often forming long chains (Huppert et al., 1984) that eventually separated from the plume and settled through the viscous layer towards the bottom of the tank. Little to no mixing occurred between the ascending plumes and the upper viscous layer (Huppert et al., 1984).

In the experiment where the viscosity ratio was the least, such that the two fluids were similar in viscosity, the system behaved similarly to experiments involving fluids of contrasting densities (Huppert and Turner, 1981; Huppert et al., 1984). As the lower layer cooled, convection currents developed in both layers, and crystallization reduced the density of the lower layer. Once the two layers had comparable densities, the lower fluid rose and mixed thoroughly with the upper layer (Huppert et al., 1984).

To further understand the effect of viscosity, Huppert et al. (1984) conducted an experiment where the viscosity of both fluids was uniformly increased, while maintaining a constant viscosity ratio. In this case, processes were similar to the early experiment with the same viscosity ratio, however plume ascent occurred at a slower rate, convection currents were less vigorous, and crystal nucleation decreased (Huppert et al., 1984).

The results from the experiments illustrate the effects of variable physical properties, such as initial temperature, viscosity contrast and density, on the interaction between two magmas. If the injected fluid has the same density and temperature as the host magma, the magmas are likely to mix soon after intrusion (Huppert et al., 1984). Experimental results show that mixing between the magmas is inhibited until they evolve to similar density (Huppert et al., 1984). Exchange of H_2O from the silicic magma into the mafic will lower the density of the mafic magma, whereas exchange of Fe from the

mafic magma into the silicic magma will increase the density (Sparks and Marshall, 1986; Snyder and Tait, 1998b). These exchanges, along with crystallization will alter the densities of the magmas and may promote mixing (Huppert et al., 1984).

The viscosity ratio, and to a smaller extent individual viscosity values, control whether the magmas will mix or mingle (Huppert et al., 1984; Sparks and Marshall, 1986). If the viscosities are similar, mixing is more likely to occur (Huppert et al., 1984; Fernandez and Barbarin, 1991). When viscosity contrasts are great, plume development and mingling processes are favored (Huppert et al., 1984; Fernandez and Barbarin, 1991).

The viscosity of the magma can be altered through temperature changes, chemical exchange and crystallization (Sparks and Marshall, 1986). Heat transfer from the mafic magma into the felsic magma may result in heating of the silicic magma as well as resorption of early crystal phases, thus reducing viscosity (Sparks and Marshall, 1986). Conversely, cooling and crystallization in the mafic layer will increase its viscosity (Fernandez and Barbarin, 1991). In addition, the presence of H_2O will reduce the viscosity (Sparks and Marshall, 1986).

Convection currents with in a magma chamber can be thermal and or, compositional driven or related to exsolution of gas phases (Huppert et al., 1984; Sparks and Huppert, 1984; Snyder and Tait, 1998b). Vigorous convection currents may disrupt the interface between the two magmas (Huppert et al., 1984). If the temperature contrasts are great, thermal exchange produces strong convection currents in the felsic magma. Consequently, if the convection velocities are higher than settling velocities, convection currents keep crystals and other particulates in suspension (Snyder and Tait, 1998b).

In additional to driving thermal plumes, temperature provides constraints on the interaction of the two magmas. When two magmas come in contact they will equilibrate in temperature (Sparks and Marshall, 1986). This is a function of the magmas' initial temperature, relative volume, and minerals present (Sparks and Marshall, 1986). Once the magmas equilibrate in temperature the felsic magma will have a reduced viscosity due to heating and crystal dissolution (Sparks and Marshall, 1986). Cooling and thus crystallization of the mafic magma will increase its viscosity (Sparks and Marshall, 1986; Fernandez and Barbarin, 1991). If the initial temperatures are very different, the mafic magma is likely to quench against the felsic magma. Quenching restricts the amount of chemical exchange and will preserve original features of the quenched magma (Sparks and Marshall, 1986; Snyder and Tait, 1998b). If the temperature between the two magmas is similar, the mafic magma will remain liquid and able to mix with the felsic magma (Sparks and Marshall, 1986).

The results of these experiments are applicable to felsic magma chambers. Although the fluids involved in the experimental models were aqueous solutions, the fluids dynamics caused by variations in physical properties would be comparable to actual magma systems. If aqueous solutions with contrasting viscosity interacted in such a manner, it is likely that two distinct magmas would behave the same way.

The numerical and experimental models support that fluids of contrasting viscosity would mingle, whereas fluids of similar viscosities would more readily mix. Huppert et al. (1984) show that the viscosity ratio, rather than individual viscosity values for each fluid determines, in part, whether the interaction of two magmas will favor mixing or mingling. By increasing the viscosity of the fluids, while maintaining a specific

viscosity ratio, Huppert et al. (1984) found that the processes were similar to the lower

viscosity values but occurred at slower rates. By this observation, the studies of aqueous

fluids can be applied to magmas, despite the significant differences in viscosity values.

Chapter 2

REGIONAL GEOLOGY AND SETTING

2.1. Regional Geology

The regional geology of the coast of Maine consists of five northeast trending fault bounded lithotectonic blocks or terranes, collectively called the Coastal Maine Lithotectonic Belt (Stewart, 1998). Each terrane has its own metamorphic and deformation history. Lithologies include bimodal volcanic rocks (rift assemblages) or shallow marine sedimentary rocks (basin deposits) with ages ranging from Precambrian to Silurian. Regional metamorphism is typically lower greenschist. These terranes were accreted to form a composite terrane prior to its Late Silurian emplacement on the North American margin during the Acadian Orogeny (Stewart et al., 1995; Stewart, 1998). The terranes have also been referred to as Avalon, Avalonia or Atlantica (Stewart, 1998).

2.2. Coastal Maine Magmatic Province

The Coastal Maine Magmatic Province, or CMMP, (Figure 2.1) covers an area of approximately 14,700 km^2 from Penobscot Bay to Passamaquoddy Bay (Hogan and Sinha, 1989). Igneous activity in the CMMP occurred during the Middle to Late Paleozoic resulting in over 100 plutons, with sizes varying from 1 to 1670 km^2. The bimodal character of the CMMP is recognized by the occurrence of predominately felsic or mafic plutons. Hybrid or intermediate igneous rocks occur only in small volumes, typically confined within an individual pluton. Many plutons are composite with both mafic and felsic components.
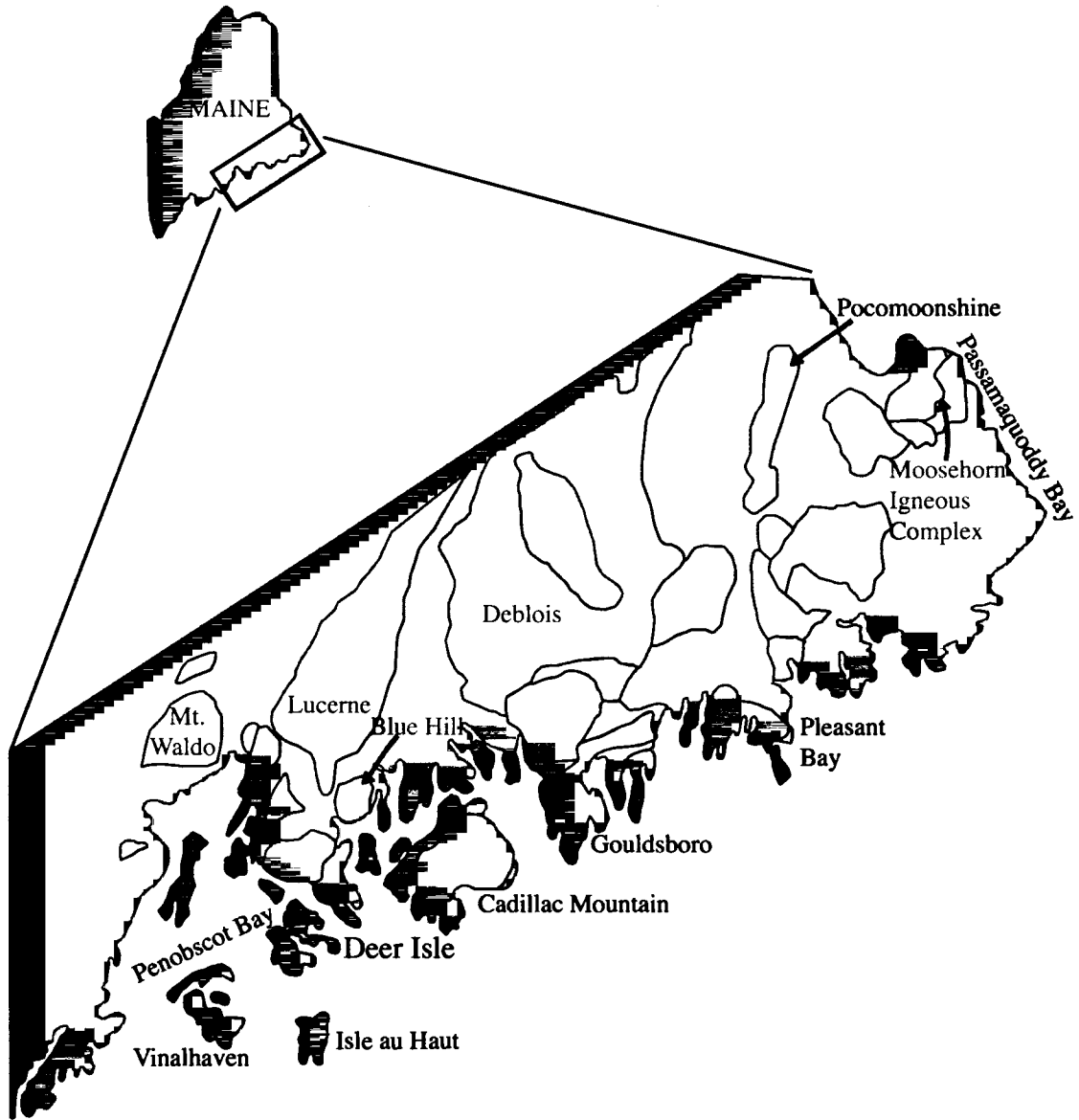
Figure 2.1: The Coastal Maine Magmatic Province (simplified after Hogan and Sinha, 1989). Labeled plutons are those refered to in the text. Orange area is non plutonic rocks.

Hogan and Sinha (1989) classified the CMMP plutons into four groups based on their ratio of felsic to mafic compositions. Type I plutons (e.g. Pocomoonshine) are characterized by overall mafic compositions, without the presence of silicic rock. These rocks are gabbros, norites and diorites. Primary mineralogy includes olivine, pyroxenes, hornblende, biotite, and plagioclase (An $_{65-38}$). Magmatic layering is common in type I plutons. Overall average silica content of type I plutons is 47.5 wt%.

Type II plutons are characterized by overall felsic compositions without significant mafic components. These plutons lack features such as mafic enclaves, composite dikes and synplutonic mafic dikes. Hogan and Sinha (1989) further divided this group on the basis of texture, mineralogy, and chemistry. Type IIa plutons (e.g. Blue Hill) are peraluminous granites with higher silica content (74.6 wt%), and typically occur as subcircular stocks. Textures within type IIa plutons are inhomogeneous, varying throughout the pluton from medium to coarse-grained and may be seriate to subporphyritic. Aplite dikes and pegmatites are common in these plutons. Type IIb plutons (e.g. Lucerne) are metaluminous granites, with lower silica content (71.9 wt.%), and occur as large (~600-1600 km^2) elongated batholiths. The inhomogeneous textures of coarse seriate to porphyritic and distinctive alkali feldspar megacrysts characterize type IIb plutons (Hogan and Sinha, 1989).

Pluton types, III and IV, show evidence of interaction between mafic and felsic magmas (Hogan and Sinha, 1989). Mafic enclaves are distributed throughout these plutons, and composite, aplite, and mafic dikes are common. These plutons can occur as individual stocks (e.g. Cadillac Mountain) or as multiple intrusions (e.g. Moosehorn Igneous Complex). The difference between type III and IV plutons is the ratio of the

felsic to mafic component. Type III plutons (e.g. Deer Isle) are predominately felsic bodies with evidence for interaction with mafic magma, whereas type IV plutons are predominately mafic and preserve evidence for interaction with felsic magmas.

2.3. Deer Isle

Deer Isle is located at the southwestern edge of the Coastal Maine Magmatic Province (Hogan and Sinha, 1989) in Penobscot Bay (Figure 2.1). It is located west of the Cadillac Mountain pluton and north of the Isle au Haut pluton. The island is roughly 20 km (SW-NW) long by 9 km wide (Stewart, 1956).

Deer Isle contains four distinct geologic units (Stewart, 1998). These are the two phases of the Deer Isle Pluton (the Oak Point Granite and the Stonington Granite), the Ellsworth Schist, and the Serpentinite of Deer Isle (Figure 2.2). The Oak Point Granite occurs on the northeastern side of Deer Isle, and the Stonington Granite is found towards the southern side. Both granites have rapakivi textures and distinguishing between the two can be difficult at times. However, the Oak Point granite contains red-orange to salmon colored alkali feldspars whereas the Stonington granite contains light purple to lavender colored alkali feldspars and often shows a pegmatitic feldspar texture. Contacts between the Stonington Granite and the Oak Point Granite are gradational (D. Stewart, 2000, personal communication).

The igneous rocks on Deer Isle are collectively called the Deer Isle Pluton (Stewart, 1956). Total area of the pluton is approximately 308 km^2 (Hogan and Sinha, 1989). Gravity data suggest the pluton has inward dipping contacts and a maximum depth of 6 km (Hodge et al., 1982). Stewart (1998) reports that both granite facies are Devonian

20

Little Deer Isle

Eggemoggin
Reach

Joyce
Point

Brooklin

Flye Point

44 15'N

Torrey Pond

Eggemoggin
Reach

Oak Point

Naskeag

Conary
Island

Hog Island

Deer Isle

Greenlaw Neck

Stinson Neck

N

Stonington

68°37' 30"W

1 km

	Stonington Granite (Devonian)
	Oak Point Granite (Devonian)
	Serpentinite (Ordovician?)
	Castine Volcanics (L. Cambrian)
	Ellsworth Schist (M. Cambrian)
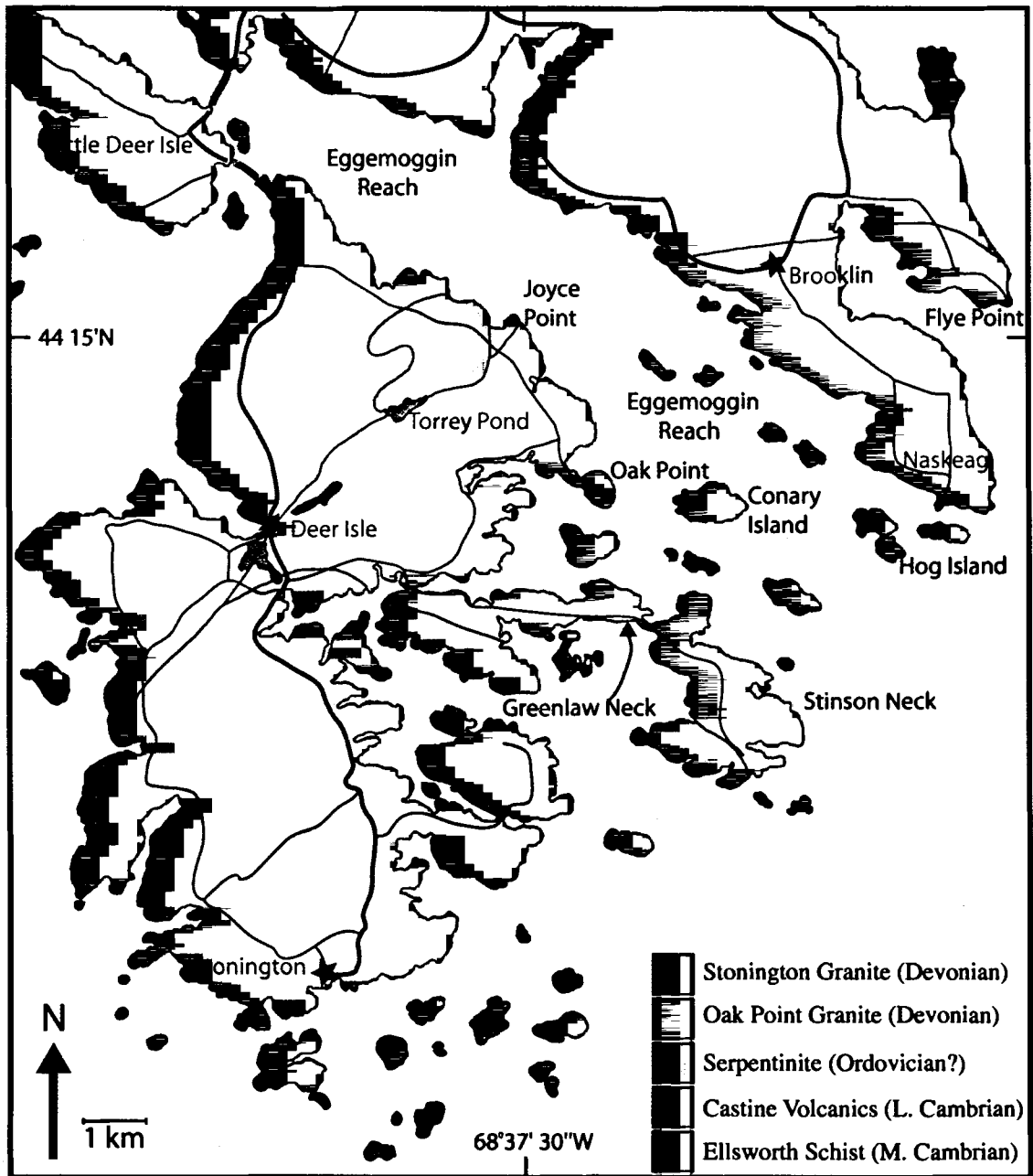
Figure 2.2: Deer Isle geologic map (simplified after Stewart, 1998).

in age and the Oak Point granite yields a U-Pb zircon age of 371 ± 2 Ma. Field relationships suggest that the Oak Point intruded the Stonington Granite (Stewart, 1998).

The Ellsworth schist occurs on the western and northern sides of Deer Isle. It consists of volcanogenic feldspathatic rocks, interbedded with metamorphosed siltstones, quartzite, iron-manganese precipitates, and some pillowed greenstones (Stewart et al., 1995; Stewart, 1998). The Ellsworth schist is interpreted to represent a marine tholeiitic basalt-rhyolite continental rift sequence. Stewart et al. (1995) reports a U-Pb zircon date of 509 ± 1 Ma. Metamorphism is lower greenschist facies with multiple folding and strong foliations (Stewart, 1998). This unit is part of the Ellsworth Terrane of the Coastal Maine Lithotectonic Block (Stewart, 1998) and is contemporaneous with the Castine Volcanics, located on Little Deer Isle (Figure 2.2).

The fourth geologic unit, the Serpentinite of Deer Isle, is a black, medium-grained enstatite-rich ultramafic stock (Stewart, 1998). The degree of serpentine alteration varies within the rock, from complete replacement to random veins. Stewart (1998) reports that it intrudes the Ellsworth schist and is intruded by the Oak Point Granite, therefore suggesting an Ordovician to Silurian age. The serpentinite is located on the north side of Deer Isle near Joyce Point, and underlies the highest point of Deer Isle (Stewart, 1956). Exposure of the serpentinite can be found along the southeastern edge of Torry Pond (R. Hooke, 2001, personal communication).

Chapter 3

STUDY METHODS

3.1. Mapping

Field mapping and sample collecting for this study occurred during the summer of 2000. To be most efficient, efforts were concentrated along the coast and during days of midday (~10am-4pm) low tide. Four 7.5' USGS topographic maps (Brooklin, Sargentville, Stinson Neck, and Deer Isle) cover the field study area. Enlarged sections of the topographic maps served as base maps. Simple orienteering methods determined the position of each site. A Brunton compass was used to measure orientations of aplite dikes, feldspar foliation and planar enclaves. For most features, three measurements were made and the average was recorded. Aplite dike measurements were limited to dikes greater than 2 cm thick. Feldspar foliation was measured only where the fabric was distinct. Enclaves, within close proximity, helped visualize the feldspar foliation. Attitudes were measured only for enclaves that had three-dimensional exposure. Locations for orientation measurements were plotted on the enlarged map sections.

A generalized geologic map of the study area was created, based on lithologies and contacts by Stewart (1998). Representative strike and dip symbols were plotted (Figure B.2). Where numerous measurements for one type of feature (i.e. enclave) exist, an average value was used. Points plotted slightly ashore or offshore are the result of overcrowding of symbols for a given location. For each site location, latitude and longitude were estimated after the field season using *Terrain Navigator*. All strike and dip measurements and approximate coordinates are shown in Table A.1.

23

3.2. Collecting

Sample collecting occurred during late summer and early fall of 2000, after most of the granite was surveyed. Sample localities were selected by access to the site, rather than any statistical pattern or method. Few samples were collected during traverses along the coast. Samples were taken in situ except for one granite sample from Greenlaw Neck, which was taken from a discard pile of rock, presumably blocks removed for the adjacent road cut. Enclaves were sampled at localities where they were most abundant. An attempt was made to collect samples representing all varieties of enclaves (i.e. composition and texture variations), however there was a bias towards the dark, fine-grained dioritic enclaves. A composite dike sample was collected from the Naskeag peninsula locality consisting of a both mafic and felsic members. Mafic dike samples came from the mafic unit on Flye Point and from a mafic dike on Brooklin. Appendix B shows locations of samples collected for point count analysis and chemical analysis.

3.3. Thin Section Preparation

Samples brought from the field were cut at random orientations at the University of Maine. Rock chips were sent to Petrographic International, in Choiceland, Saskatchewan, for standard and polished thin sections. Due to the larger grain sizes, 5 x 8 cm thin sections were made for the granite samples.

3.4. Modal Data

Modal analysis of granite samples was completed on un-oriented slab cuts using a 1 cm grid. Rapakivi rims were counted as plagioclase, and the cores as alkali feldspar. Each granite sample consisted of over 1000 points. Modal amounts are listed in Table A.2.

Due to fine grain sizes, enclave data were counted on thin section using a mechanical stage. One increment on the mechanical stage (approximately 1 mm) determined the spacing. At least 400 points were counted for each thin section. Total counts per thin section varied depending on the size of the sample. Although mafic minerals were counted separately, a total value was used for a mafic modal percent.

3.5. Whole Rock Chemistry

Sample preparation for whole rock chemistry analysis was conducted at the University of Maine. The following procedure was used to prepare whole rock samples for chemical analysis. Samples were cut into slabs or slices with rock saws. Approximately 1 cm was trimmed off the edge of the slabs to minimize weathering effects. Feldspar inclusions in enclaves were removed prior to crushing.

Rock slabs were broken with a rock hammer and the pieces were passed through a jaw crusher, breaking them into smaller (<2 cm) pieces. Crushed pieces were washed in a #6 sieve (3.35 mm) with tap water, allowing smaller pieces and dust to pass. The washed sample was allowed to dry over night. The dry crushed sample pieces were pulverized in an alumina shatter box for about 3 minutes. After each run, the powder was transferred into a 20 ml (6 dram) vial using a stainless steel spatula.

To prevent cross contamination of samples equipment was cleaned between samples. Jaw crusher plates were scrubbed with a wire brush and rinsed with methanol. Once dry, the plates were then wiped with large chemwipes. The shatter box components (puck, lid, bowl) and spatula were rinsed with tap water, and wiped with a chemwipe to remove excess water. Each component was then rinsed with methanol and wiped dry with a chemwipe.

Total whole rock chemical analysis consisted of five granite samples (four in duplicate), 13 enclaves, two aplite dikes, a felsic and mafic member of a composite dike, and two mafic dikes. David Slauenwhite at The Regional Geochemical Center, St. Mary's University, Halifax, Nova Scotia, performed X-ray Fluorescence trace and major element chemical analysis. Values were determined on a Philips PW2400 X-Ray Spectrometer. Analysts at St, Mary's University performed a second pulverizing event since the samples prepared at the University of Maine were too coarse. Appendix A includes the results for the whole rock analysis (Table A.3).

3.6. Microprobe Analysis

Individual mineral chemistry was determined at the University of Maine on an ARL SEMQ electron microprobe equipped with Advanced Mircobeam, Inc. automation and a Tractor Northern Energy Dispersive Spectrometer. Accelerating potential was 15 kilovolts and beam current was 10 nanoamps with 10-second counts. Spot diameter was 3 µm. Back-scattered SEM images and energy dispersive spectra were used to locate analytical locations on mineral grains.

Four enclaves and two granite samples were analyzed. Analysis focused on plagioclase, biotite, hornblende and suspect clinopyroxene grains. Ten analyses were collected for each sample point.

Measurements greater than 40 wt. % had a relative standard deviation ranging from 1.87 % to 0.11 %, with an average of 0.8 %. Measured values between 20 and 40 wt. % vary in standard deviation from 0.14 % to 2.41 %, with an average of 0.78. Standard deviation varies from 0.08 % to 35.16 % for weight percents between 10 % and 20%. Weight percent measurements less than 10 wt. % and greater than 1 wt. % have a range of deviation from 0.2 to 220 %, with an average of 8.73 %.

Formula units were recalculated per 24 oxygens for hornblende and biotite, 8 oxygens for plagioclase, and 6 oxygens for pyroxene. Calculations were performed as described by Deer, Howie and Zussman (1992).

Chapter 4

PETROGRAPHY

4.1. Oak Point Granite

The Oak Point Granite (OPG) (371± 2 Ma) is a coarse grained, seriate, red-orange to salmon, hornblende-bearing, rapakivi granite (Figure 4.1). Accessory minerals in the OPG include magnetite, zircon, apatite, and allanite (Stewart, 1956). Modal percents are shown in Figure 4.2. Some localities of the OPG are red colored, characterized by massive feldspar, round quartz and lack of mafic minerals. These sections are interpreted to reflect hydrothermal alteration and are associated with numerous epidote-bearing fractures. Microfractures commonly develop through all minerals of cut hand samples. Small sections of pegmatite grains of quartz and alkali feldspars were observed at three outcrops. These sections are irregular to ovoid and range from 30 cm to 1 m in diameter.

Plagioclase feldspar in the OPG occurs as individual crystals and as rapakivi rims on alkali feldspars. Individual plagioclase crystals are anhedral to subhedral and range in size from 0.5 mm to 1 cm. Hornblende, biotite and opaque minerals are included in plagioclase. Some plagioclase grains contain small anhedral microcline crystals. Sericite alteration occurs in variable amounts, and it is typically concentrated near the crystal center.

Zoning in plagioclase varies. A few grains have two simple zones: a relatively uniform core with a thin compositionally different rim. The contact between these zones is irregular. Most grains, however, have more complex zoning patterns. Core shapes are typically round to ovoid, although some are more rectangular. These cores often have
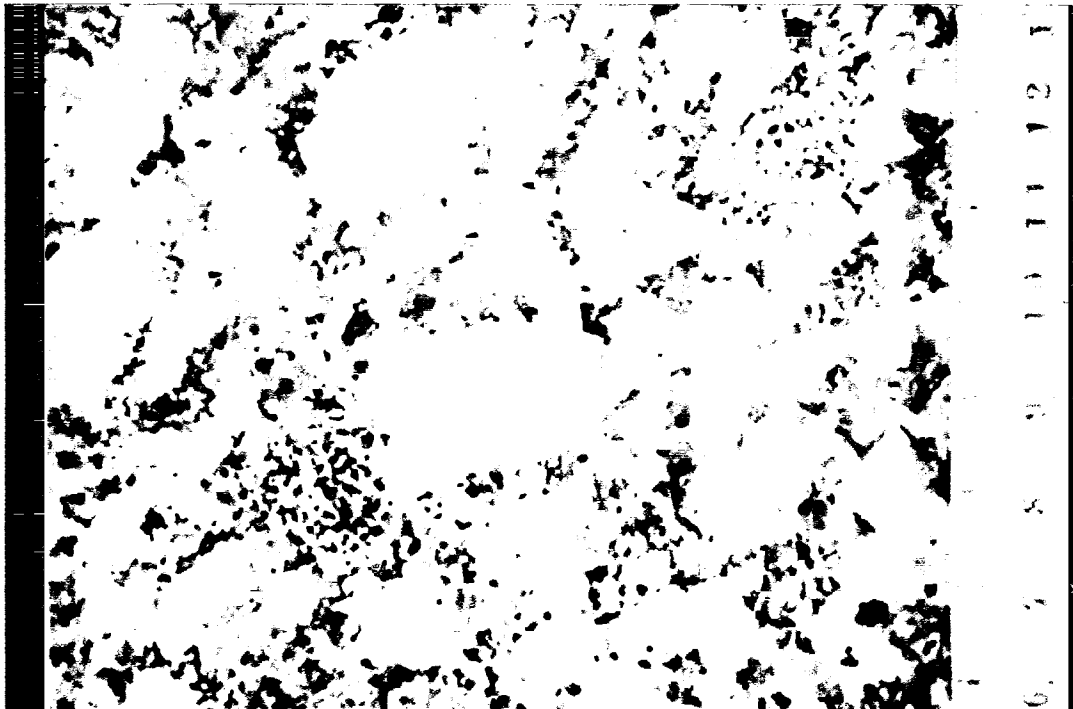
Figure 4.1: Photographs of Oak Point Granite hand samples. Top picture is from a sample collected from Oak Point. Bottom picture is from a sample collected from Greenlaw Neck. Ruler units are in cm.
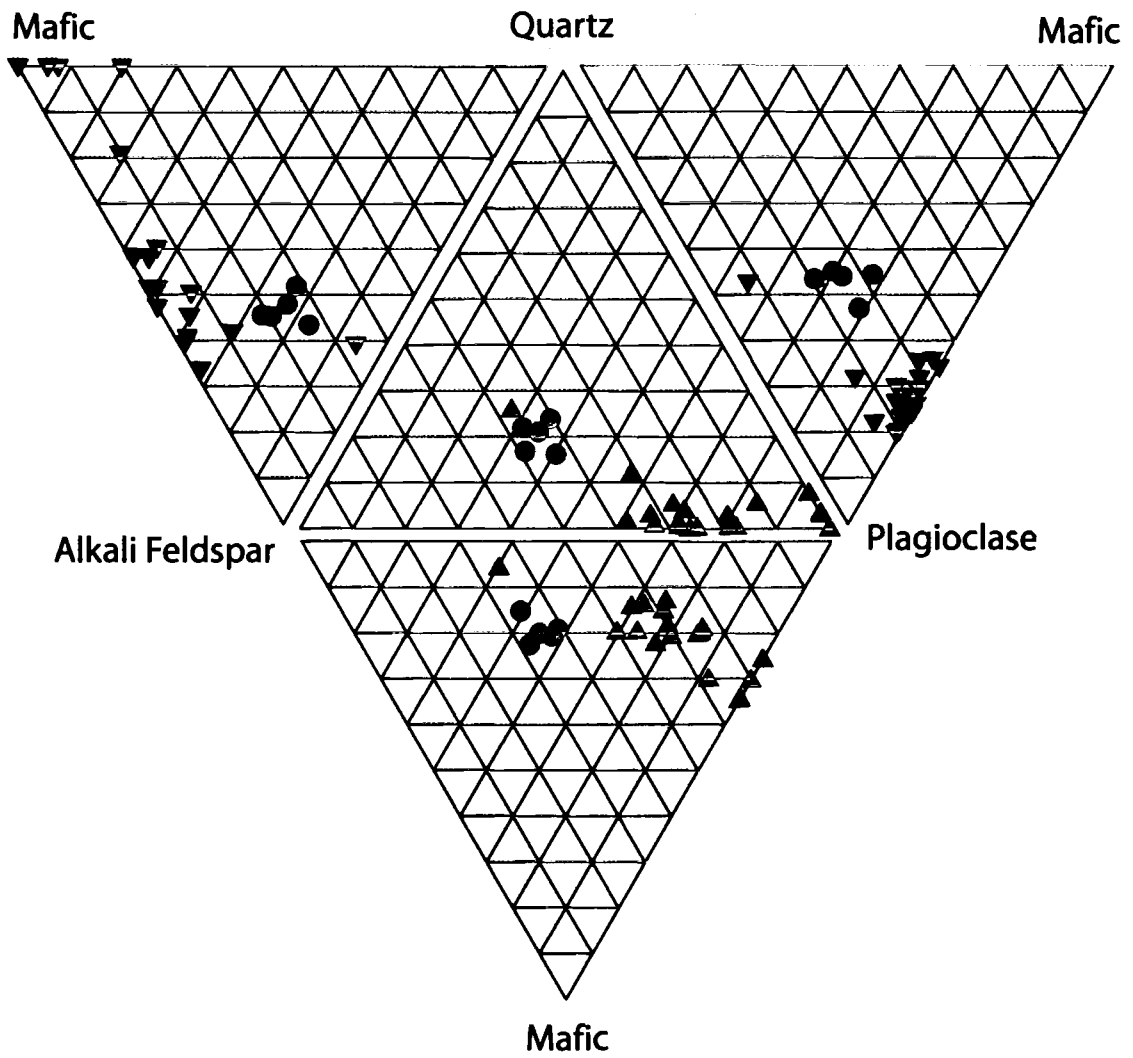
Figure 4.2: Modal analysis for granite and enclave samples.

numerous fine opaque inclusions and as well as sericite alteration. Extinction patterns in cores can be patchy, continuous or uniform. A ring of alteration or an increased concentration of fine inclusions often defines the core boundary. Zoning in outer portions of the plagioclase grains is either continuous or oscillatory. The oscillatory zones vary in thickness and can have round, ovoid or rectangular shapes. Some oscillatory zones show signs of alteration. Near the crystal margin, some grains show a curved line of inclusions, often cutting oscillatory zones.

Some granite samples (FLYE, OAKPT, NSKPT) contain a composite plagioclase grains, consisting of several randomly oriented individual 0.5 to 1.5 mm anhedral grains. The composite grains are anhedral and range in size from 1.5 mm to 4 mm. Individual grain contacts are noted by fine inclusions and alteration, as well as composition differences characterized by extinction. Zoning and albite twin direction is different for each individual grain. In one such composite grain (FLYE) from Flye Point, an alteration ring often overprints all the smaller grains.

Alkali feldspars are large, anhedral to subhedral, red-orange to salmon colored crystals. This phase mostly occurs as large (5 mm to 2 cm) crystals and less common as small (0.5 mm to 1.5 mm) interstitial grains. Many large alkali feldspars have plagioclase rims or rapakivi texture. Some alkali feldspars show faint round to oval white rings, possibly chemical zones or micro-rapakivi rims followed by alkali overgrowth. Most alkali feldspar grain contacts are irregular, although less common are planar and curved. Carlsbad twin planes are typically jagged and irregular. Fine rounded, interlocking irregular quartz grains are concentrated along some crystal margins. Alkali feldspars often contain small (< 1 mm) continuous or oscillatory-zoned anhedral plagioclase

inclusions throughout the grain. Other common inclusions are biotite, hornblende, quartz and sphene.

Most alkali feldspars have perthitic textures, often visible in hand sample. Perthitic lamellae vary in thickness and are often sub-parallel. The lamellae often contain plagioclase grains. Some perthite lamellae near the crystal margin have rounded shapes.

Rapakivi feldspars are common throughout the OPG. The alkali perthitic cores are rounded and the plagioclase rims are subhedral to anhedral. Rapakivi feldspars next to one another do not show similar shapes in either their cores or rims. Cores are typically 1 to 2 cm in length, where the rims are 1 to 6 mm thick. Core and rim contacts are irregularly shaped and jagged, and some contacts appear to be gradational. Plagioclase rim thickness varies among feldspars, as well as on individual crystals. The rims consist of several individual plagioclase grains with various sizes and orientations. These plagioclase grains do not have similar zoning patterns, nor do they contain a common overgrowth. Poikilitic quartz is present in some rapakivi rims.

Quartz occurs as an anhedral interstitial phase, ranging in grain size from less than 0.25 mm to 5 mm. Aggregates of small quartz grains may exceed 1 cm. Quartz is typically inclusion free, however biotite, hornblende, plagioclase may be included. Undulatory extinction is common and some grains are poikilitic.

Mafic and accessory minerals in the OPG include biotite, hornblende, opaques, sphene and apatite. Biotite is the most abundant of the mafic minerals. This phase occurs as orange-brown, weakly pleochroic, or red-brown to yellow, pleochroic grains. Grains are anhedral to subhedral and ranges in sizes from 0.25 mm to 3 mm. Small (0.25 mm to 0.5 mm) randomly oriented biotite grains often form 2 mm long aggregates. Slightly bent

cleavage planes in some biotite crystals suggest minor deformation. Weak to moderate chlorite alteration is common among biotite grains. Green or olive green to pale yellow hornblende occurs as anhedral to subhedral 0.5 mm to 2.5 mm grains. These grains often show twinning and zoning and some have suspect clinopyroxene cores. Sphene is typically anhedral to subhedral, although some euhedral grains exist and are typically from less than 0.5 mm to 1 mm. Sphene often has embayed morphologies enclosing quartz. Opaque minerals rarely exceed 0.5 mm although > 1 mm aggregates are common. These occur as round to angular anhedral grains, and less commonly as elongated laths. Opaque minerals are associated with hornblende, and are often included in biotite. Apatite is most abundant in close proximity with mafic minerals. It occurs mostly as short (0.25 mm) needles, although some are as long as 0.5 mm. Some grains have almost perfect hexagon shapes.

Small (5 mm to 1 cm) sub-circular concentrations of mafic minerals (micro-enclaves) exist in the OPG (Figure 4.3). These consist of subhedral to anhedral 0.5 mm to 1.5 mm hornblende, biotite, and rare sphene, along with weak to extensively altered plagioclase. Minerals are tightly spaced, with minor amounts of interstitial, poikilitic quartz grains, often containing apatite inclusions. Within these sections, apatite reaches its longest lengths (0.5 mm).

4.2. Aplite Dikes

Aplite dikes occur throughout the Oak Point Granite. They have a uniform granular sugary texture, pink to red color, and a low mafic mineral content (<1%). Typical aplite dike thickness is between 5 to 50 cm, although some greater than 0.5 m
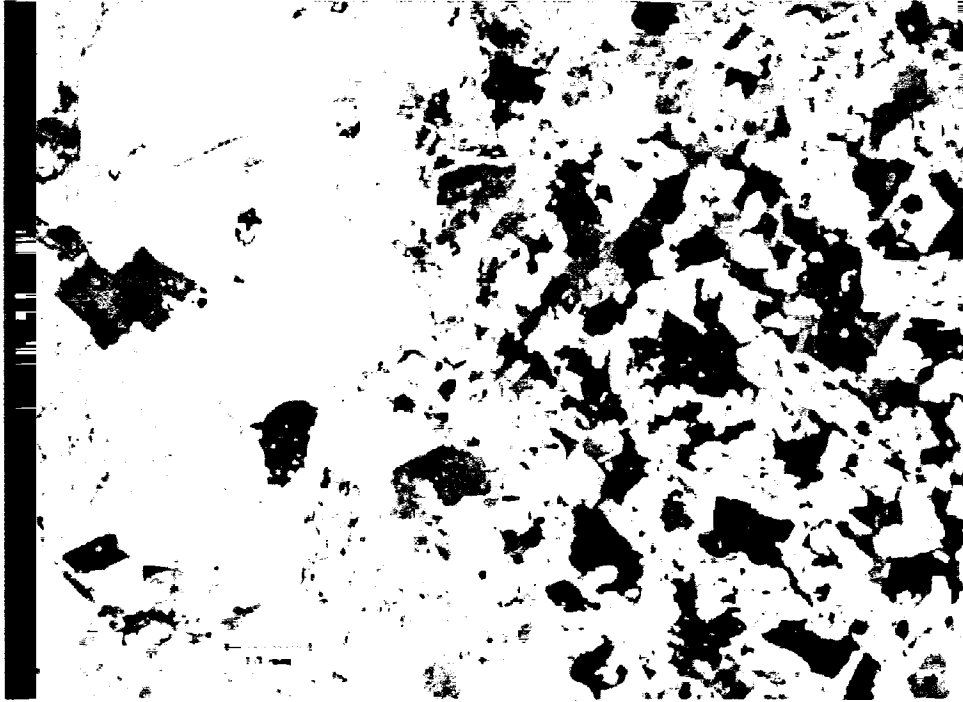
Figure 4.3: Photomicrograph of a micro-enclave (Sample GRNLW). Scale
   bar is 1.0 mm.

exist. Contacts with Oak Point Granite are sharp and weakly crenulated. Most dikes are planar but few do have minor bends. The largest fault displacement observed across an aplite dikes is 30 cm. Both dextral and sinistral movement across faulted aplite dikes is apparent. Some localities show a network pattern of shorter dikes connecting several (4-5) larger relatively parallel dikes. Aplite dikes cross cut enclaves, as well as other aplite dikes. Strikes and dips of aplite dikes are random.

Aplite dikes have two distinct grain sizes (Figure 4.4). The small and larger grains consist of microcline, quartz, and plagioclase. The small grains are typically less than 0.15 mm and are anhedral to sub-round. The small plagioclase grains have albite twinning, minor alteration, and lacks distinct chemical zonation. Biotite is rare and occurs as anhedral laths. The larger grains range in size from 0.5 mm to 3 mm. These are anhedral to some subhedral grains. Some alkali feldspars have perthitic textures, as well as plagioclase and quartz inclusions. Quartz grains often show undulatory extinction. Plagioclase phenocrysts have continuous zoning, and rarely show oscillatory zoning. Many grains have alteration on the grain margin, rather than the crystal core.

4.3. Composite Dikes

Four individual composite dikes have been observed in the OPG (Figure 4.5) and they all occur on the southeast side of the Brooklin Peninsula, west of Naskeag Point. Contacts between the composite dike and the OPG are sharp, and are irregular, lobate, wavy, or relatively linear.

Three of the composite dikes are located in close proximity (see Figure B.1). They each have a similar north-south orientation, with a 73^0 eastward dip direction. Their
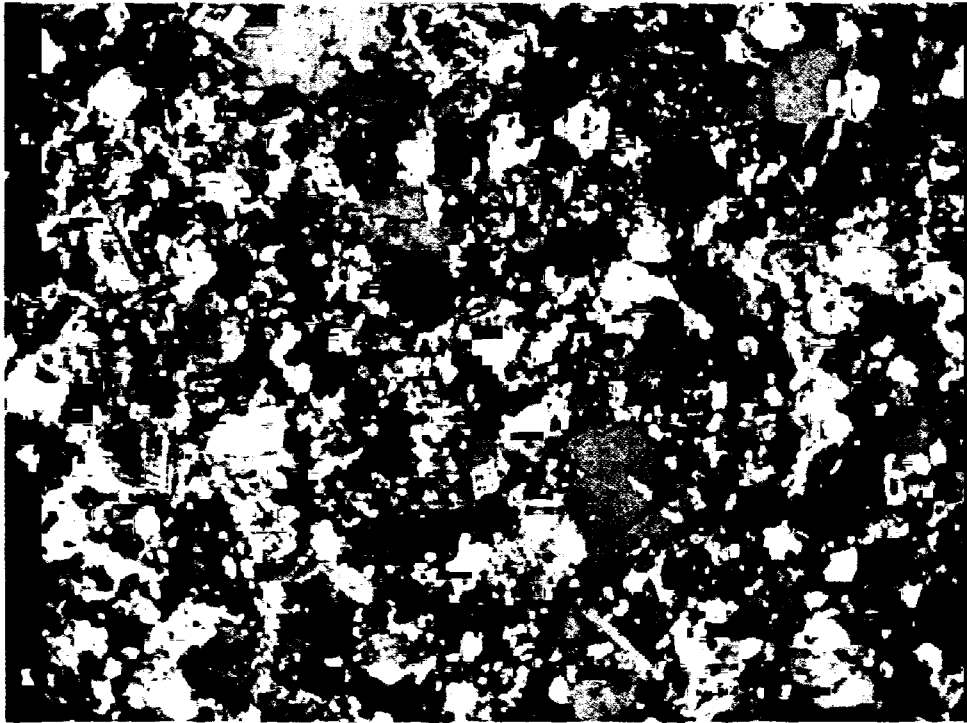
Figure 4.4: Photomicrograph of an aplite dike (from Sample NKPT-2).
Scale bar is 1.0 mm.

Figure 4.5: Photographs of composite dikes. Top photo is from the solo dike near Little Babson Island (backpack for scale). Bottom picture is from one of the three composite dikes west of Naskeag Point (pocket knife for scale).

sub-parallel trends suggest these three may be interconnected; however such a relation is not observed. The dikes are commonly less than 1 m they can be traced for about 8 m beneath the surficial deposits inland, and below the beach cover of the tidal zone.

A fourth composite dike exists approximately due east of Little Babson Island. It has a rounded, wave eroded exposure surface with a width of approximately 2 m and exposure length is 5 m. Orientation is approximately 140^0, and dips towards the northeast.

Three lithologies can be described from the composite dikes: fine-grained mafic component, felsic component, and gray porphyritic component. The mafic component is dark gray to black and with a relatively uniform, aphanitic texture. It occurs as sub-round to elongated pillow forms, ranging in size from a few cm in diameter to a meter in length. Elongated pillows have a general orientation parallel with the dike margins. The mafic pillows are separated by felsic material that ranges in thickness between a few mm to several cm. Contacts between the felsic and mafic units have fine lobe and diapiric structures.

In thin section, the mafic component reveals a micro-porphyritic texture consisting of fine-grained anhedral biotite-hornblende-rich matrix with random oriented subhedral plagioclase laths (Figure 4.6). Biotite has an orange to golden color and hornblende is light green. These grains are mostly 0.25 mm or smaller, however some do reach 0.5 mm. Hornblende also occurs in 0.25 to 0.5 mm irregular to anhedral aggregates. These have patchy pleochroism and birefringence. Other minor grains included in the groundmass are small, anhedral opaque minerals, and rare anhedral sphene.
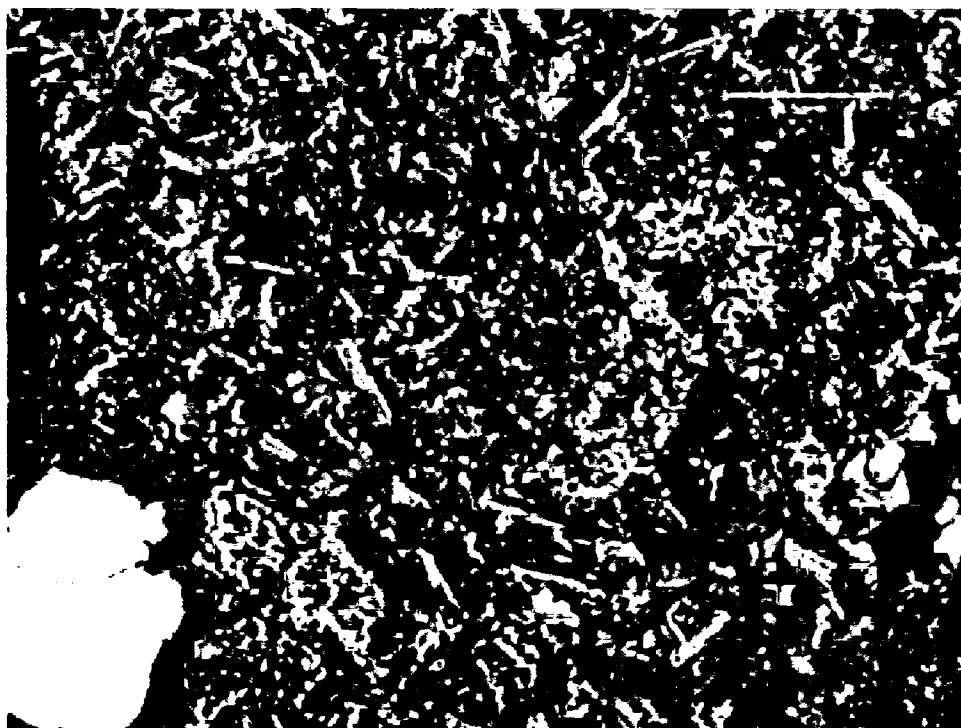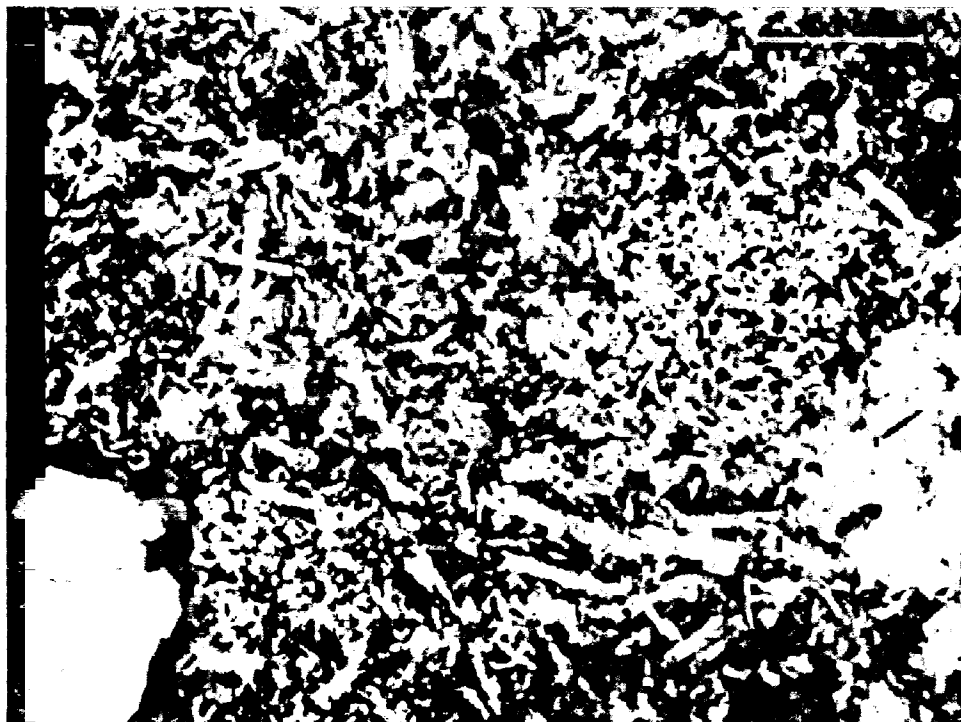
Figure 4.6: Photomicrograph of the mafic component of a composite dike (Sample NKG-6). Scale bar is 0.5 mm.

Plagioclase laths are typically 0.5 mm, but may be as large as 1 mm. These are continuously zoned, although zones are not clearly defined. Plagioclase often has fine opaque inclusions. A few subhedral plagioclase grains are also present. The cores of these grains are unaltered and generally free of inclusions. Crystal margins have sieve textures with high concentration of biotite and opaque inclusions.

Several round to ovoid quartz grains are present. These range in size from 0.5 mm to 1 mm and are rimmed by fine hornblende grains. Quartz and plagioclase also occur as interlocking 0.25 to 0.5 mm grains in 1 to 1.5 mm diameter, sub-round pods.

The felsic unit of the composite dikes has a light pink color and aplitic texture. This unit fully encloses the mafic material. Pillows are separated by felsic material a few millimeters to several centimeters thick. The felsic unit has colors and textures resembling the aplite dikes in the OPG.

The felsic material consists dominantly of quartz, plagioclase and microcline (Figure 4.7). Generally, there are two grain sizes with in the felsic unit. The smaller grains are sub-round and irregular with serrate contacts. These grains are typically less than 0.15 mm, and rarely exceed 0.25 mm. Inclusions and alterations are rare among the finer grains. Larger grains range from 0.5 mm to 3 mm. Quartz occurs as irregular to subrounded grains. Grains greater than 1.5 mm are typically more irregularly shaped whereas smaller grains (0.5 mm) are more equant. Undulatory extinction is common in many grains. Plagioclase is anhedral to subhedral. These have oscillatory zoning in the cores, which are commonly altered. Crystal margins are typically unaltered, lack pronounced zones, and have irregular shapes. Round quartz inclusions are common near plagioclase boundaries. Small plagioclase grains are anhedral and some are sub-round.
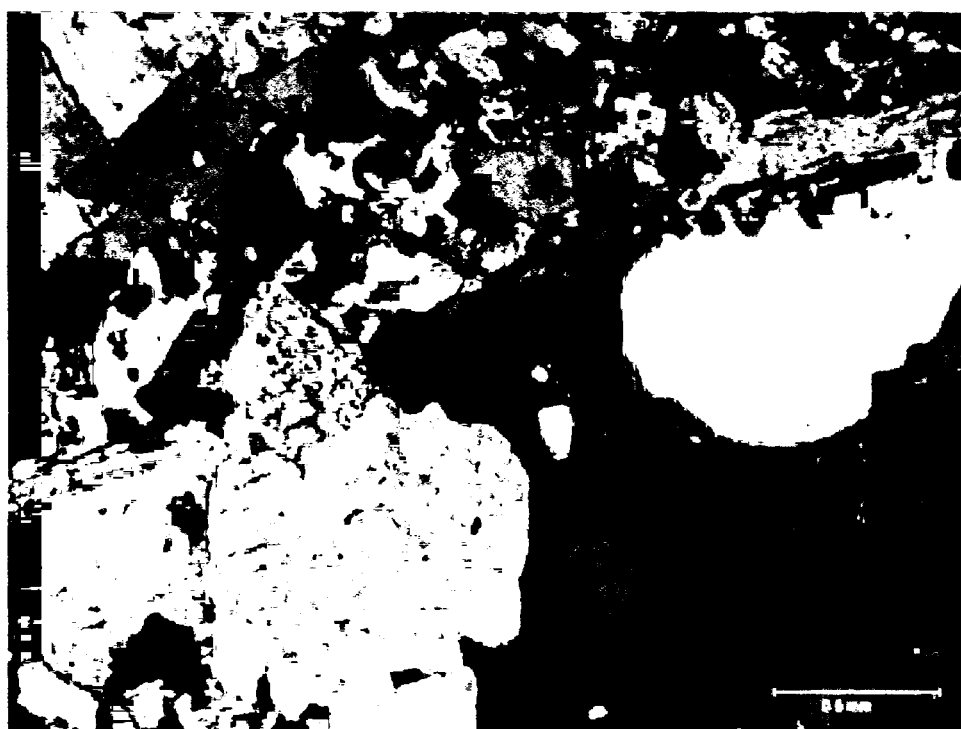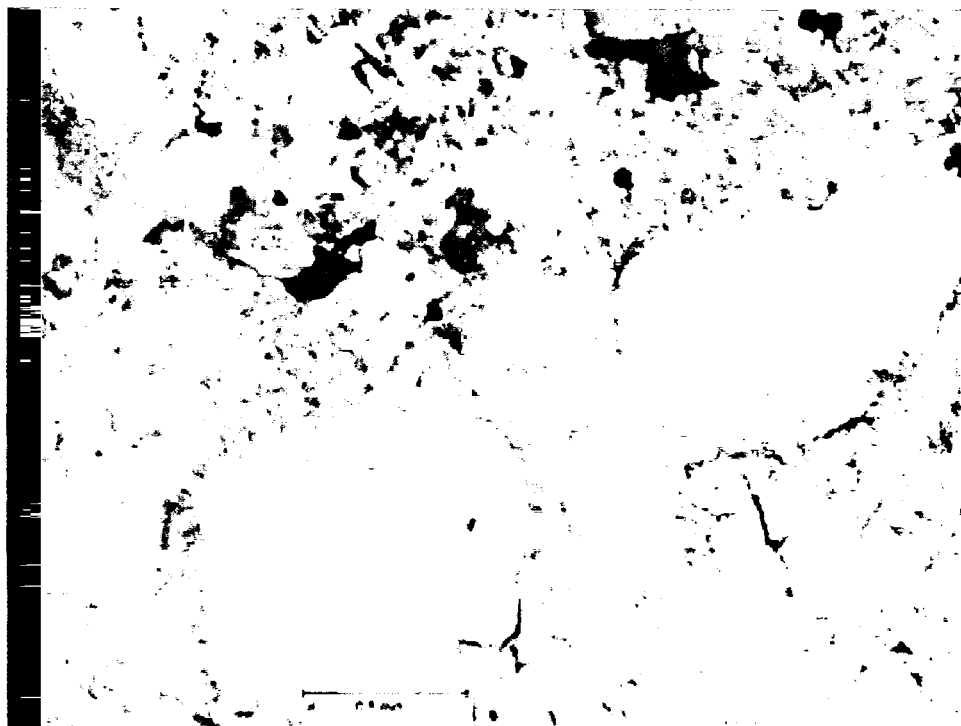
Figure 4.7: Photomicrograph of the felsic component of a composite dike
(Sample NKG-6). Scale bar is 0.5 mm.

These have minor alteration, and rarely show zoning. Microcline grains often have small, zoned plagioclase or round quartz inclusions.

Biotite is the only mafic phase present. It occurs as fine (< 0.5 mm) laths and makes up less than 1 % of the sample. Biotite grains are more abundant near the contact with the mafic unit.

The gray unit is present in some composite dikes and is porphyritic. Phenocrysts are light pink to white colored < 1 mm quartz and feldspar. Inclusions of the mafic unit are small (<1 cm) dark, rounded shapes. This unit also occurs as veins of various thickness surrounding the mafic unit.

The gray unit consists of anhedral plagioclase, microcline and quartz phenocrysts in a groundmass of fine-grained (< 0.25 mm) quartz, alkali feldspar (microcline) and plagioclase (Figure 4.8). The groundmass has anhedral, serrated grain contacts. Microcline grains in the groundmass often have small plagioclase inclusions. Acicular apatite occurs in minor amounts in the groundmass.

Some plagioclase phenocrysts are rounded, anhedral 0.5 to 2 mm grains. Many of these grains exhibit well-defined subhedral, oscillatory zones in their core. A ring of alteration and fine inclusions surrounds the oscillatory zones. This ring structure has a curved and embayed path and often cuts the outer most oscillatory zones. Between the ring and the grain boundary, the plagioclase is unaltered and may contain fine apatite needles. Other plagioclase grains have moderate to extensive alteration. These are subhedral to anhedral 0.5 to 1.5 mm grains and do not show similar ring features or zoning.
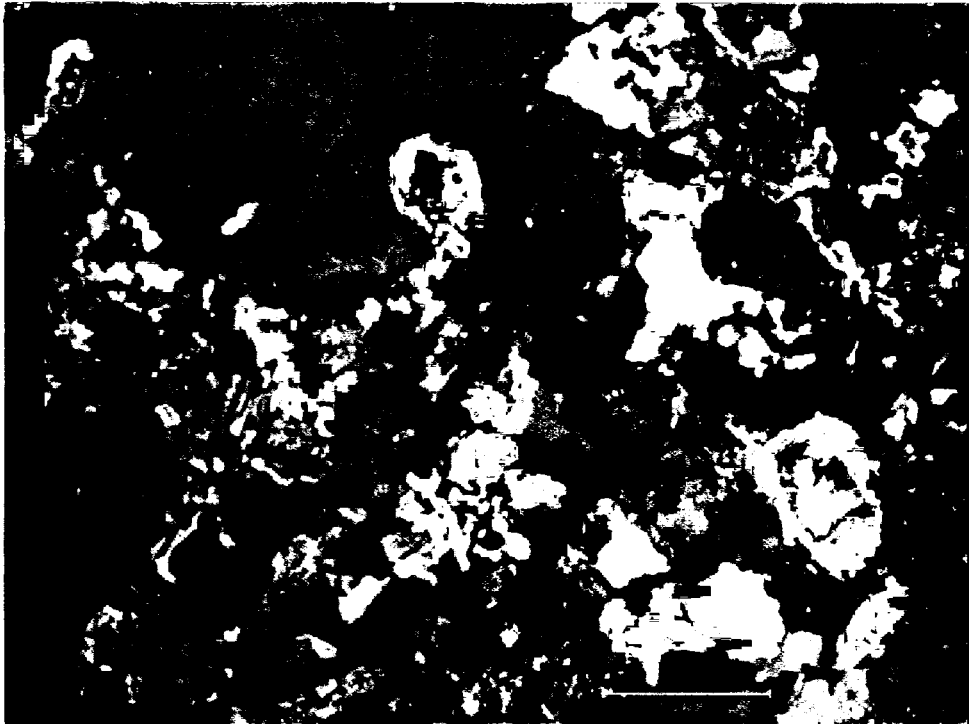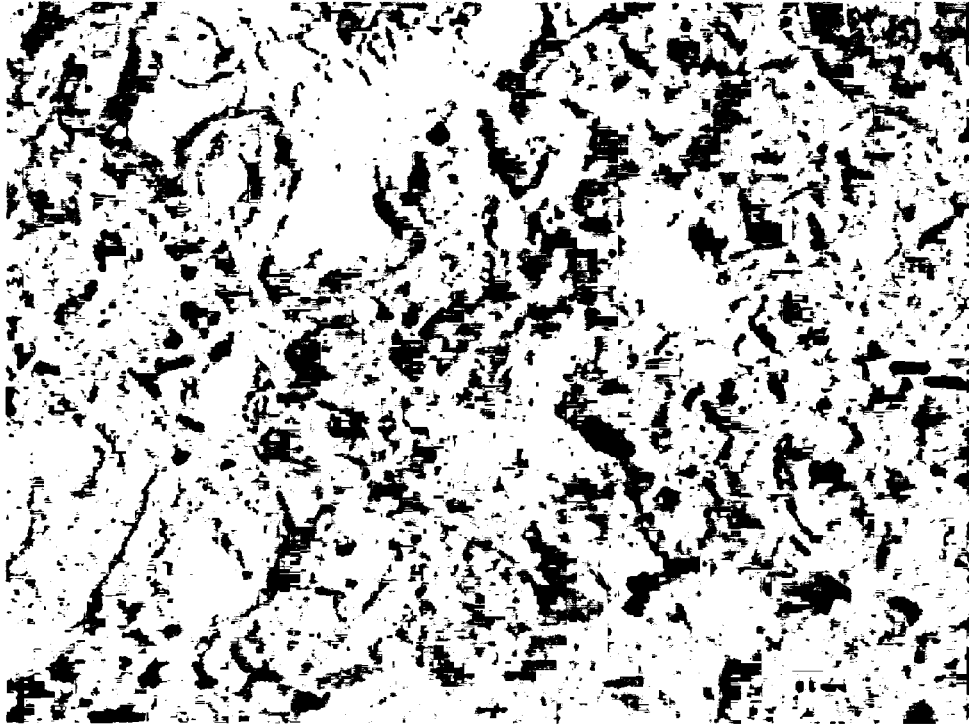
Figure 4.8: Photomicrograph of the gray component of a composite dike
(Sample NKG-13). Scale bar is 0.5 mm.

Most alkali feldspar grains are constituents of the groundmass. Phenocrysts are anhedral and range from 0.5 mm to 2 mm in size. Many have thin plagioclase rims that lack twinning or zoning.

Quartz occurs as sub-round, to ovoid anhedral 0.25 to 1 mm grains. Fine, interlocking, anhedral plagioclase, microcline and quartz grains often surround the larger quartz grains. Few angular quartz grains also exist.

Biotite occurs throughout the sample mostly as individual < 0.25 mm anhedral laths or as 1 mm aggregates exists. Scattered 0.5 mm subhedral biotite is present. Round opaque grains surround and are included in biotite grains.

The gray unit also contains rounded 3 to 5 mm sections of biotite and plagioclase that are presumably derived from the mafic component. One such pod contains poikilitic anhedral (0.5 mm) plagioclase grains. These plagioclase grains are tightly packed and have minor alteration. Opaque minerals are scattered throughout the section, and never exceed 0.25 mm. Biotite forms subhedral green-brown to golden laths. In comparison to the interior, the margin of the mafic pod has more coarse and higher concentrations of biotite. Apatite needles occur throughout the pod, and are also in greater abundance near the margin.

The contact between the mafic and felsic components is irregular, consisting of several "bays and peninsulas" (Figure 4.9). Some rounded fragments of either component have separated and become enclosed by the other. The mafic component is slightly finer grained, more biotite-rich, and the plagioclase is smaller and less abundant at the contact. A few 1 mm subhedral plagioclase grains are situated on the contact. In both components, apatite needles are most abundant along the contact. Interlocking anhedral quartz and

44
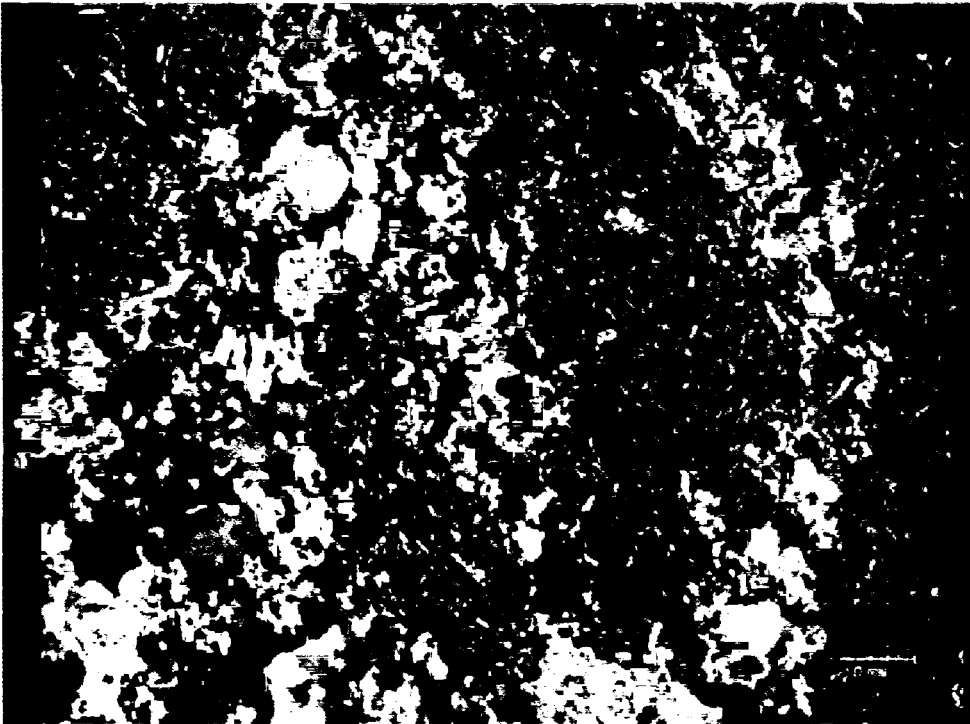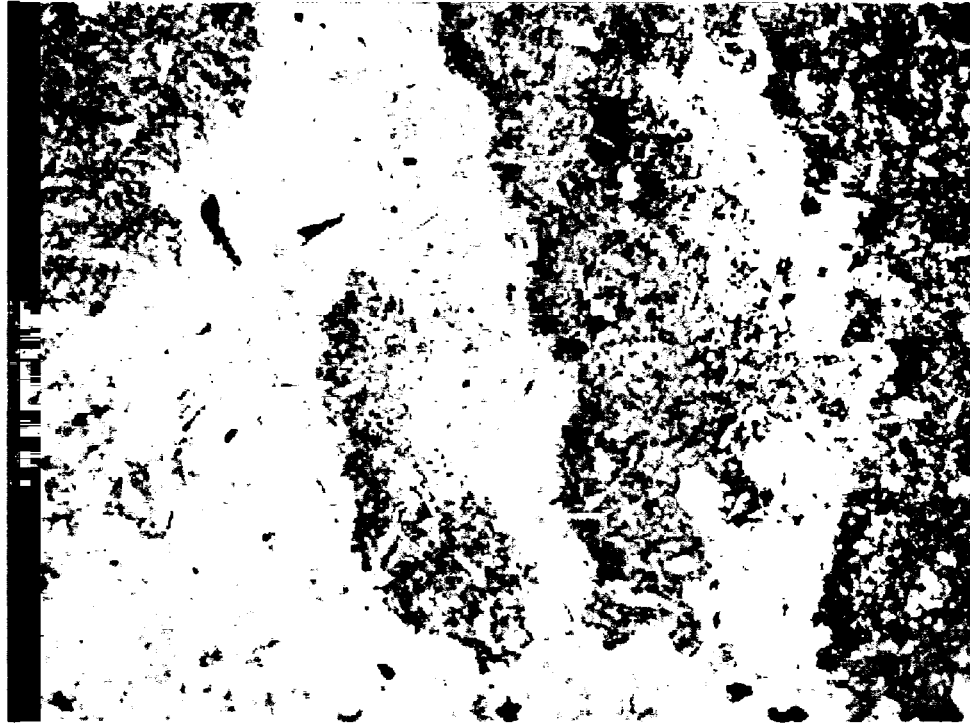
Figure 4.9: Photomicrograph of the contact between composite dike units (Sample NKG-6). Scale bar is 1.0 mm.

plagioclase occur along the contact. They rarely exceeding 0.5 mm and are more commonly less than 0.25 mm. The contact between the gray unit and the mafic unit is similar to the felsic-mafic contact. However, in this case, the mafic unit does not decrease in grain size, and there is a higher abundance of hornblende at the contact. Contact between the gray unit and the felsic component is gradational and relatively straight.

4.4. Mafic Dikes

Mafic dikes occur on the Brooklin peninsula and on Flye Point. Stewart (1998) describes the mafic dikes on Brooklin as Jurassic age monchiquite dikes. Three individual mafic dike locations occur on the Brooklin peninsula. These have aphanitic to micro-porphyritic textures. One dike has been eroded such that it is preserved in the Oak Point Granite by its remnant shape. Beach gravel deposits cover what is left of this dike, although its orientation (47^0-75^0 SE) and width (0.5 mm) can be determined. At a short distance west of this dike are two small mafic dikes. These trend toward one another but terminate in points 1 m apart. Neither of these dikes is straight but have a general northeast trend. Their width is < 20 cm and their contact with the Oak Point Granite is sharp.

A third mafic dike is found in close proximity to the solo composite dike, described previously. The exposure is three dimensional, approximately 0.5 m wide, 1 m high and 1.5 m long. It strikes at 50^0 and is vertical. It is similar in color and texture as the other mafic dikes.

These dikes on the Brooklin peninsula are similar in color and have micro-porphyritic textures (Figure 4.10). The phenocrysts are 0.25 to 1.5 mm subhedral to

anhedral olivine that occur as individual grains or as glomeroporphs of 5-6 crystals. Serpentine alteration is present in some olivine grains. The groundmass consists of pyroxene, minor plagioclase and opaque minerals. The latter occurs as thin short needles and as round grains. Acicular apatite is very abundant in one of the mafic dike samples but was not observed in the other samples.

The mafic dike on Flye Point is exposed only during low tide. Stewart (1998) marked this dike location and described it as a massive, non-foliated rock. Its exposure is approximately 5 m x 10 m, and trends 50^0 NE. The contact with the Oak Point granite is not exposed, so a dip direction was not determined. This dike has a medium grain size (Figure 4.11).

In the Flye Point dike, olivine occurs as subhedral to anhedral crystals ranging in size from 1 to 4 mm. Some grains are zoned as indicated by changes in birefringence. Minor serpentine alteration is common along fractures and grain margins. Clinopyroxene occurs as pale yellow or colorless, elongated subhedral blades (0.25 to 4 mm) or as anhedral grains (0.25 to 1 mm). Most clinopyroxene grains have numerous zones. Some grains appear in clusters and radiate from a central point. Biotite occurs as subhedral to anhedral 0.25 to 2 mm grains. These typically have a dark red-brown to yellow color, although some grains are bright orange. Opaque minerals are blocky to irregularly shape. Most opaque grains are between 0.25 and 0.5 mm, although some are close to 1 mm. Many are surrounded by red hematite and are associated with biotite. Plagioclase occurs in minor amounts. These grains are subhedral to anhedral and appear to be interstitial.
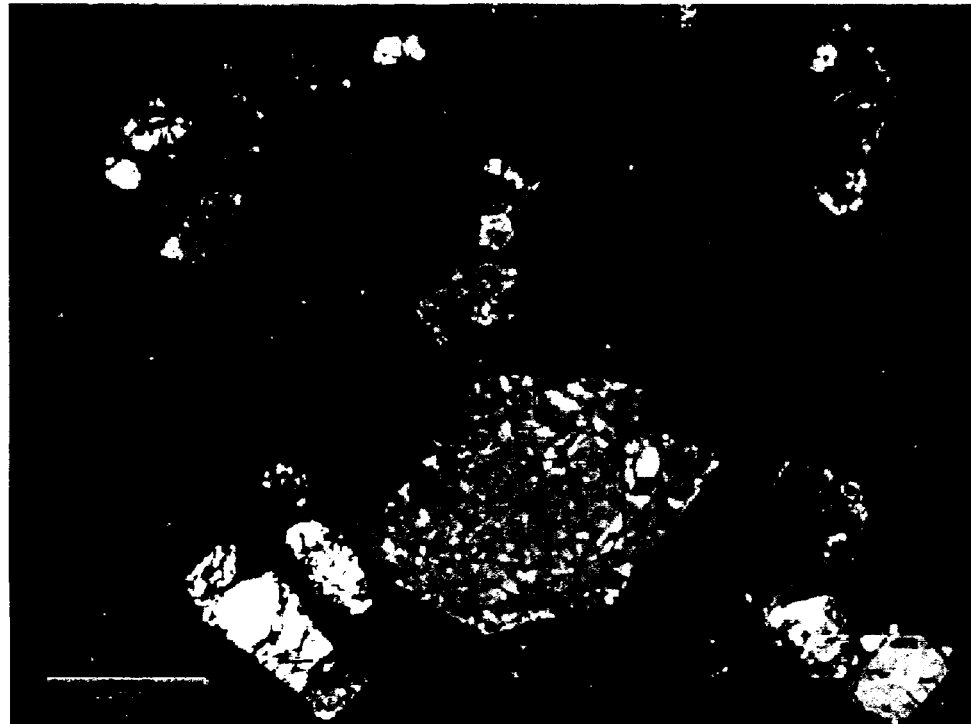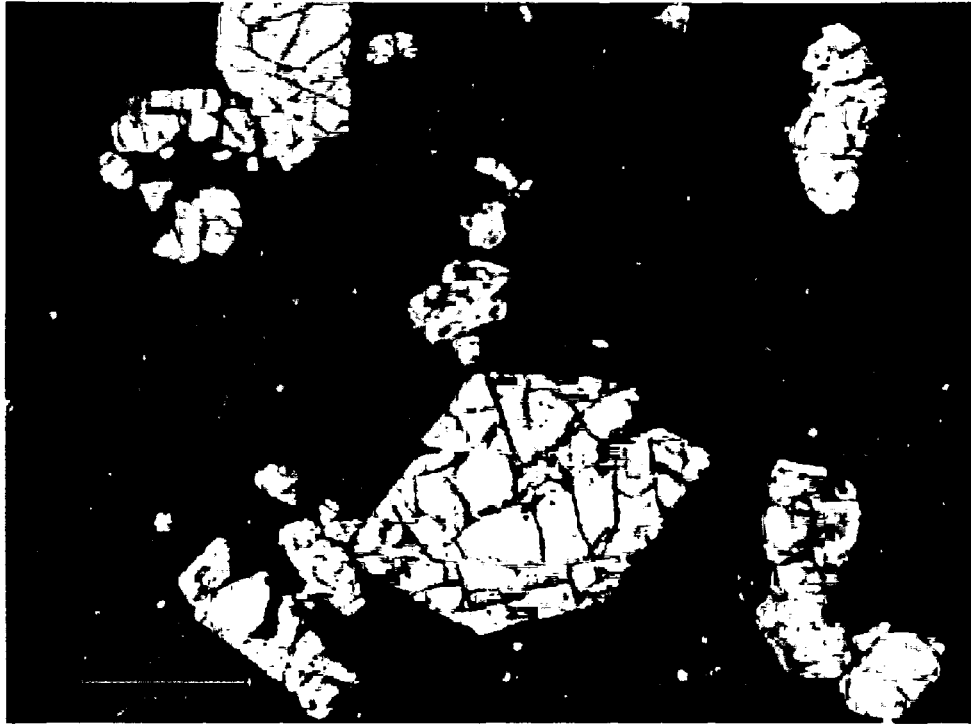
Figure 4.10: Photomicrograph of a mafic dike from the Brooklin peninsula (Sample NKG-9). Scale bar is 0.5 mm.
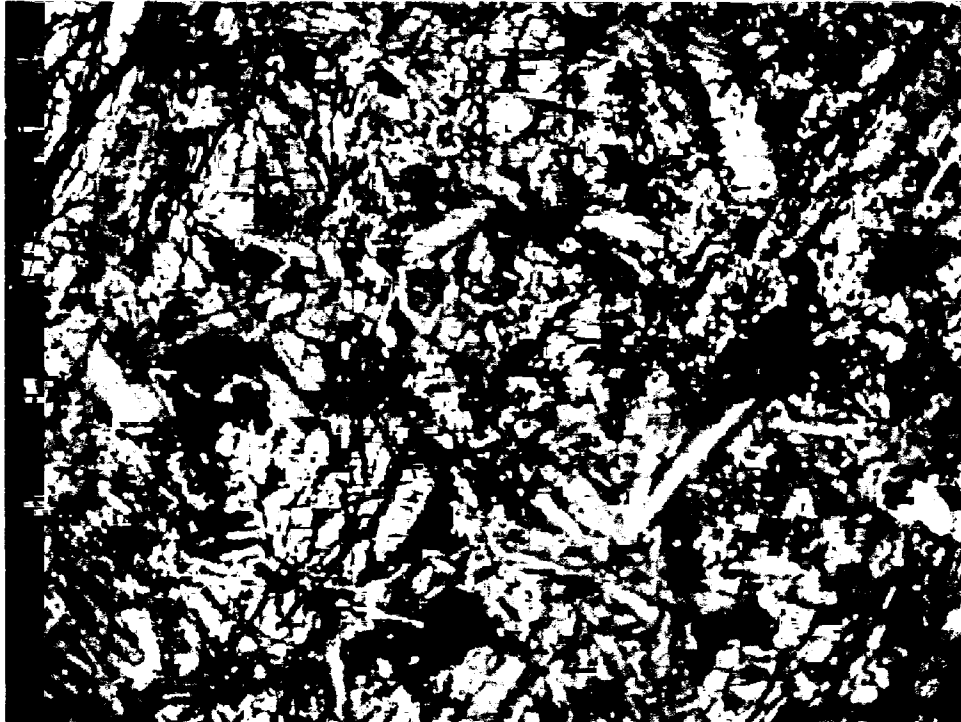
Figure 4.11: Photomicrograph of the mafic dike from Flye Point (Sample FYPT-1).
Scale bar is 1.0 mm.

They have uniform extinction and do not show albite twinning. Apatite occurs as blades or thin needles. Most apatite grains are approximately 0.25 mm although some are close to 0.5 mm.

4.5. Enclaves in the Oak Point Granite

Enclaves are a prominent feature of the OPG and although they occur throughout the Oak Point Granite, their abundance varies at each outcrop. For example, at some localities enclaves are scarce and even at times absent in sections over several meters. However, at other localities there are large numbers of enclaves in small areas.

The enclaves range in composition from dioritic to granitic (Figure 4.2). Enclaves within the OPG have similar characteristics with fine-grained textures relative to the host granite. Most enclaves are typically equigranular with the exception of large feldspar megacrysts.

Composition, texture and grain size define three groups of enclaves collected from the field: medium-grained felsic, medium-grained dioritic, and fine-grained dioritic. The felsic variety is medium-grained, occurring as amorphous to sub-round masses. Sizes are approximately 15 cm in diameter, although some exceed 30 cm. The texture is subporphyritic, with a color index less than 5%. The larger grains are alkali feldspar and quartz. In hand sample, alkali feldspar is perthitic, and plagioclase mantles are common.

In thin section, alkali feldspar occurs as anhedral microcline and perthite and makes up approximately 45 modal percent of these rocks (Figure 4.12). Individual crystals are mostly 1 to 2 mm although some as large as 3 mm are present. Plagioclase
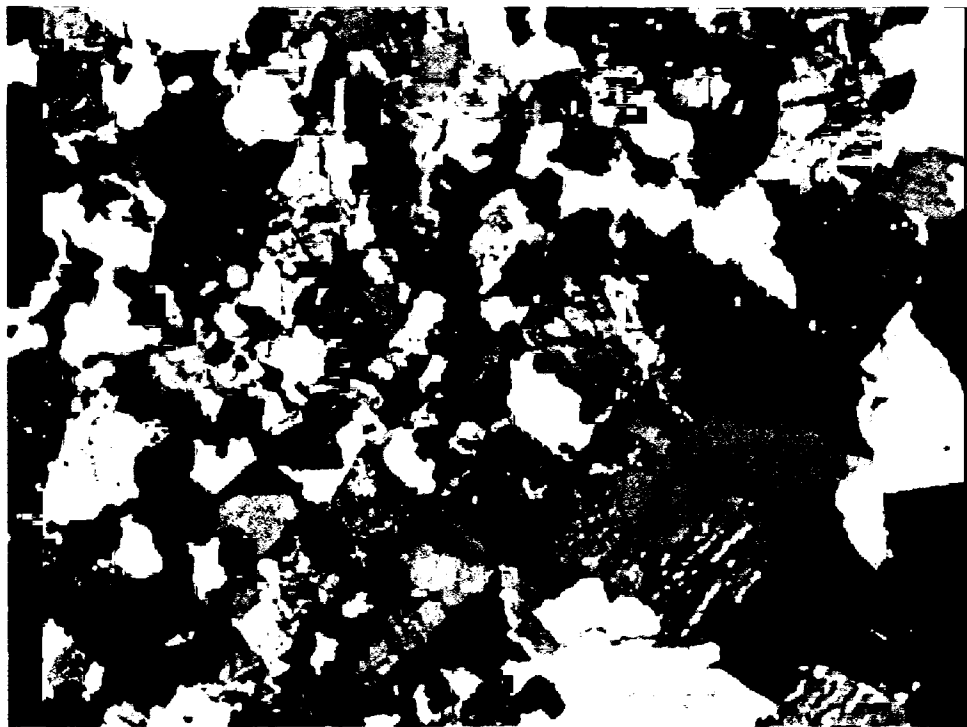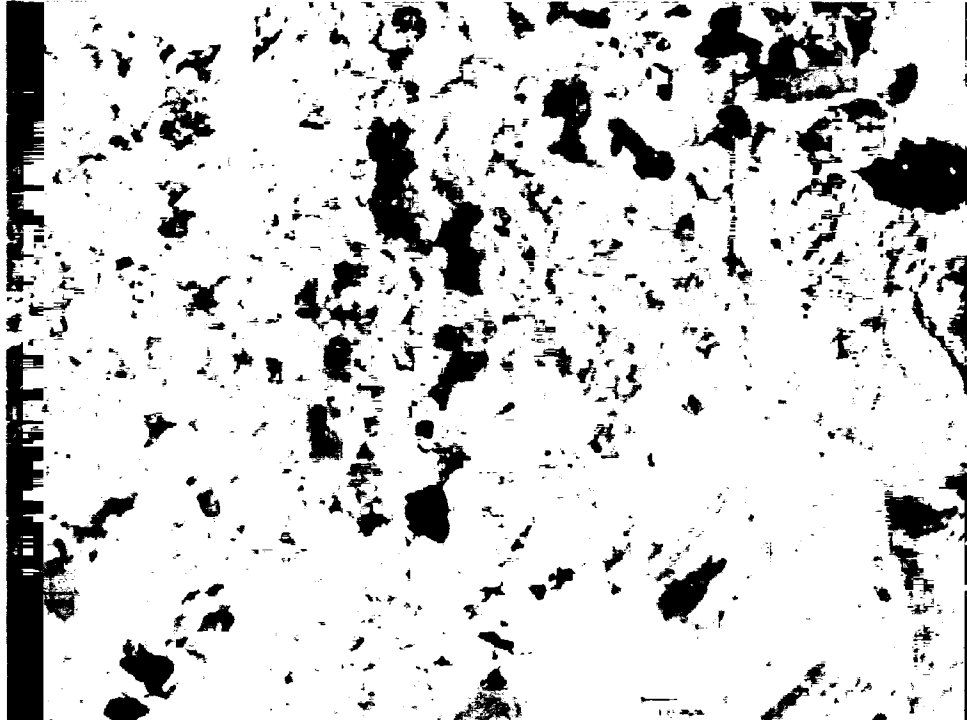
Figure 4.12: Photomicrograph of a felsic enclave (Sample SNS-7). Scale bar is 1.0 mm.

inclusions are often located near the center of the alkali feldspars. A large (~1 cm) perthite grain contains several anhedral zoned plagioclase grains (~1 mm) with in the central portion. Extinction of the large perthitic grain reveals a rounded dissolution surface towards the grain boundary. The outer perthitic overgrowth contains coarse anhedral quartz grains.

Quartz is anhedral ranging from 0.5 mm to 2 mm and comprising approximately 25 modal percent of the rock. These occur as single crystals or in aggregates of several smaller crystals. All quartz grains show weak undulatory extinction and many grains have poikilitic texture.

Plagioclase makes up about 25 % of the rock volume. Grain sizes range from 0.25 mm to 1 mm, having irregular to elongated ovoid shapes. Zoning in plagioclase grains typically consists of a moderately to extensive altered core and an unaltered rim. Composition zone boundaries are irregular and sub-rounded shapes. Some rare grains have three zones, the altered core and two unaltered overgrowths.

Mafic minerals are a minor component (<5 %) of the felsic enclaves. Biotite is the dominant mafic phase and it occurs as subhedral to anhedral red-brown, golden brown to yellow grains. Other mafic phases include sphene and opaques. Mafic minerals do not exceed 1 mm and are typically less than 0.5 mm. Small amounts of acicular apatite occur in some biotite and adjacent plagioclase grains.

The medium-grained dioritic enclaves are equigranular and contain 1 to 3 mm crystals. These have a frosted white weathered appearance, with black specks. Their shapes are sub-round with diameters not exceeding 20 cm. Collected samples of this group were extensively altered (Figure 4.13).
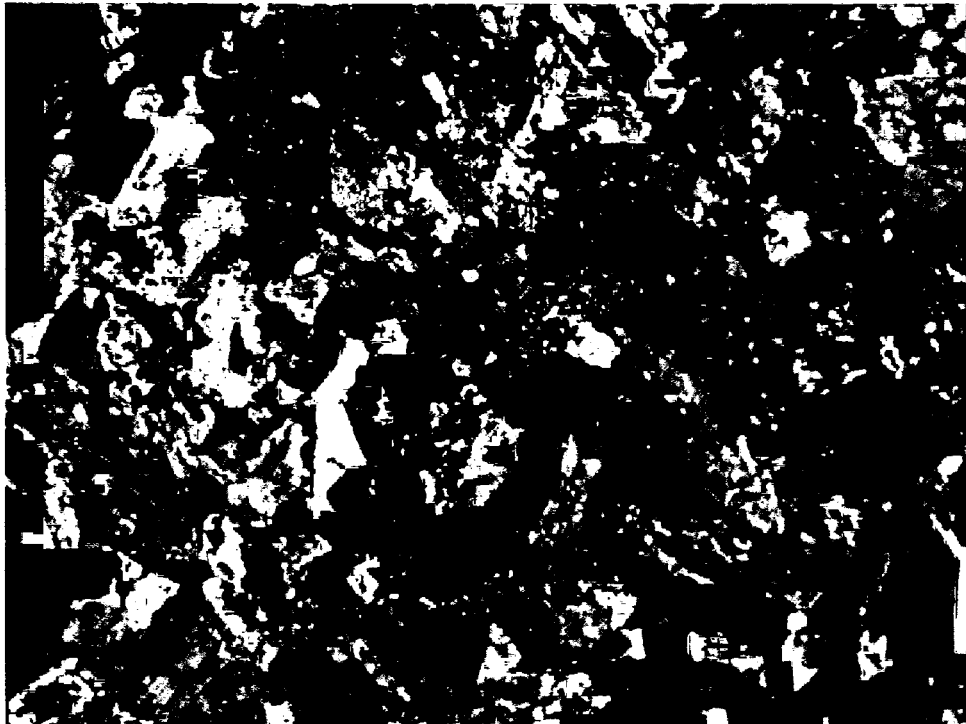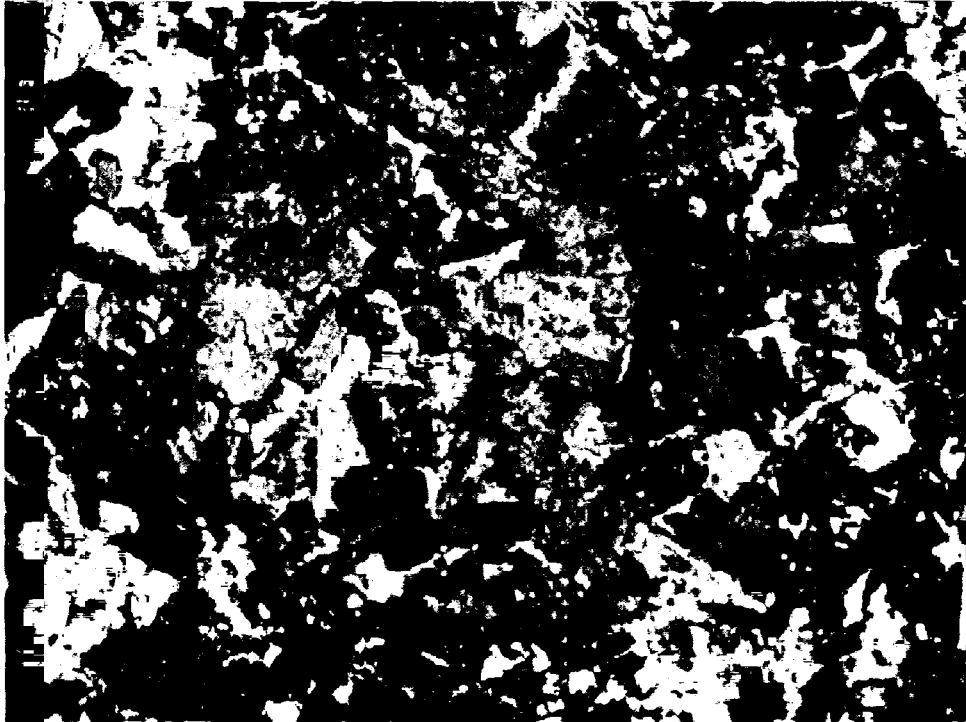
Figure 4.13: Photomicrograph of a medium-grained dioritic enclave (Sample SNS-29). Scale bar is 1.0 mm.

The dominant mineral of this group is plagioclase, comprising about 65 modal % of the rock volume. Most grains are about 1 mm in length but some are as long as 3 mm. Shapes are anhedral, elongated ovoid to irregular, although some grains are subhedral. Sericite alteration varies among the samples and individual grains with in a sample. The smaller grains are extensively altered whereas the larger grains have alteration localized in central portions. Plagioclase has continuous zoning, and some grains show patchy zoning patterns towards the crystal centers. Extinction patterns reveal irregular zone boundaries. Plagioclase grains have inclusions of all other phases present in this type of enclave.

Alkali feldspar and quartz occur as minor phases, approximately 3% and 4%, respectively. Both grains occur randomly and often have poikilitic textures. Quartz shows undulatory extinction. Acicular apatite is included in both phases.

Mafic minerals constitute approximately 30% of the medium-grained dioritic enclaves. Hornblende and biotite are weakly to extensively altered to epidote and/or chlorite. Biotite and hornblende occur in roughly equal proportions. Anhedral to subhedral, olive to light green and dark green hornblende occurs as individual 1 to 2 mm grains or in aggregates of several smaller crystals. Many grains have poikilitic texture, due to high amount of round plagioclase inclusions. Several hornblende grains show relic clinopyroxene grains with in the crystal. Biotite occurs as red-brown to faint yellow-brown anhedral grains, although some subhedral grains exist. These grains are randomly distributed throughout the samples. Sizes range from 0.5 mm to 1.5 mm.

Other mafic minerals include sphene and opaques. Sphene occurs as anhedral to subhedral grains ranging in size from 0.5 mm to 2 mm. Opaque minerals occur as

anhedral blocky to round shapes. Large anhedral opaque grains are associated with hornblende aggregates.

Apatite needles are included in all minerals and some are situated across crystal contacts. Thickness of the needles varies, such that shorter grains are thicker, and longer grains thinner. Lengths of the apatite grains range from less than 0.25 mm to 1 mm.

The fine-grained dioritic enclaves are also equigranular in texture and are a black, tan-brown to dark gray on weathered surfaces and light to dark gray on fresh surfaces (Figure 4.14). In some hand samples, a prominent red coloring exists due to higher alkali feldspar concentrations or sub-round ocellar grains. Color index among these enclaves range approximately from about 12-34%. Some of these enclaves have a weak foliation, defined by biotite and hornblende as well as elongated-ovoid plagioclase and alkali feldspars.

Most of these enclaves consist of 0.25 mm to 1 mm anhedral grains of alkali feldspar and plagioclase (Figure 4.15). These minerals also occur as larger (1 to 3 mm) grains. Plagioclase has normal and reversed compositional zoning, as well as fine oscillatory zoning in some grains. Albite twinning is present in some grains. Alteration of plagioclase typically occurs in the central portion of the grain and some plagioclase grains have thin rims of alkali feldspar.

Alkali feldspar mostly occurs as small 0.25 mm to 1 mm anhedral microcline grains. Its abundance varies from 14 to 44 modal percent of the rock volume. Perthitic texture is rare in these enclaves and limited to the larger grains. Most microcline grains contain small inclusions of plagioclase. Acicular apatite is a common inclusion in both alkali feldspar and plagioclase.
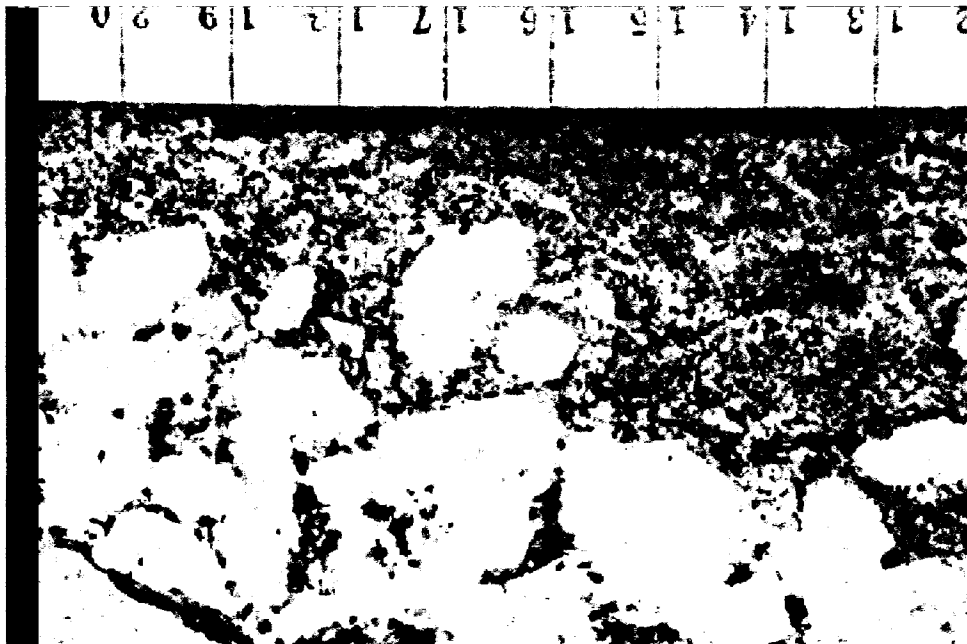
Figure 4.14: Photographs of fine-grained dioritic enclave hand samples. Top picture is sample OPE-9 and bottom picture is sample FYPT-7. Ruler units are in cm.
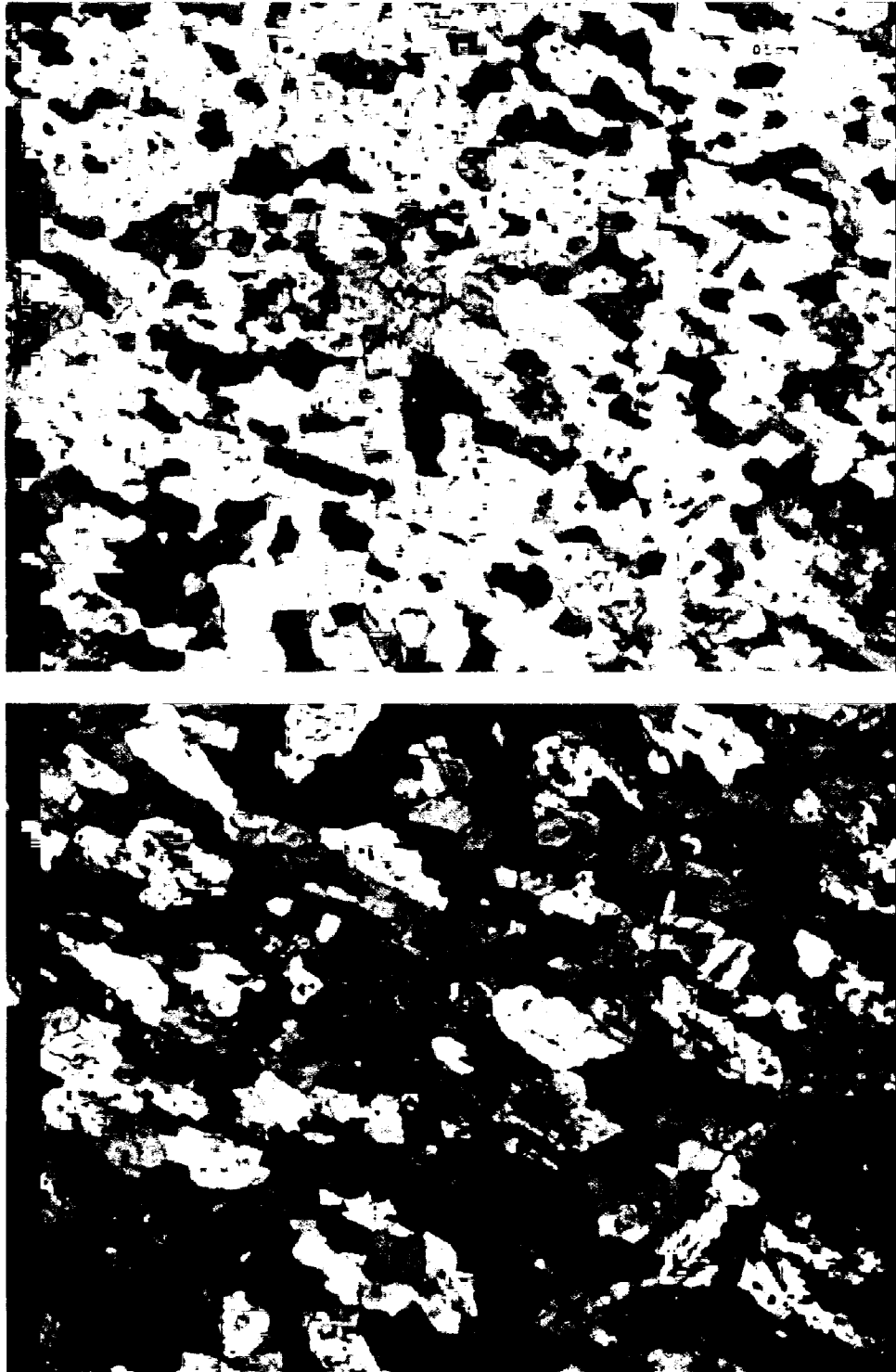
Figure 4.15: Photomicrograph of a fine-grained dioritic enclave (Sample ESC-1).
Scale bar is 0.5 mm.

Quartz is rare in most samples, averages about 4%, but makes up 10% in one sample. It occurs as an interstitial phase or associated with megacrystic feldspar inclusions. Undulatory extinction and poikilitic textures are common of quartz grains. Crystal sizes range from 0.5 mm to 1 mm. Acicular apatite occurs in small amounts in some quartz grains.

Mafic minerals range in abundance from 12% and up to 34%, with an approximate average of 20%. Biotite and hornblende are the dominant phases, although their relative abundances vary among samples. Hornblende occurs as 0.5 mm to 2.5 mm olive green to dark green anhedral to less common subhedral grains. These can be either irregular or elongated individual grains or aggregates of several small crystals. Twinning and zoning is common among hornblende grains. Most grains have a poikilitic texture, characterized by round embayments and inclusions, such as opaques, plagioclase, microcline and biotite. Relic clinopyroxene crystals occur in many hornblende grains.

Biotite occurs as red-brown to faint yellow-brown anhedral to subhedral grains. These are typically amorphous masses, as well as elongated laths. They can also exhibit rounded embayments and poikilitic textures, although this is less common than as in hornblende. Sizes are from 0.25 mm to 1 mm, although some grains are as large as 3 mm. Fe-oxides, hornblende, and other smaller biotite grains are included in biotite.

Sphene and opaque minerals are less abundant. Sphene occurs as anhedral to subhedral grains, although some euhedral grains are present. Sphene rarely exceeds 1 mm in length and is typically closer to 0.5 mm. Opaques are anhedral, rounded to sub-rounded grains. These can be either larger grains, up to 0.5 mm in diameter or as small

round grains. The larger opaque grains occur in association with hornblende, where as the small anhedral round grains are randomly scattered through out the sample.

Acicular apatite is ubiquitous in plagioclase and alkali feldspars, however, it occurs less common in hornblende and biotite. These are uniform in thickness and do not exceed 0.5 mm in length. Apatite needles are weakly aligned to the sample foliation.

Clinopyroxene occurs in some samples as small rounded anhedral to elongated ovoid grains. Elongated grains are 0.5 mm in length, and the anhedral grains are typically 0.25 mm in diameter. Red-orange to yellow staining occurs around some grains. Clinopyroxene grains are included in some large plagioclase grains. Suspect clinopyroxene grains occur in some hornblende grains (Figure 4.16). These are colorless to faint green patches within hornblende. Cleavage is recognizable in some cases. In crossed nicols, the relict section is identifiable by its blue birefringence, contrasted by green or violet-red birefringence of the hornblende crystal and by different extinction angles. The relict patches are irregular, ovoid and rectangular shapes, never exceeding 0.25 mm in diameter. Some relic sections have a red-orange to yellow staining. This staining is concentrated in the suspect grain, and confined to the hornblende grain. Small round opaque inclusions are common in some relic clinopyroxene. Some hornblende grains show cores of hornblende showing different birefringence, and pleochroism.

Field measurements, such as orientations and dimensions, focused on the fine-grained dioritic enclaves. These are the largest, most abundant, and most easily observed enclaves in the Oak Point Granite. The longest dimension of the enclaves is typically 15 to 25 cm, although some exceed 1 m. Enclaves are relatively planar and have ellipsoid to disk shapes. The thickness of the enclaves ranges from 5 to 60 cm, but typically they are

Figure 4.16: Photomicrograph of a suspect clinopyroxene grain
(Sample SNCC-2). Scale bar is 0.1 mm.

about 6-20 cm. Adjacent enclaves with in single outcrops typically have different sizes and shapes. The enclaves on the east side of Eggemoggin Reach are typically larger, more amorphous and have higher abundance of feldspar inclusions than enclaves on Deer Isle.

Although some enclaves are planar, many enclaves have a wavy or lobate irregular form (Figure 4.17). Two dimension horizontal exposures of enclaves show that many have a bow or bulge on one side (Figure 4.18). The bulge of the enclave is consistently on the NE side of the exposure.

Large megacrysts occur in many of the fine-grained dioritic enclaves. These consist mostly of perthitic alkali feldspars, often with rapakivi textures. They closely resemble rapakivi feldspars from the host granite, in both similar color and size. The abundance of such inclusions varies greatly among enclaves, ranging from a few to over 30% of the enclave. High percentages of inclusions in some enclaves can mask or hide the nature of the enclave. Less common are megacrysts of ovoid 0.5 to 2 cm plagioclase. Many plagioclase megacrysts have a faint red color. Occasionally, megacrysts are found situated across the contact between the host and enclave.

In thin section, the rapakivi megacrysts consists of an rounded perthitic core (Figure 4.19) with a few small strong to weakly zoned, weakly altered, anhedral 0.25 mm to 1 mm plagioclase grains. Contact of the perthite with the plagioclase rim is irregular. The rapakivi rim consists of several individual plagioclase grains. These range in size from 1 mm to 5 mm and are anhedral to subhedral. Plagioclase grains are in contact with one another by irregular, sharp contacts. Albite twins are randomly oriented with respects to other grains. Sericite alteration is typically minor, although some grains
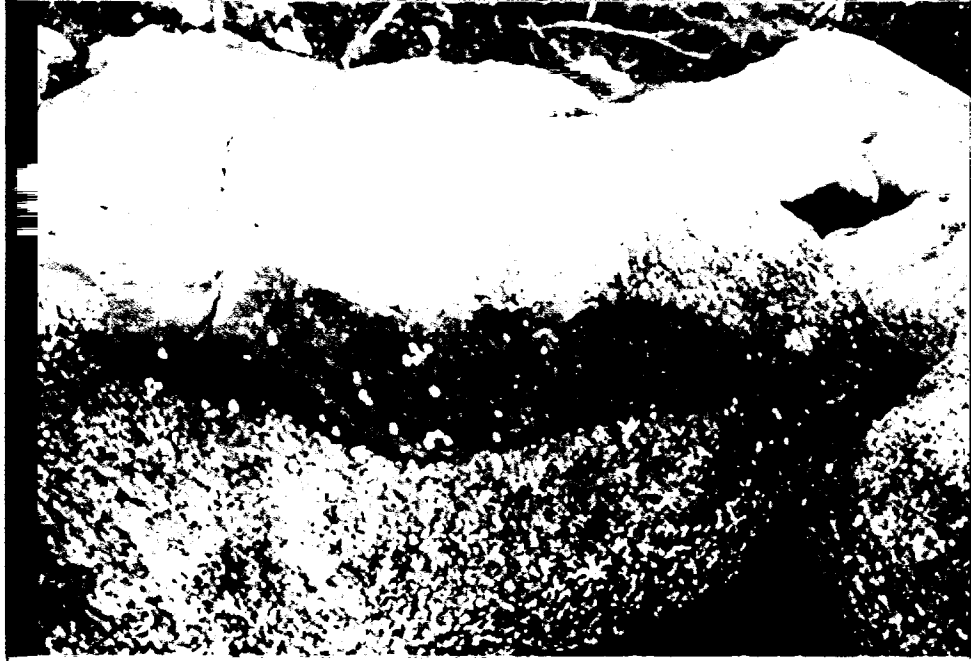
Figure 4.17: Profiles of two enclaves. Top photograph is from the eastside of Oak Point (green pen for scale). Bottom photograph is from Naskeag Point (hammer for scale).
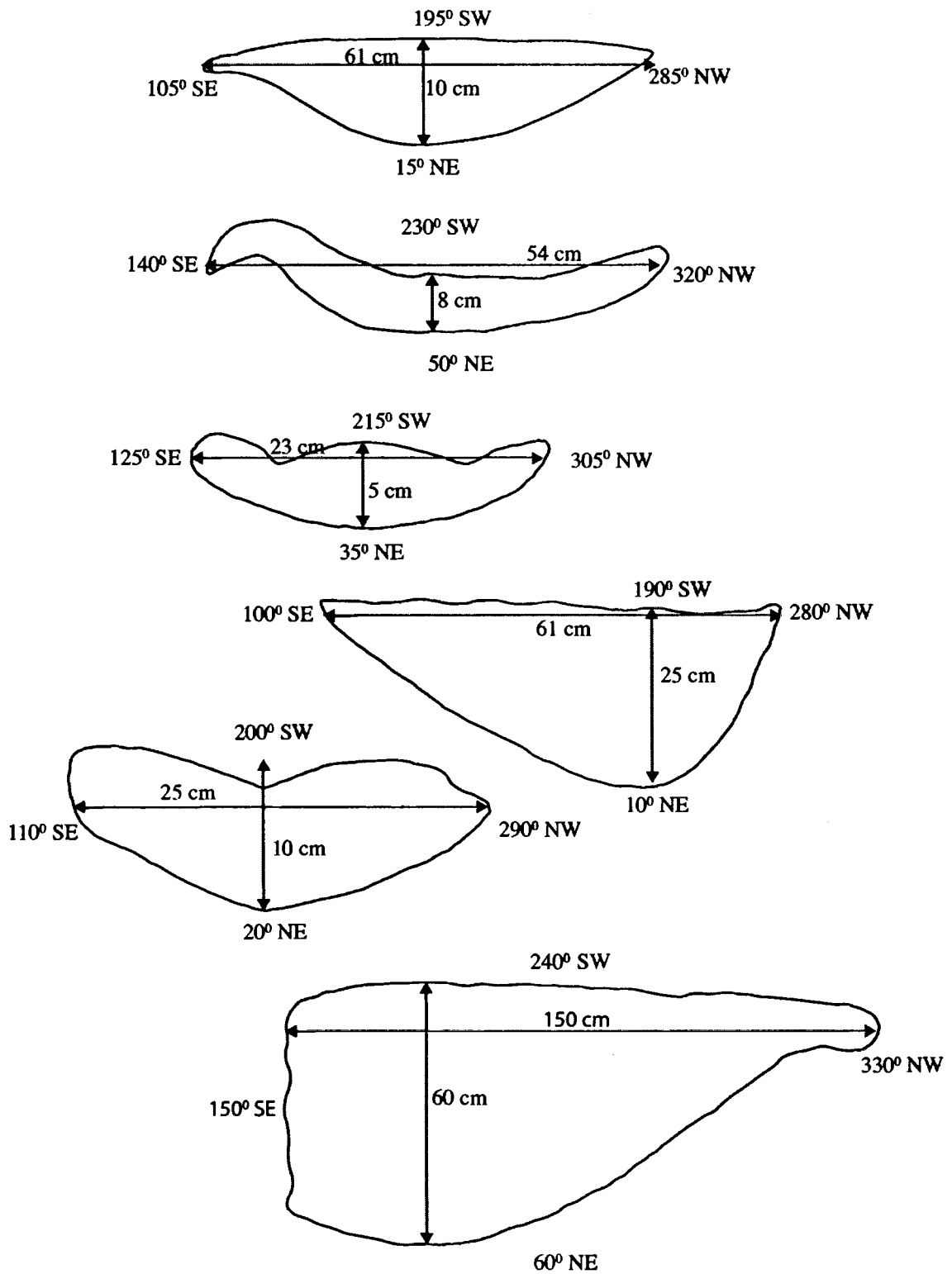
Figure 4.18: Field sketches of enclaves from horizontal surfaces.
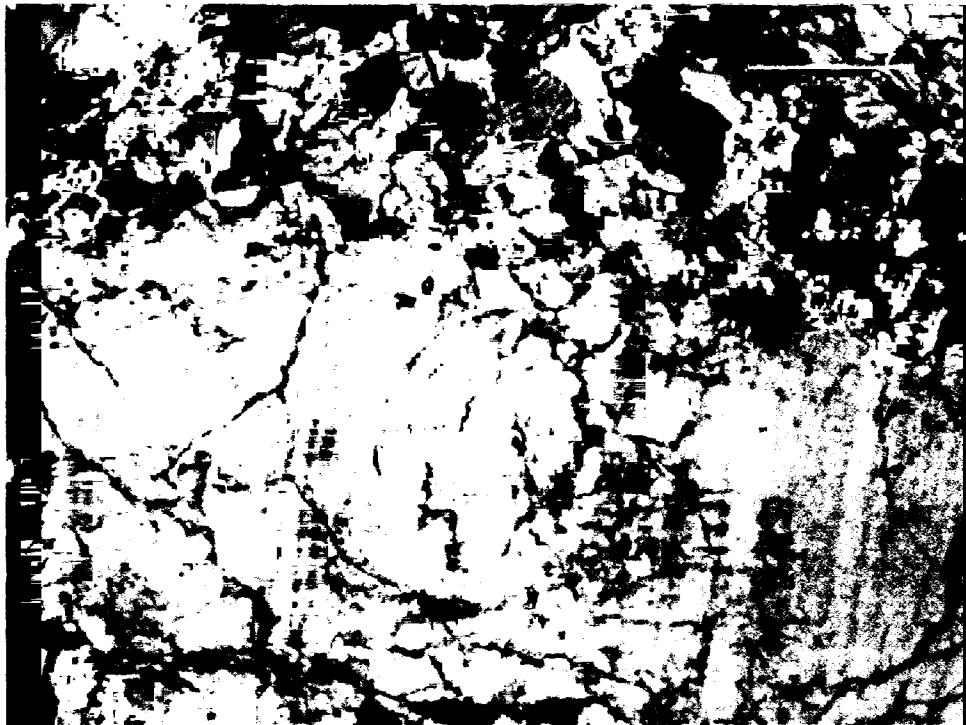
Figure 4.19: Photomicrographs of a feldspar inclusion in an enclave host (Sample FYPT 7). Top figure scale bar is 1.0 mm. Lower figure is a close up of contact of feldspar with the enclave host. Scale bar is 0.5 mm.

are have extensively altered sections. Plagioclase grains have inclusions of small anhedral elongated quartz, some of which are poikilitic. Zoning varies among the grains. Some grains have strong continuous composition zones between core and rim, whereas others have oscillatory zoning. Round to ovoid "trails" of fine opaque inclusions are present in some plagioclase grains. These surfaces are confined to the grain and do not cross into adjacent grains. Overgrowths towards the crystal margins are subhedral. Contact of the rapakivi rim and the enclave host is sharp and it is irregular to sub-planar, depending on the plagioclase grain morphology. Fine biotite, round opaque minerals and apatite needles are included in plagioclase rims. The apatite grains are restricted between the mafic inclusion trails and the crystal margin.

Chapter 5

RESULTS

5.1. Structural Data

Enclaves and feldspar foliations have similar attitudes (Figure 5.1). Enclaves range from 3^0-177^0, with an average of 99.5^0. Dip angles range from 5^0-73^0 and average at 33.6^0. Feldspar foliation varies from 0^0 to 173^0 with an average of 114.6^0, and the dip angle ranges from 20^0-55^0, with an average of 37.1^0. Both enclaves and feldspars have dip direction toward the west, with a higher frequency to the southwest.

Aplite dikes have a relatively random pattern (Figure 5.1). Dip angles range from 5^0 to 90^0 with an average of 54.2^0. Figure 5.2 shows histograms for west and east dipping dikes. Most aplite dikes dip toward the east, with a slight preference to the southeast. West dipping dikes are less common, and show a preference toward the northwest. Twelve (12) vertical dikes were measured in the Oak Point Granite. These strike between 0^0-16^0 and average at 59^0.

5.2. Whole Rock Chemistry

A total of twenty samples were analyzed by XRF. Ten (10) major (wt%) and eighteen (18) trace (ppm) elements were measured. Appendix A (Table A.3) includes the whole rock chemical data. Figure 5.3 shows Harker diagrams for MgO and total alkali for all samples.

Two mafic dikes were analyzed, one sample from Flye Point (FYPT1) and the other from the Brooklin peninsula (NKG9). They have SiO_2 values of 41.51 and 44.78
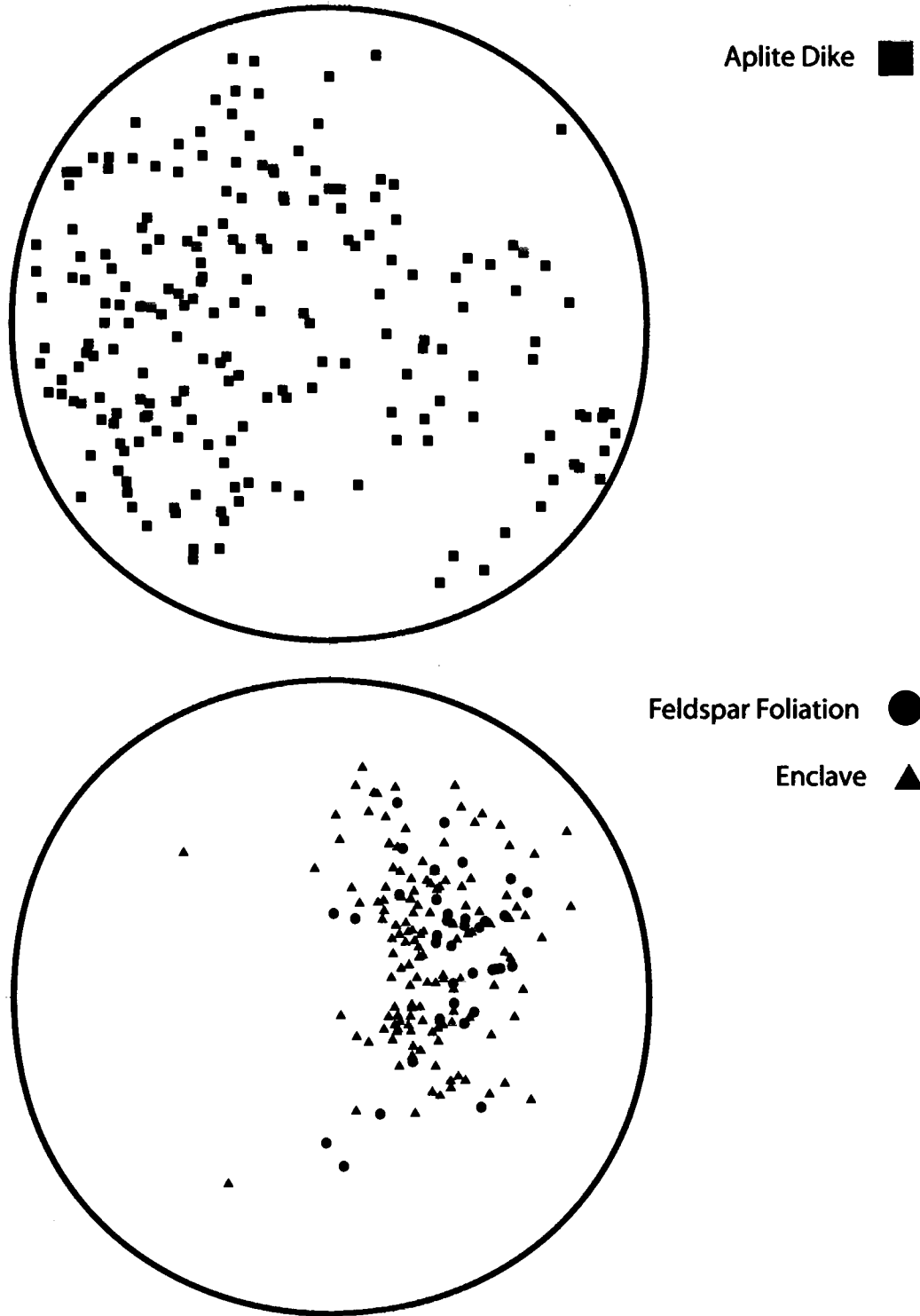
Figure 5.1: Stereo diagram of planar features (Lower hemisphere, equal area projection).
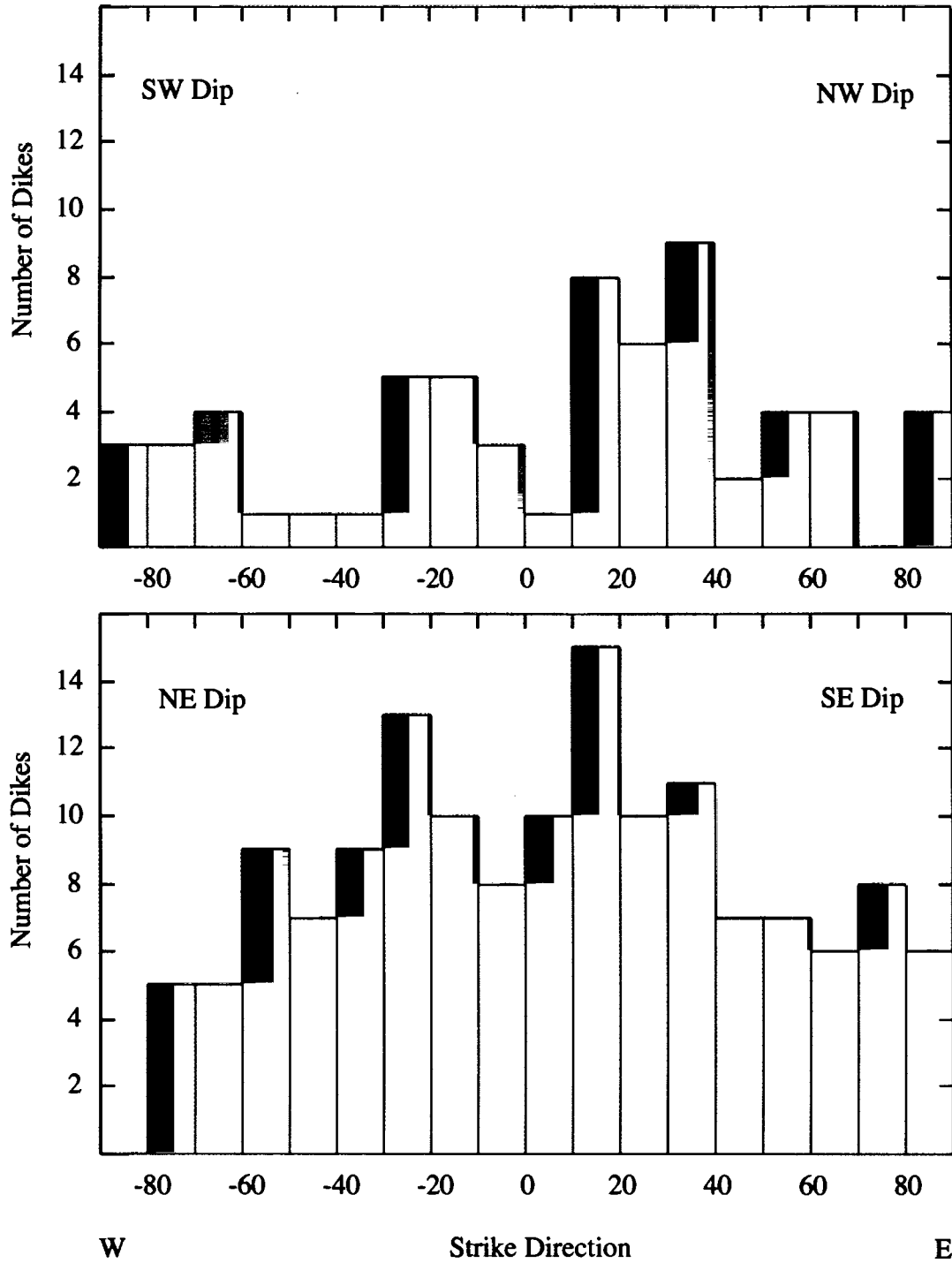
Figure 5.2: Histograms of aplite dikes. Top figure shows dikes with west dipping orientations. Lower figure shows east dipping dikes.
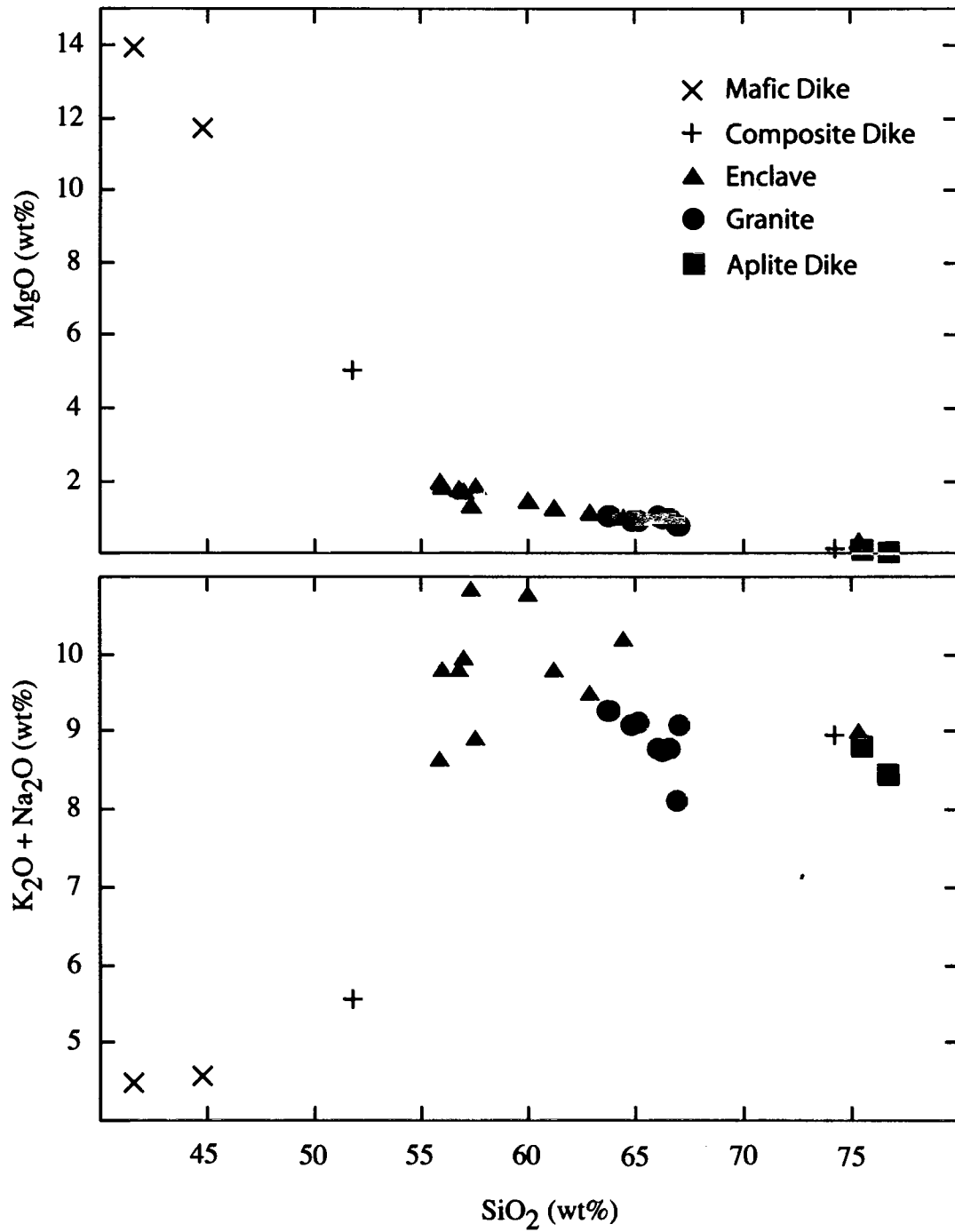
Figure 5.3: Harker diagrams for all whole rock chemical analysis samples.

wt. %, respectively. These dikes have similar concentrations of all major elements, with minor variation in trace element chemistry. The mafic dikes have high MgO (13.95, 11.70 wt. %) and low total alkali (2.13, 2.16 wt. %) concentrations in comparison to other samples (Figure 5.3). Although an age is not known for the mafic dike of Flye Point, the chemical similarity with the Brooklin dike suggests that both are of similar age (Jurassic) and origin. Therefore these samples are not included in later diagrams or discussions.

The mafic and felsic components of the composite dike have SiO_2 wt. % of 51.76 and 74.27, respectively. The mafic component is enriched in most major elements excluding SiO_2 and K_2O. The felsic component has enrichment of Y, Rb, K, Pb, and Th. The composite dike units have relatively similar concentrations of Na_2O, Ga, and Nb.

Enclave samples plot in three groups based on SiO_2 concentration. All enclave samples are fine-grained diorite enclaves except one felsic enclave. Six of the fine-grained enclaves have lower SiO_2 values ranging between 55.8 and 57.6 wt. %. These six samples have similar major element chemistry and Rb, Nb, V, Ga concentrations. They show the most variation for K_2O, Ba, and Cu. Four enclaves have slightly higher ("intermediate") SiO_2 concentrations ranging from 59.9 to 64.4 wt. %. These four are depleted in major elements and most minor elements when compared to the low SiO_2 enclaves. However, both groups have comparable concentrations of Rb, Ba, and Nb. The intermediate enclaves are slightly enriched in Zr when compared with the low SiO_2 enclaves. The single felsic enclave has a SiO_2 value of 75.31 wt. %. It is depleted in most major elements (excluding K_2O) and in several trace elements (Zn, Zr, Nb, Y, Ga, and Co) compared to the other enclaves. It shows enrichment in Rb and has comparable Cr, Cu and Pb concentrations to some enclaves.

Oak Point granite samples range from 63.63 to 67.00 wt. % SiO_2. All major elements decrease as SiO_2 increases. Most trace element concentrations decrease or remain relatively constant as SiO_2 increases, although Th and Rb increase as SiO_2 increases. The granite samples have minor overlap with two intermediate enclave samples.

The two aplite dike samples have SiO_2 values of 75.45 and 76.63 wt. %. Major element composition is similar in these samples. Concentrations of V, Co, and U show the least variation while the greatest trace element variation occurs in Th, Nb, Y, Rb, Sr, Cu, Ni, Ba, and Zr. The aplite dikes are chemically similar to the felsic component of the composite dike for major and some trace elements.

Harker diagrams reveal five distinct groups based on SiO_2: the mafic component of the composite dike (MCCD), the low SiO_2 enclaves, the intermediate SiO_2 enclaves, the granite samples, and the felsic group, consisting of the aplite dikes, the felsic enclave and the felsic component of the composite dike (FCCD). Harker diagrams for almost elements show a decrease in concentration with increasing SiO_2. Exceptions to this include the major element K_2O and minor elements Pb, Rb, Th and U.

Major element Harker diagrams are shown in Figures 5.4, 5.5, and 5.6. Excluding K_2O, major elements decrease with increasing SiO_2. There is a strong correlation for all major elements on Harker diagrams except for K_2O. Correlation coefficients commonly exceed 0.9 (Table 5.1). The MCCD plots relatively close to the line for P_2O_5, Fe_2O_3, MnO and TiO_2. It is depleted with respects to the line for Al_2O_3, Na_2O and K_2O, but shows strong enrichment for Fe_2O_3, CaO and MgO. Bivariant plots for Na_2O and K_2O show the most scatter.
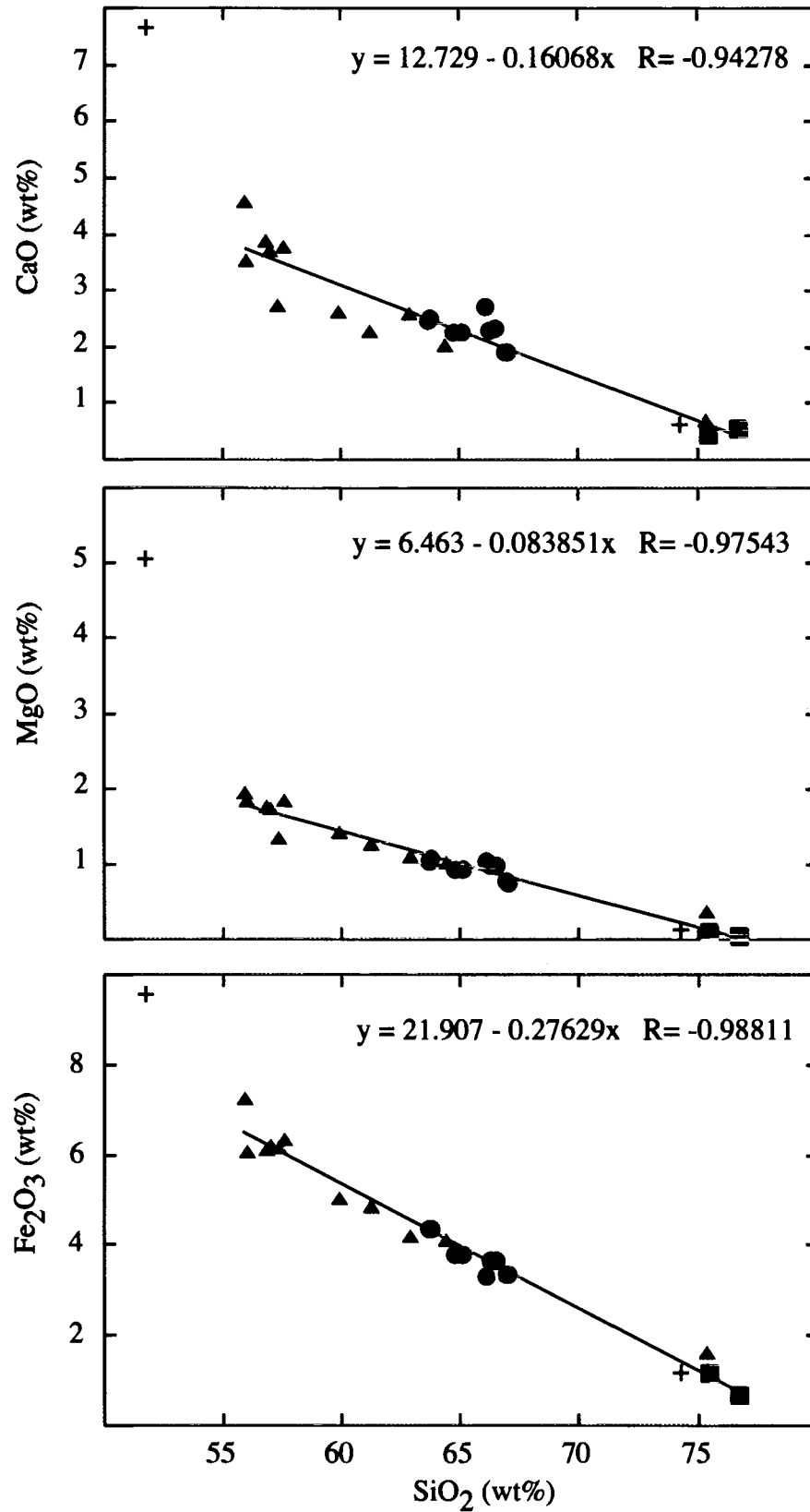
Figure 5.4: Harker diagrams of CaO, MgO and Fe_2O_3.
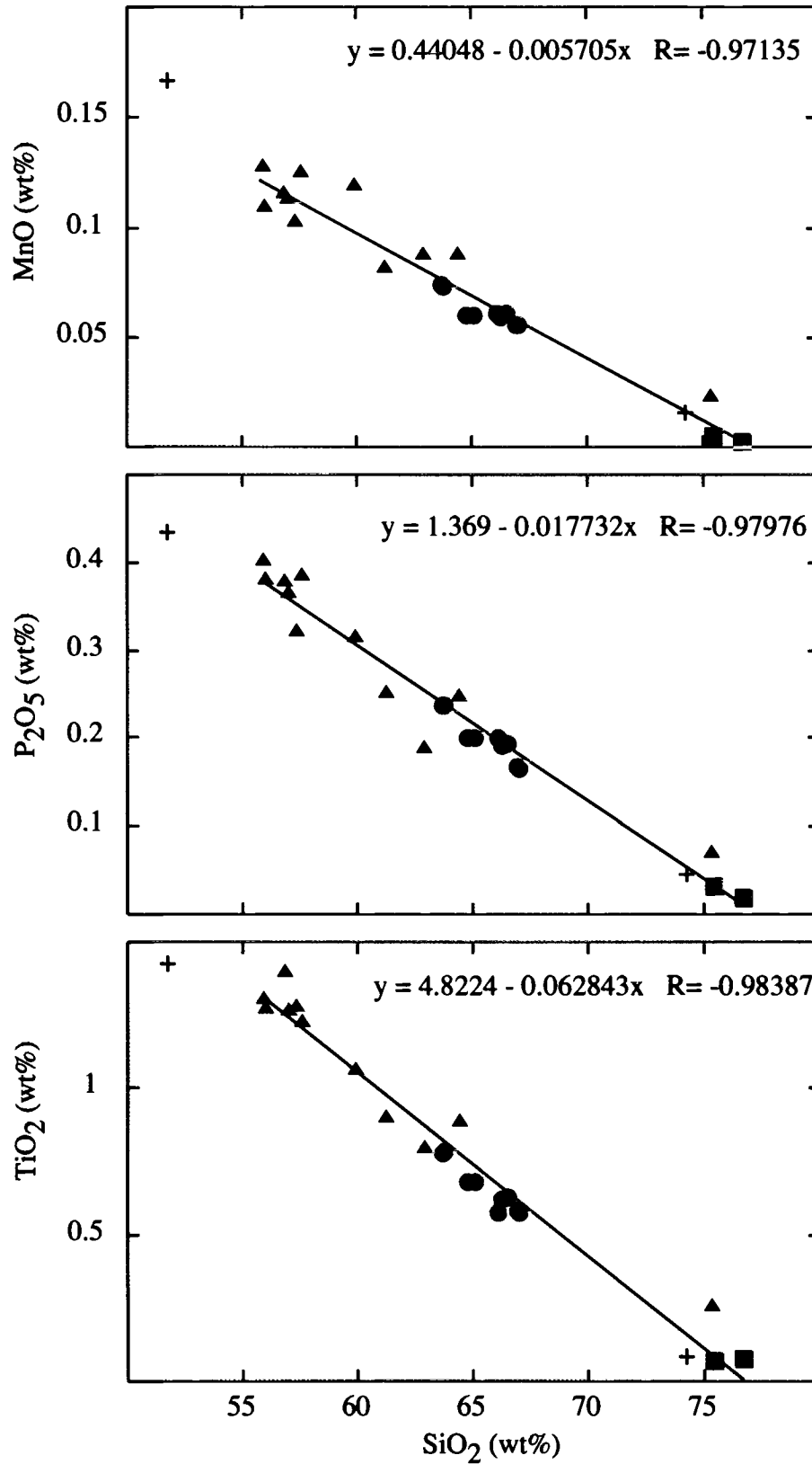
Figure 5.5: Harker diagrams of MnO, P_2O_5 and TiO_2.
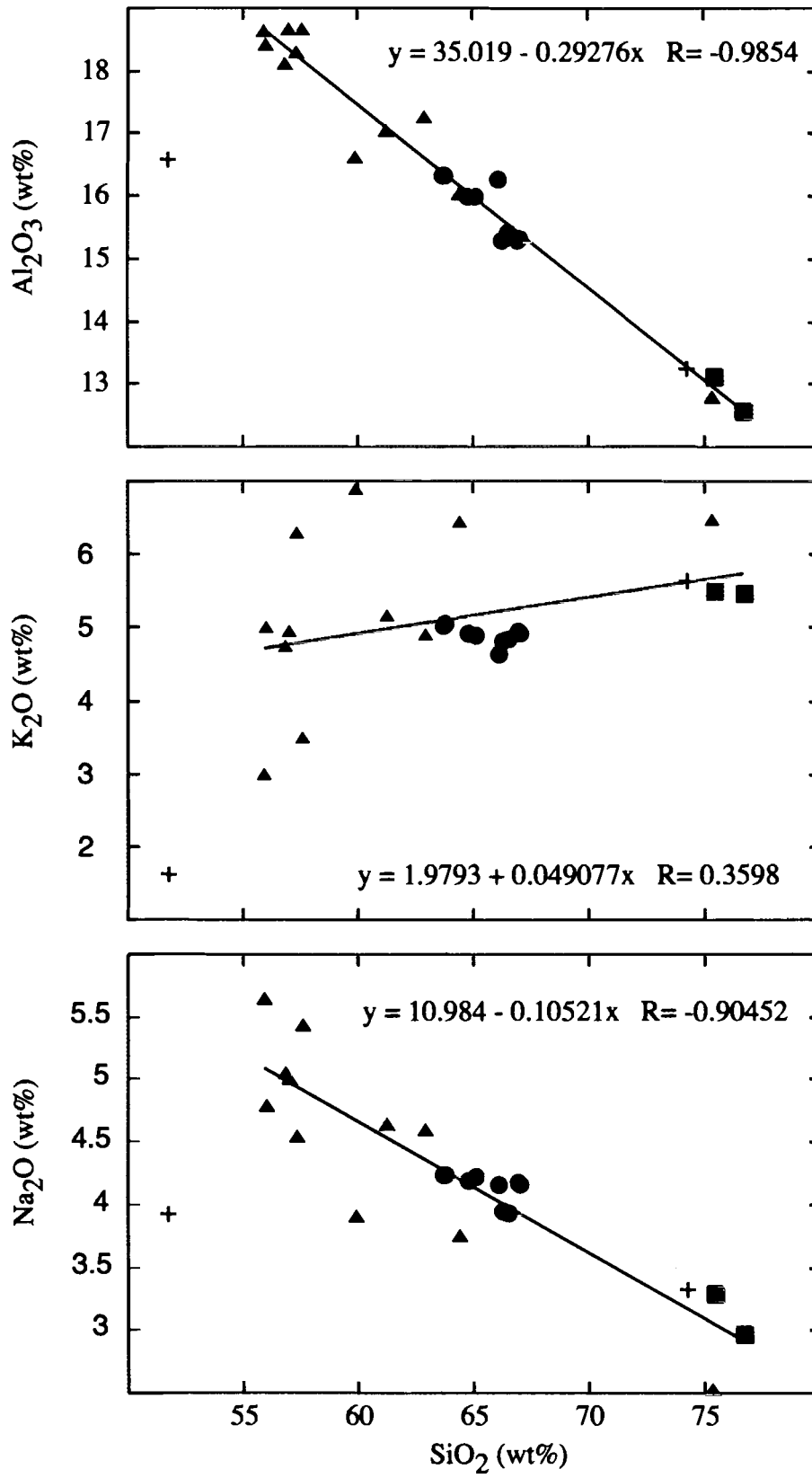
Figure 5.6: Harker diagrams of Al_2O_3, K_2O and Na_2O.

74

	TiO_2	Al_2O_3	Fe_2O_3	MnO	MgO	CaO	Na_2O	K_2O	P_2O_5
Al_2O_3	0.961								
Fe_2O_3	0.984	0.974							
MnO	0.975	0.951	0.970						
MgO	0.969	0.964	0.978	0.970					
CaO	0.925	0.947	0.954	0.926	0.975				
Na_2O	0.858	0.935	0.909	0.854	0.900	0.932			
K_2O	-0.291	-0.432	-0.407	-0.305	-0.447	-0.583	-0.687		
P_2O_5	0.985	0.957	0.985	0.954	0.988	0.953	0.877	-0.371	
SiO_2	-.0984	-0.985	-0.988	-0.971	-0.975	-0.943	-0.904	0.360	-0.980

Table 5.1: Inter-element correlation coefficients (R) for major elements.

With the exception of U, Th, Pb and Rb, all trace elements show a general decrease with increasing SiO_2 (Figures 5.7, 5.8, 5.9, 5.10, 5.11 and 5.12). Some trace element trends show strong (R > 0.90) correlations (i.e. Zn, V, Zr), although several others have moderate (R > 0.77) correlations (i.e. Nd, Nb, Ga, Sr, Co, La). Poor correlations exist for the minor elements Cr, Cu, Ni, Rb, Ba, and Y. The concentrations of Ni, Cr, and Cu show the least variation among the samples. Trace elements U, Th, Pb and Rb show increases for increasing SiO_2.
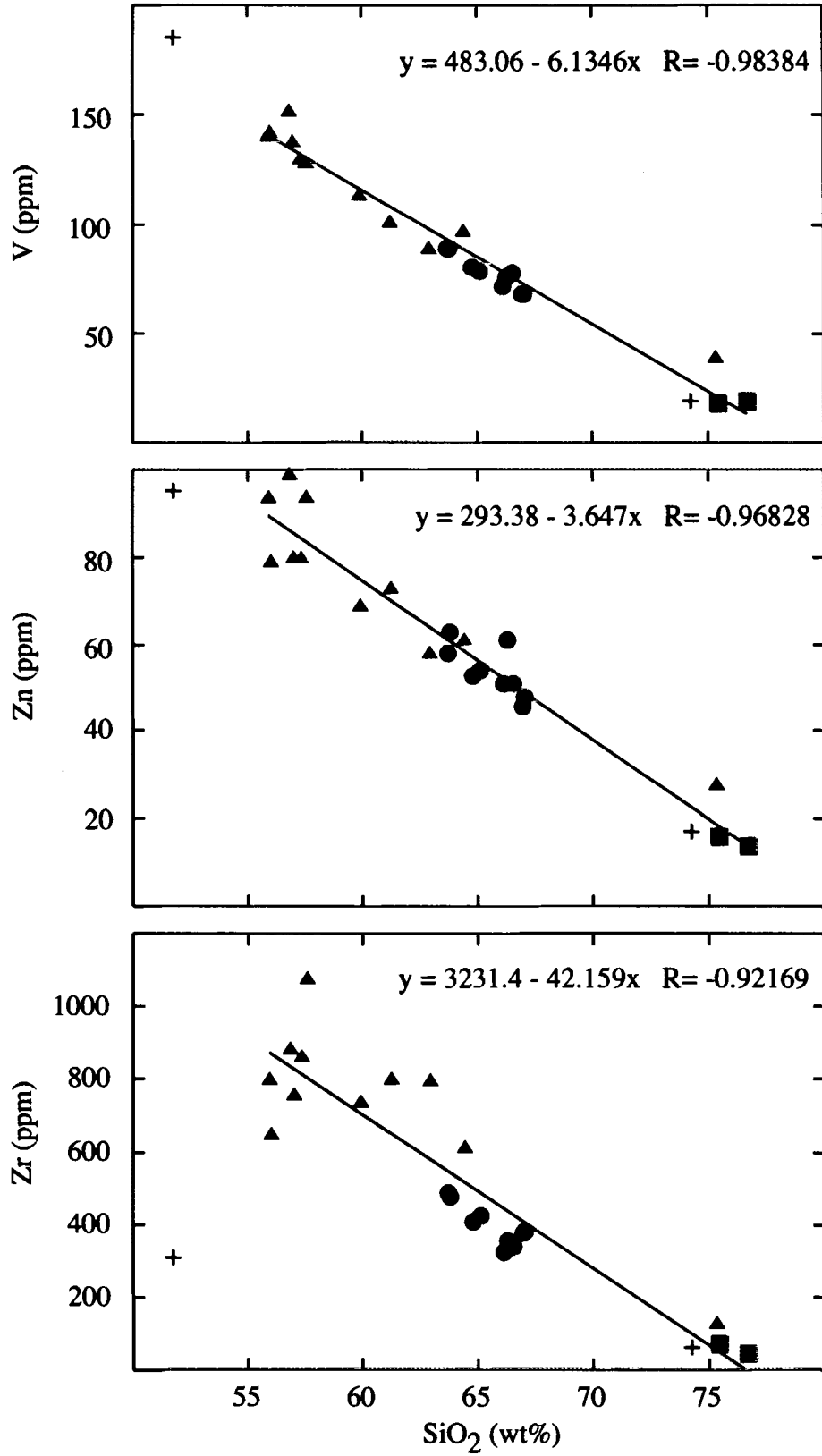
Figure 5.7: Harker diagrams of V, Zn and Zr.

76

$$y = 40.936 - 0.49536x \quad R = -0.88835$$

$$y = 44.378 - 0.37053x \quad R = -0.88367$$

$$y = 95.866 - 1.1068x \quad R = -0.83785$$
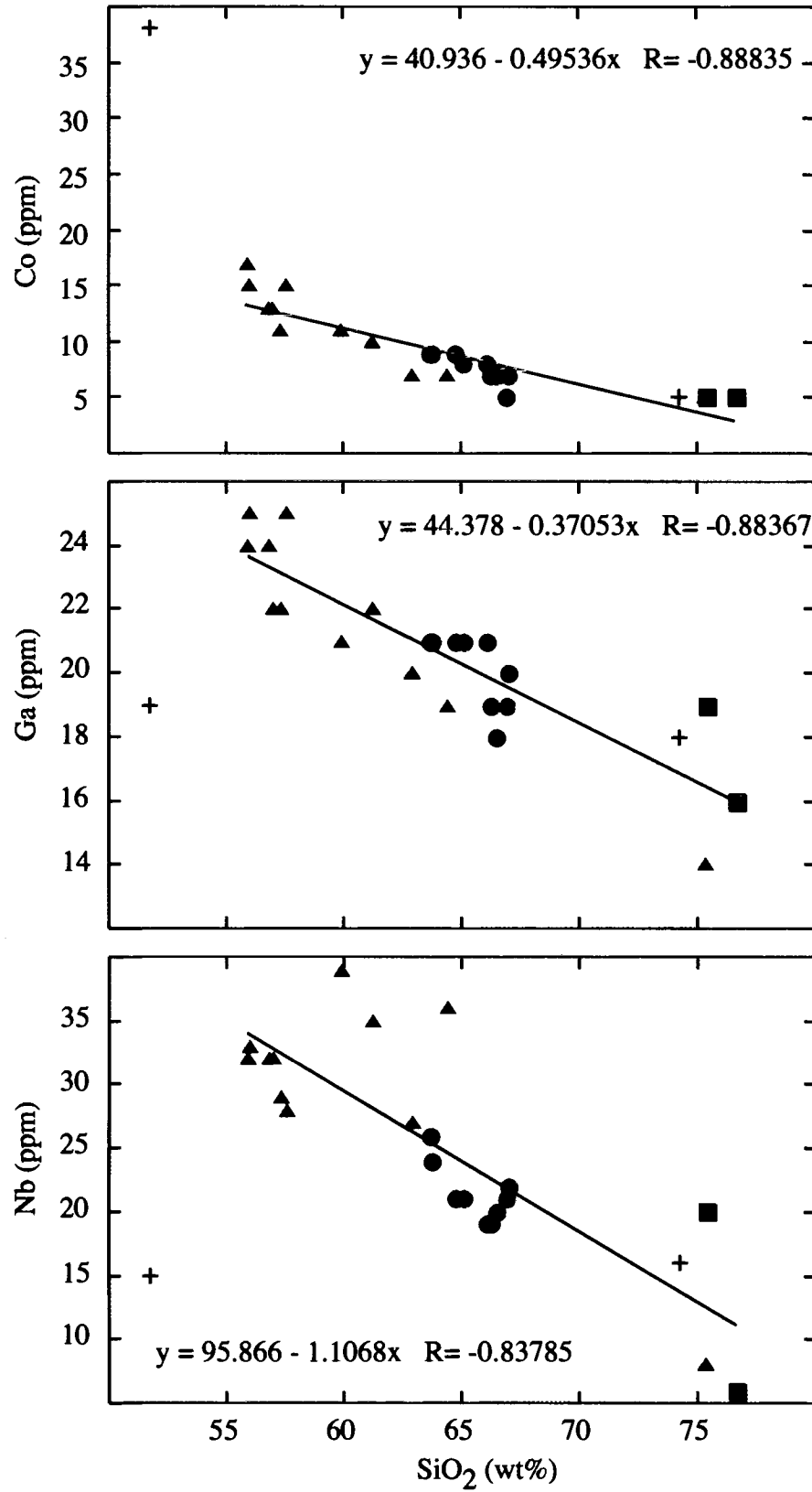
Figure 5.8: Harker diagrams for Co, Ga, and Nb.
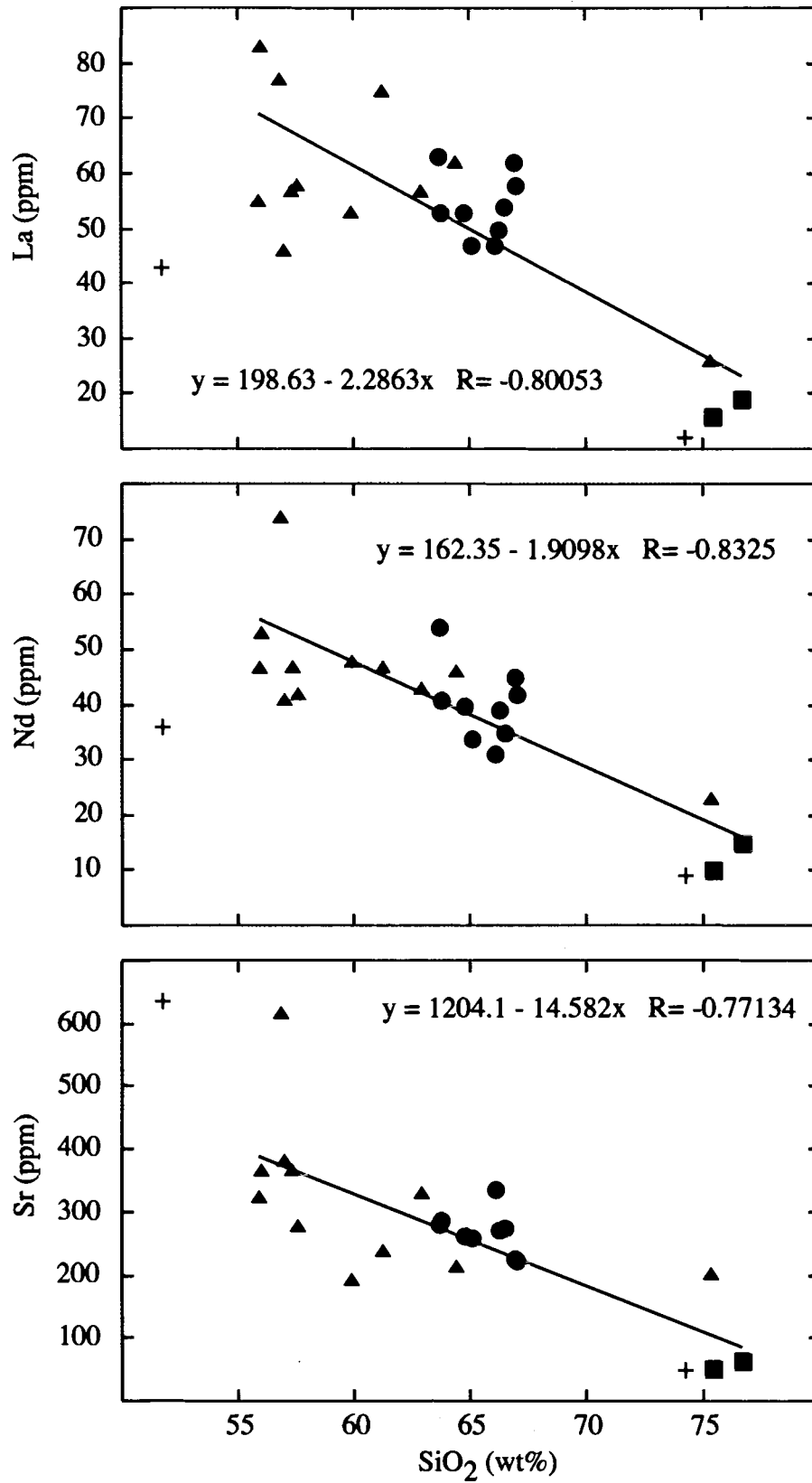
Figure 5.9: Harker diagrams of La, Nd, and Sr.
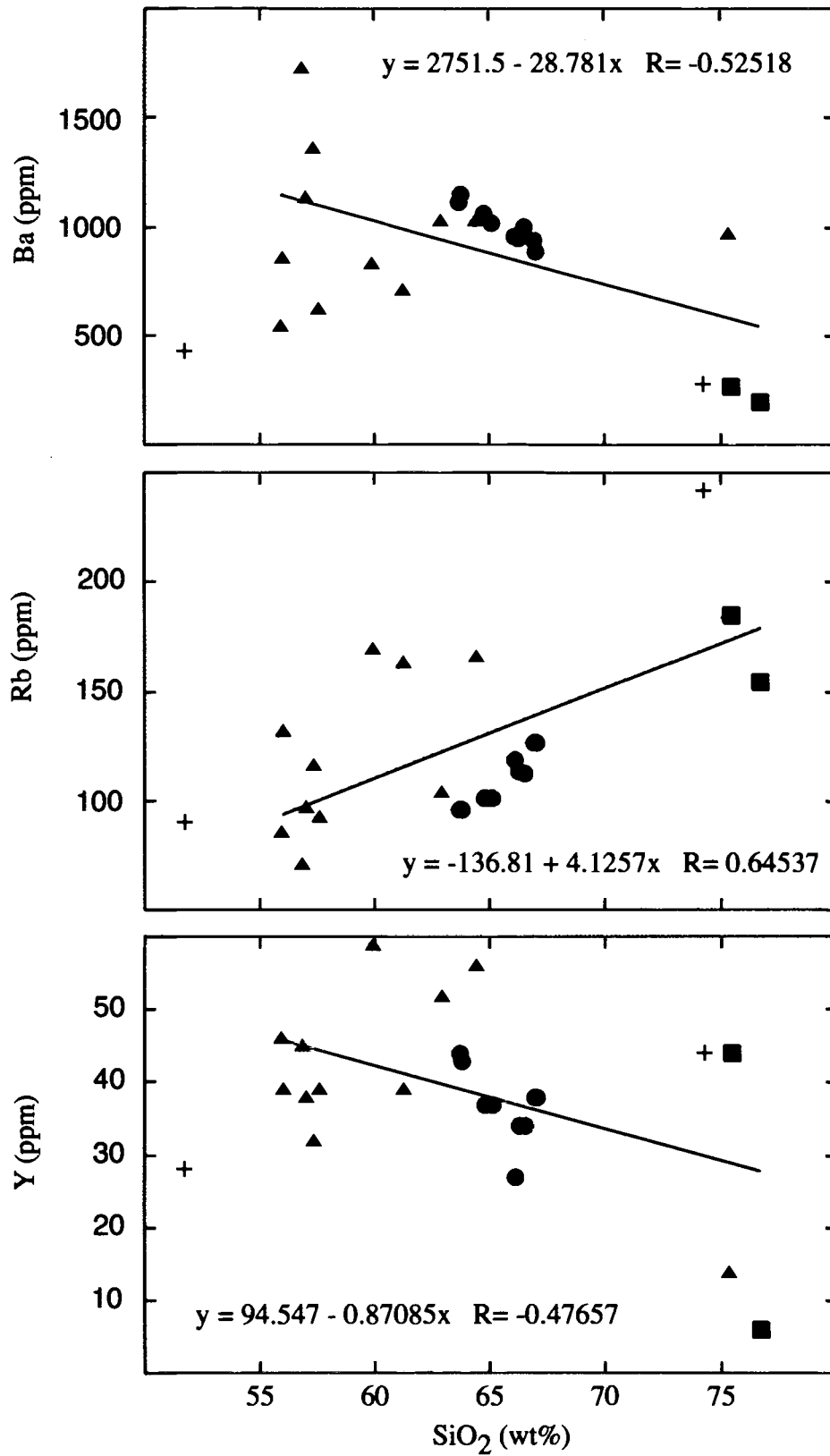
Figure 5.10: Harker diagrams of Ba, Rb, and Y
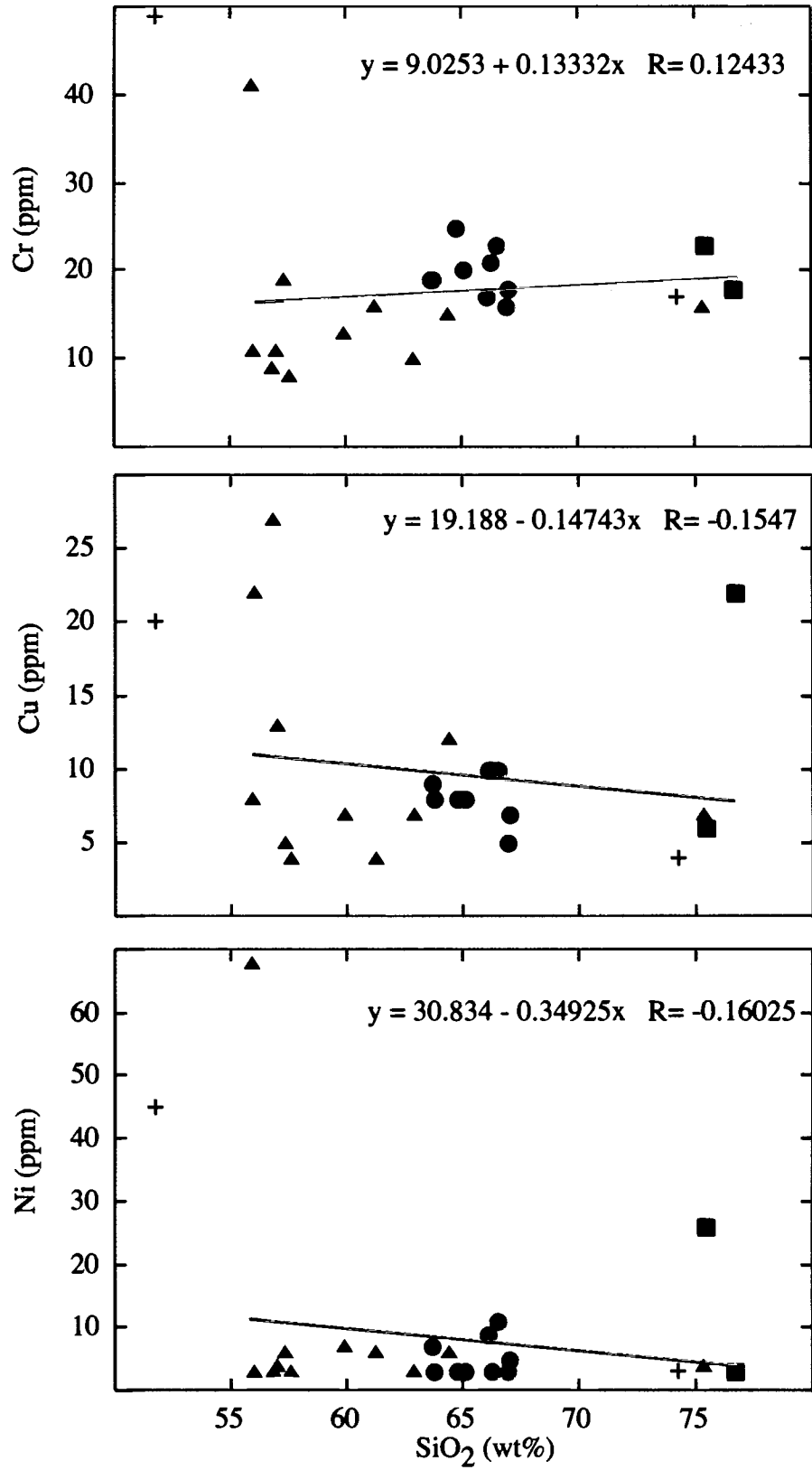
Figure 5.11: Harker diagrams of Cr, Cu and Ni.
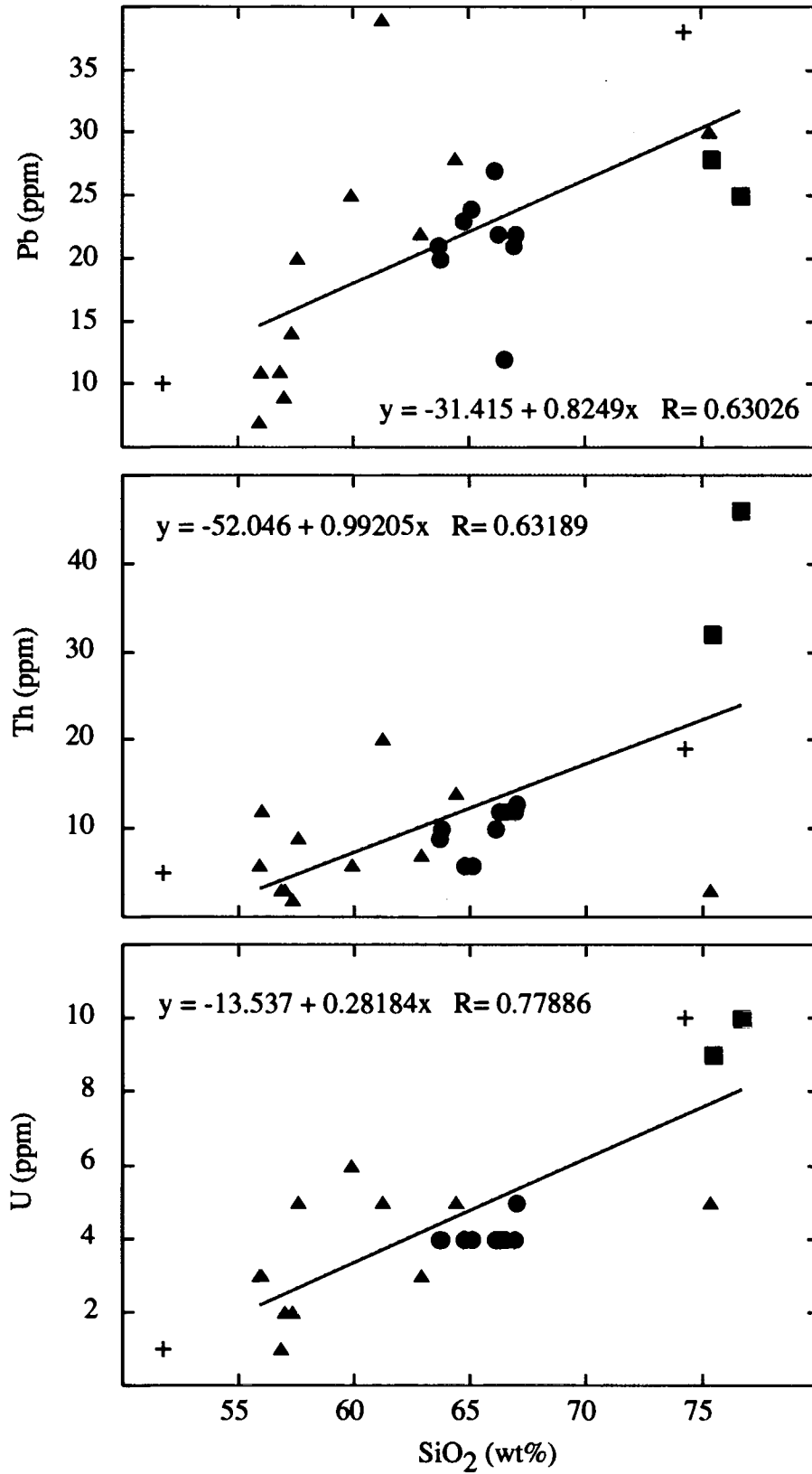
Figure 5.12: Harker diagrams of Pb, Th, and U.

The three plots (top to bottom) show:

Pb plot: $y = -31.415 + 0.8249x$ R= 0.63026

Th plot: $y = -52.046 + 0.99205x$ R= 0.63189

U plot: $y = -13.537 + 0.28184x$ R= 0.77886

X-axis: SiO_2 (wt%)

5.3. Electron Microprobe

Microprobe results are shown in Appendix A (Tables A.4, A.5, A.6 and A.7). Three fine-grained diorite enclaves, one felsic enclave and two granite samples were analyzed.

Plagioclase in both enclave types contained normal and reversed zoned grains (Table 5.2). Plagioclase core compositions in the fine-grained enclaves range in An content from 18.3 to 29.3 with an average of 24.3. Rims vary from 18.1 to 24.6 with an average of 21.4 An. The greatest An content change in a normal zoned plagioclase was 11.4, and the greatest change for a reversed zoned plagioclase was 4.0.

The felsic enclave (SNS-7) has plagioclase cores ranging from 0.5 to 25.7, with an average of 19.9. The rim compositions range from 18.2 to 26.8 with an average of 23.1. The greatest change in An content for a normal zoned plagioclase is 5.5 and the greatest for a reversed zoned plagioclase is 3.7.

Only one plagioclase grain from a granite sample contained a reversed zoned plagioclase (Sample GRNLW-Pl1). The anorthite contents for plagioclase cores ranged from 17.5 to 24.3 % with an average of 21.5. The rims ranged from 14.6 to 21.5 with an average of 18.2. The greatest anorthite change in a normal zoned plagioclase was greatest at 6.6, with the least variation of 1.2. The plagioclase grain that showed reverse zoning had a change of 1.1 %.

Hornblende chemistry shows an overlap among granite and enclave samples (Figure 5.13). Most compositions plot into the edenite field (Deer, Howie and Zussman, 1992). Biotite chemistry in both enclave and granite samples is also

Enclave	Core	Rim	Change
SNCC1-Pl4	20.4	21.2	-0.8
SNCC1-Pl5	30.0	24.6	5.4
SNCC1-Pl6	22.5	23.1	-0.6
SNCC1-Pl7	18.3	22.3	-4.0
NKG3-Pl1	29.5	18.1	11.4
NKG3-Pl2	23.0	20.5	2.5
NKG3-Pl3	25.5	19.2	6.3
NKG3-Pl4	26.5	21.5	5.0
NKPT1-Pl2	23.1	21.9	1.2
SNS7-Pl13	23.1	26.8	-3.7
SNS7-Pl14	23.8	18.2	5.5
SNS7-Pl15	26.3	22.3	4.0
SNS7-Pl16	25.7	25.2	0.4
Granite			
FLYPT-Pl1	21.3	14.6	6.6
FLYPT-Pl2	17.5	14.7	2.8
FLYPT-Pl3	21.1	16.8	4.4
FLYPT-Pl4	22.6	21.4	1.2
GRNLW-Pl1	20.2	21.5	-1.3
GRNLW-Pl2	23.4	18.8	4.6
GRNLW-Pl4	24.3	19.9	4.4

Table 5.2: An content of plagioclase grains from enclave and granite samples. A negative change indicates reversed zoning.
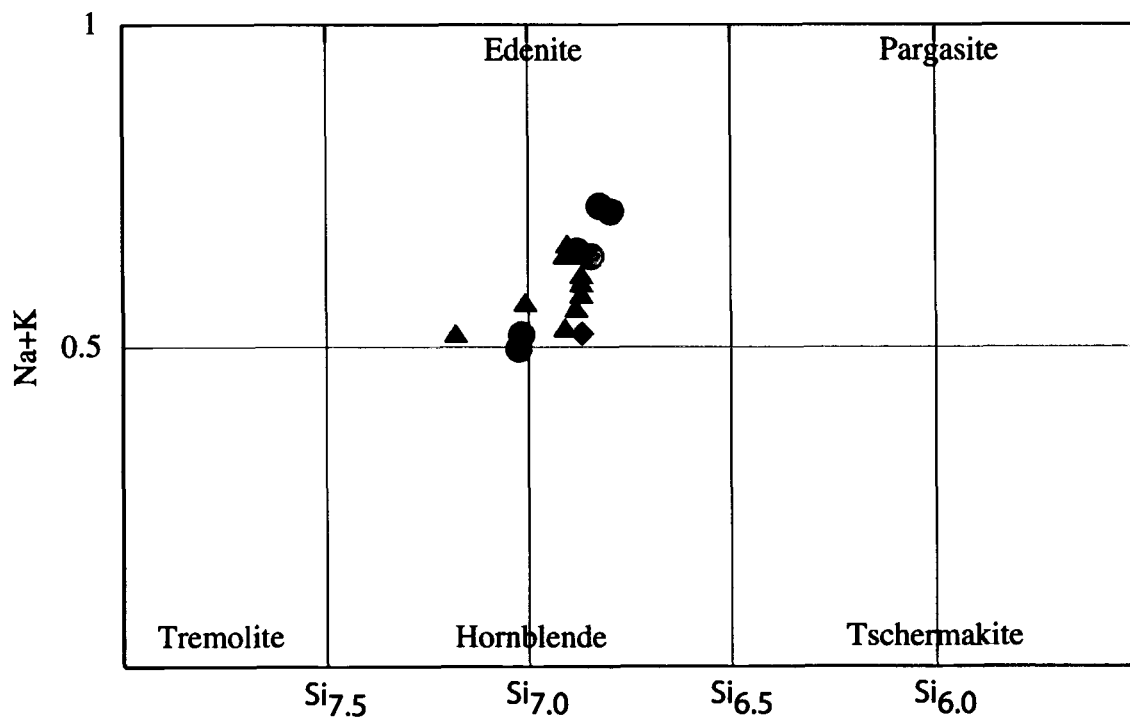
Figure 5.13: Chemical variation diagram for hornblende grains (after Deer, Howie and Zussman, 1992). Green triangles are from enclave samples and blue circles are from granite samples. The red diamond is a suspect clinopyroxene core.

similar among grains (Figure 5.14). Relative proportions of MgO and FeO are nearly equal in each biotite grain, although the biotite grains from the felsic enclave are slightly more magnesium enriched with respects to the fine-grained enclaves, which have a slight enrichment of FeO.

Of the two pyroxene samples analyzed, one was an independent grain (NKPT1 px3), whereas the other one was a core in a hornblende grain (NKPT1 px1). Both have similar chemistry (Figure 5.14). One suspect pyroxene grain analyzed produced a hornblende composition (Figure 5.13).
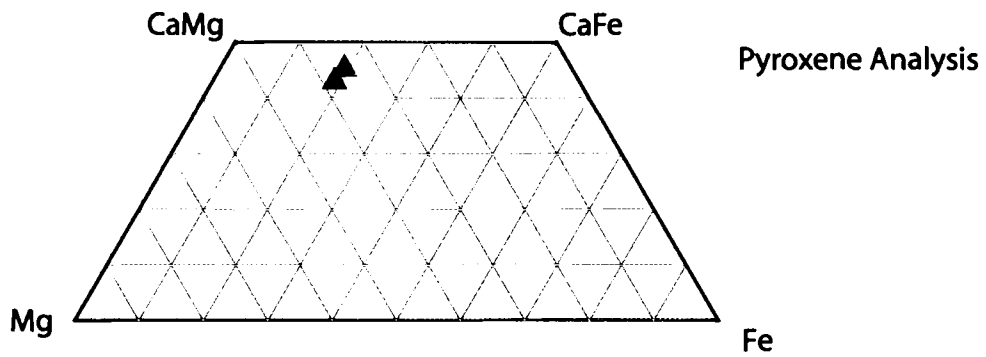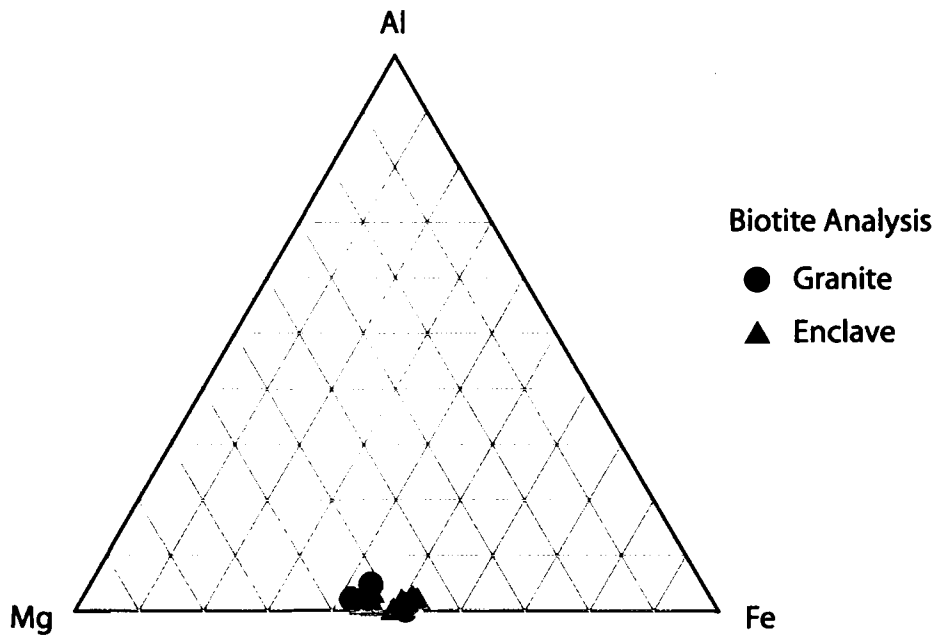
Figure 5.14: Ternary diagrams for biotite and pyroxene microprobe analysis. Top figure shows biotite chemistry results. Bottom figure shows pyroxene results.

Chapter 6

INTERPRETATIONS

6.1. Structural

The foliation of magmatic enclaves and that defined by alkali feldspar in the Oak Point Granite are similar (Figure 5.1). This relationship could reflect either settling of the enclaves and feldspars (i.e. cumulates) or alignment due to magmatic flow. Wiebe and Collins (1998) report parallel attitudes among MASLI gabbroic layers, tabular feldspars and associated magmatic enclaves. They interpreted this to reflect settling of materials to a semi-rigid floor. Feldspar cumulates are common in leucocratic layers of MASLI plutons (Wiebe, 1993, Wiebe et al., 2000). If the feldspar foliation in the Oak Point Granite is a result of crystal settling, then it is possible that enclave orientations are the result of similar cumulate processes. Compaction of the enclave would result in foliation of elongated minerals in the enclaves, as well as the relatively planar shape of most enclaves.

An alternative hypothesis to explain the agreement between enclave and feldspar foliation orientations is magmatic flow. In Sierra Nevada granitoids, the long axis and mineral foliation in enclaves are parallel to the magmatic fabrics of the host granite (Barbarin, 1991; Fernandez and Barbarin, 1991). Vernon (2000) and Paterson et al. (1989) list the alignment of elongated minerals in the enclaves as micro-structural evidence for identifying magmatic flow. They report that a relatively high percentage of melt with in the enclave must be present, permitting rotation the crystals without undergoing deformation (Vernon, 1984; Paterson et al., 1989). The wide distribution of

87

the enclaves throughout the Oak Point granite is also evidence that a flow regime (or possibly convection currents) were present in the magma chamber during petrogenesis (Wiebe, 1994).

Some enclaves from the OPG have a foliation of elongated minerals and acicular apatite. This suggests that the enclave was at least semi liquid during alignment, prior to complete quenching. If magmatic flow was the mechanism for the mineral foliation in the enclaves and their similar orientation, it must have occurred during magmatic conditions, due to the lack of mineral deformation in the enclaves (Vernon, 1984). Because feldspar foliation was not consistently present, nor clearly defined, magmatic flow was likely to be at low to moderate rates, and not continuous.

6.2. Magmatic Enclaves

Two hypotheses exist for the origin for magmatic enclaves. One is they are re-melted xenoliths, and the other is that they are from a contemporaneous magma (Vernon, 1984; Didier and Barbarin, 1991; Wiebe et al., 1997). The enclaves in the OPG show similar features, such as textures and feldspar inclusions that support a magmatic origin.

The irregular contacts between the enclaves and the host granite support a magmatic origin. Irregular contacts are indicative of mingling of two fluids of contrasting properties (Wiebe, 1991). If the enclaves originated as solid fragments of country rock, i.e. xenoliths, some original angularity should have been preserved (Vernon, 1984).

Elongated grain shapes, fine-grained textures and acicular apatite are microstructures associated with rapid cooling and quenching of magma (Fernandez and Barbarin, 1991; Vernon, 1991). The dioritic composition indicates that the enclave melt

88

had a higher temperature than the granitic host. Once in contact with the host magma, the dioritic melt is chilled to the host magma temperature (Vernon, 1990), producing fine-grained textures. Acicular apatite in the enclaves is also a characteristic of magma quenching (Wyllie et al., 1962; Vernon, 1984). Furthermore, the preferred orientation of elongated grains also supports a magmatic origin. A high percentage of melt must have been present to permit rotation of crystals without experiencing deformation (Vernon, 1984).

A hypothesis to explain the origin of the rapakivi feldspar inclusions in many enclaves is that they are the product of metasomatism caused by the granitic melt, and that they grew in the enclave (Vernon, 1991). However, because the feldspar inclusions do not contain inclusions of the enclave minerals near the crystal core, the feldspars must have nucleated and grew either earlier than minerals in the enclave or grew in another environment. Enclave mineral inclusions are limited to the outer portions of the rapakivi rims, suggesting that some growth of the feldspar megacrysts did occur in the enclave (Vernon, 1991).

The common occurrence of rapakivi feldspar inclusions in many enclaves supports a liquid origin (Vernon, 1991). These feldspars have textures, sizes and color similar to those in the host rock. The transfer of the feldspars from the granitic melt must have occurred prior to quenching of the enclave. Because other solid components of the granite are not present in the enclave, it is conceivable that the only solids in the granitic magma were the alkali feldspar crystals.

Many studies of plutonic (Barbarin, 1988; Wiebe et al., 1997) and volcanic (Gourgaud, 1991; Koyaguchi, 1991) systems conclude that enclaves are the product of

magmas derived from hybridization processes between two distinct magmas. Petrographic and chemical data for enclaves and associated rocks from the Oak Point Granite suggests that these enclaves were produced by hybridization. Petrographic evidence includes the presence of clinopyroxene, feldspar inclusions and chemical variation in plagioclase (Vernon, 1990; Gourgaud, 1991).

The rapakivi feldspar inclusions common in enclaves are a significant line of evidence indicating mixing between two magmas (Vernon, 1990). These feldspar grains are similar in texture, size and color as the host granite. As previously discussed, these grains must have been mixed into the enclave magma prior to quenching. If the feldspar inclusions were able to transfer, it is plausible that some melt and chemical constituents from the host was also transferred during the mixing process.

The large size, rounded shapes and lack of inclusions of enclave minerals suggest the feldspar inclusions grew in the host granitic magma prior to mixing event. The rims of these rapakivi feldspar inclusions consist of several plagioclase grains with different crystallization histories. Similar structures are present in the large rapakivi feldspar grains within the host granite. This suggests that the rims formed prior to the mixing event as well. The occurrence of some enclave mineral inclusions in the outer portions of the feldspar megacryst rims, indicate that some growth did occur in the enclave magma (Vernon, 1990).

Some enclave samples have individual clinopyroxene grains, and many hornblende crystals have suspect or relic clinopyroxene cores. The presence of clinopyroxene indicates that an anhydrous, more mafic magma was involved in the mixing process (Orsini et al., 1991). These clinopyroxene grains nucleated and grew prior

to the mixing event. During mixing, exchange of K_2O and H_2O from the granitic magma promoted the nucleation and growth of hornblende and biotite (Foster and Hyndman, 1990). The clinopyroxene cores in the hornblende indicate that the hybridization process was not complete.

Plagioclase grains can be used to evaluate hybridization processes. For example, the presence of both normal and reversed zoning in plagioclase support dynamic processes and temperature fluctuation (Gourgaud, 1991). In one enclave sample, microprobe analysis of adjacent plagioclase grains showed normal and reversed zoning. Furthermore, rapakivi textures and plagioclase cores within alkali feldspars are textures reflecting mixing processes (Hibbard, 1991). Many enclaves contained both of these feldspar textures. Both plagioclase and alkali feldspar cores must have existed prior to the overgrowths, however it is unlikely that both nucleated within the same magma under the same conditions. These relations indicate mechanical exchange between the host granite and the enclave magma.

6.3. Composite Dike Interpretations

Petrographic and field evidence indicates that the mafic and felsic components of the composite dikes were contemporaneous magmas. The round pillows, diapiric type structures and irregular contacts indicate that the mafic component was liquid at the time of emplacement in the felsic host (Vogel and Wilband, 1978; Snyder et al., 1997). The slight decrease in crystal size and the presence of apatite needles near the contact indicate quenching of the mafic magma against the felsic unit (Wiebe, 1973; Vernon, 1984). Evidence for exchange between the two magmas includes hornblende-armored quartz

grains, rounded quartz and plagioclase grains, and ovoid inclusions of the mafic component within the felsic unit. Biotite enrichment at the contact of the mafic component reflects dehydration and K_2O transfer from the felsic magma.

The composite dike most likely originated as a felsic dike, similar as the numerous aplite dikes in the Oak Point granite. Slight wavy forms, some minor bends in the strike and cross cutting of enclaves and feldspar foliation suggest that the aplite dikes are late possible felsic replenishments, presumably filling fractures formed as the granite host cooled (Fernandez and Barbarin, 1991). Mafic magma subsequently either intruded along same fracture or flowed into the dike (Snyder et al., 1997). The pillow structures form due to viscosity contrast of the mafic magma in the felsic host (Snyder et al., 1997). The rounded grain shapes and complex zoning patterns in the blue gray unit suggest that it is a product of hybridization between the other two components (Taylor et al., 1980).

6.4. Magma Mixing and the Mafic End Member

Strong linear geochemical trends on bivariant major element plots suggest magma mixing (Foster and Hyndman, 1990; Tindle, 1991; D'Lemos, 1996). Although the data shows high correlations, the coefficients are not perfect. Variability in the linear trends may result from inhomegenetity of the mixing end members, loss and/or gain of components, mobility of elements, and fractionation during mixing (D'Lemos, 1996). The samples of this study show linear relationships on Harker diagrams for most major elements and some trace elements. More importantly, the major elements show strong coefficients for all inter-element correlations, except for K_2O (Table 5.1). These strong

92

linear relationships provide evidence for mixing as a significant process during in the formation of the Oak Point Granite (D'Lemos, 1996).

In fractionation processes, $MgO/(MgO+Fe_2O_3)$ concentrations should produce exponential trends with increasing SiO_2. Similarly, the ratio of $CaO/(CaO+Na_2O)$ will also have the same curve in response to fractionation. However, for both of these ratios, linear regressions are produced for increasing SiO_2 (Figure 6.1). Although the correlation coefficient for $MgO/(MgO+Fe_2O_3)$ is not as strong as other inter-element correlations (Table 5.1), these diagrams clear do not reflect fractionation processes.

In several diagrams, the MCCD plots near the line defined by all other samples, however in other diagrams it plots either above (i.e. MgO, CaO) or below (i.e. Al_2O_3) the line. Most correlation coefficients increase when the MCCD is disregarded. This relationship suggests that the MCCD is not the mafic end member and is not directly related to the mixing process.

In studies of MASLI type plutons, mafic dikes and mafic components in composite dikes have compositions similar to gabbroic layers (Wiebe, 1993; Wiebe et al., 1997). In the Pleasant Bay Pluton, the basaltic dikes, chilled mafic layers and gabbroic layers have similar compatible and incompatible element concentrations suggesting that they originated from similar mafic magmas. However, more primitive incompatible compositions of the basaltic dikes infer that these dikes best represent the parental mafic magmas that intruded the active chamber (Wiebe, 1993). In addition, mafic dike compositions in the Cadillac Mountain pluton are more primitive compositions than the most mafic cumulate layers (Wiebe et al., 1997). In the Gouldsboro granite, the basaltic dikes are similar in composition to the mafic units in composite dikes as well as the
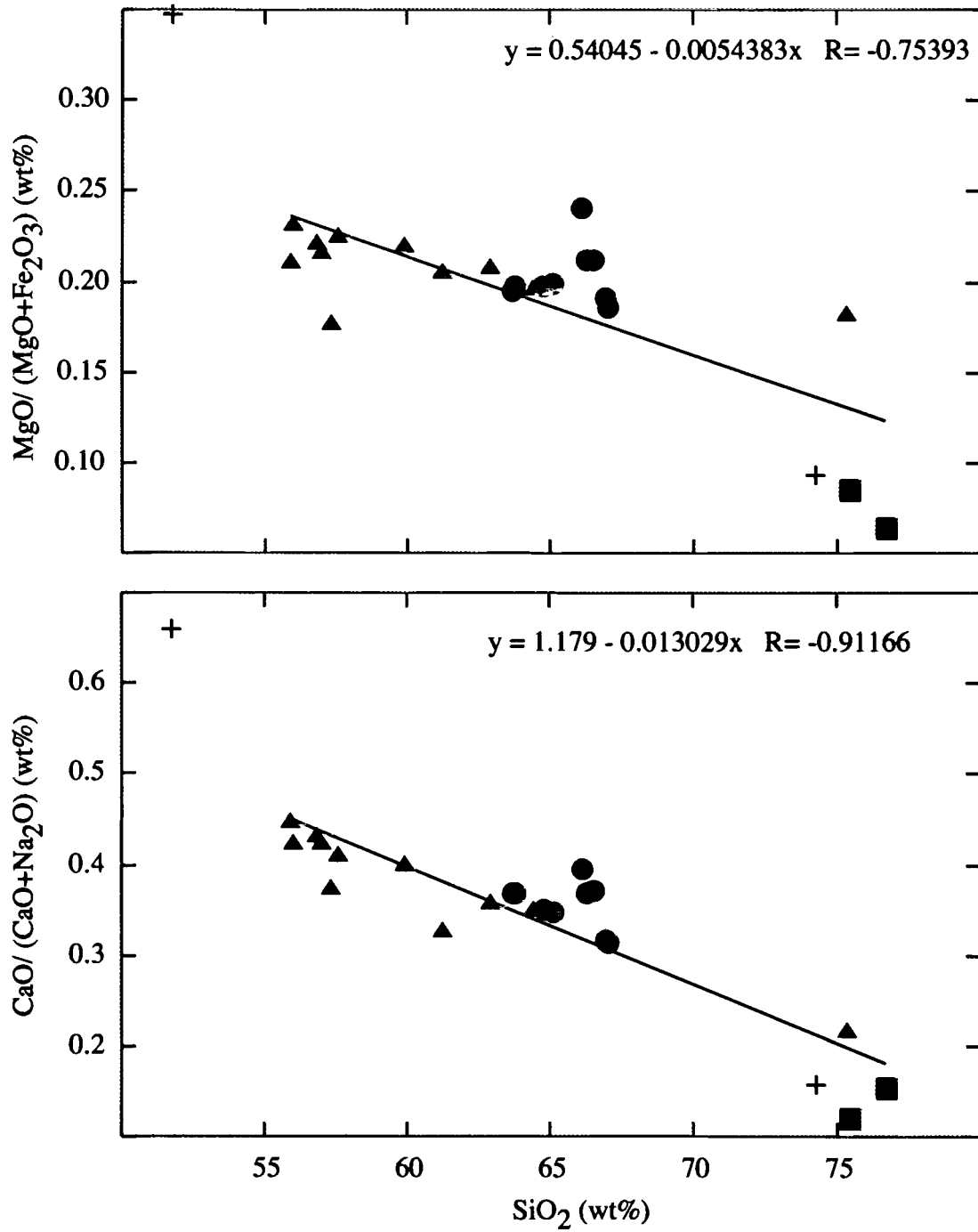
Figure 6.1: Harker diagrams for $MgO/(MgO+Fe_2O_3)$ and $CaO/(CaO+Na_2O)$.

gabbroic rocks are similar suggesting all have the same source (Wiebe and Ulrich, 1997). These studies conclude that the mafic dikes represent feeders into the granitic pluton, and they are the mechanism for emplacement of the gabbroic layers (Wiebe, 1993; Wiebe and Ulrich, 1997; Wiebe et al., 1997). By analogy to these studies, the MCCD represents a best estimate of the composition of a parental mafic magma injection in the OPG pluton.

If the MCCD represents a mafic injection into the OPG, a significant viscosity contrast with the felsic end member would inhibit immediate mixing between the two magmas (Huppert et al., 1984; Fernadez and Barbarin, 1991). More dense mafic magma would pond at the base of the chamber (Campbell and Turner, 1985; Wiebe, 1996). Subsequently fractional crystallization of this mafic magma would produce a less dense, more viscous residual magma. Once the residual magma reached a viscosity similar to that of the felsic end member, mixing between the residual and the felsic end member could occur (Huppert et al., 1984), producing a hybrid magma that is most likely the source of the enclaves. The MCCD does not plot on the mixing lines and can not be the mafic end member. However, the data suggests that it has fractionated to an evolved magma, which became the mafic end member.

Chemical relationships between the enclaves and the MCCD support this hypothesis. The enrichment of the MCCD in most majors and compatible trace elements reflect a more primitive composition and early crystallizing phases. Furthermore high incompatible element concentrations support that the enclaves had derived from a residual magma. Orsini et al. (1991) reached a similar conclusion for the origin of enclaves from a granitoid in northern Sardinia.

Fractional crystallization of olivine, plagioclase and augite effectively removes MgO and CaO from a mafic magma. Compatible elements, such as Cr, Ni, and Co, are strongly partitioned into ferromagnesium minerals and will also be rapidly depleted (Mason and Moore, 1966; Cox et al., 1979; Philpotts, 1991). Fractionation of these minerals will produce a residual magma depleted in these elements. Fractionation of olivine and pyroxene in a parental mafic magma explains the significant difference in compatible trace elements between the MCCD and the enclaves.

The slight enrichment of Fe_2O_3 and MnO concentrations in the MCCD can also be explained by fractional crystallization. Magnesium ions are preferred in early, high temperature ferromagnesian minerals over iron ions. The less drastic difference between iron concentrations in the MCCD and the enclaves as compared to Mg concentrations, suggests that the residual magma separated from the parental magma near temperatures that favor the precipitation of Fe-bearing minerals. Because Mn^{+2} is able to substitute for Fe^{+2} in many iron-bearing minerals (Mason and Moore, 1966), Mn concentrations mimic the processes for Fe.

The MCCD concentrations of TiO_2, P_2O_5, are slightly depleted whereas Al_2O_3 is more significantly depleted with respect to the mixing trend line. Al_2O_3 is preferred in plagioclase, where as P_2O_5 and TiO_2 are favored in the minerals apatite and ilmenite, respectively (Mason and Moore, 1966). The relatively low concentration of these elements in the MCCD suggests that minerals in which these elements are favored had not nucleated at the time the residual magma separated from the parental magma.

The enclaves are enriched in Na_2O and K_2O with respect to the MCCD. These elements are not preferred in early crystallizing mafic minerals, thus fractionation would

produce enrichment of these elements in a residual magma. Sodium shows good linear relationships with the other samples, further supporting the mixing process.

A residual magma produced by fractional crystallization will have high concentrations of incompatible elements. The concentrations of the incompatible elements, such as Ga, Zr, Nb, Y, Nd, Ba and La, are depleted in the MCCD with respects to the enclaves. Also, some of these elements show linear trends for bivariant plots. These relations indicate that the enclaves originated from a hybrid magma, produced from the mixing of a fractionated mafic end member (i.e. MCCD) and a felsic host end member.

6.5. The Felsic End Member

The bivariant diagrams show linear relations, indicating that mixing processes occurred during the formation of the Oak Point Granite. As discussed above, the composition of the mafic end member is interpreted to be an evolved magma that was originally chemically similar to the MCCD. The data suggest two possible interpretations for best estimates of the composition of the felsic end member. The first is a composition similar to the OPG samples and the other is a composition similar to that of the felsic group.

The OPG samples fall on trend lines and have some chemical similarities with enclave samples. The overall size of the OPG body makes it conceivable that this is the original felsic magma chamber, in which mafic magmas intruded. If this is the felsic end member, the felsic group is then best interpreted to represent late or filter pressed fluids filling cavities (i.e. felsic enclaves) and early fractures (aplite dikes). The low

concentrations of most major elements in the felsic group supports this model, however the incompatible trace element chemistry does not. The low concentration of incompatible elements (i.e. La, Zr, Ga) in the felsic group does not support the hypothesis that they are highly evolved fluids.

The second possibility is that the felsic group are felsic end members. In MASLI plutons, felsic dikes are chemically similar to the felsic layers, and are interpreted to be conduits through which felsic magma was replenished (Wiebe, 1993, Wiebe et al., 1997). As the felsic dikes have high SiO_2 and fall at the end of the mixing line, it is likely they represent the felsic end member.

The felsic group consistently plots together and at the opposite extreme from the MCCD for Harker and other variation diagrams (i.e. V and P_2O_5). These samples show minor deviation from mixing lines, and have minor chemical variation amongst them. This suggests that these had derived from a similar magma.

For some incompatible elements (i.e. U, Pb, Th, Rb) the felsic group is enriched with respect to other samples. Harker diagrams for these elements show a weakly defined elemental increase with increasing SiO_2 for all samples (Figure 5.12). If the fractionation is attributed to the enrichment of these elements (i.e. U, Pb, Th, Rb), the concentrations of other incompatible elements (i.e. Y, Zr, Sr, Nd, La) should also be enriched in the felsic group. As this is not true, enrichment of U, Pb, Th, and Rb reflects the original composition of the felsic end member magma. These relationships support the representation of the felsic group as the felsic end member.

Chemical data from high silica rhyolites have similar chemical compositions to the felsic group (Hildreth, 1981). This relationship further supports the interpretation that

the felsic group may represent the felsic end member. The felsic dikes are most likely late felsic magma replenishment into the magma chamber.

The interpretation that the felsic group represents the felsic end member suggests that the Oak Point Granite is also a product of hybridization between the two end member magmas. Two other observations support this hypothesis. First the composition of the Oak Point Granite is intermediate in composition with respect to the most mafic enclaves and the felsic group (D'Lemos, 1996). Second, petrographic features of the Oak Point Granite, such as rapakivi feldspars with rounded cores and plagioclase grains with numerous oscillatory zones, indicate chamber dynamics in response to magma mixing (Vernon, 1990; Hibbard, 1991).

As enclaves and the Oak Point Granite are both a product of magma mixing, the latter most likely had experienced a mixing event before distribution of the former. The rapakivi feldspars common to both hybrid units suggest this hypothesis. Textures, sizes and morphologies of the feldspars indicate that these had originated in the Oak Point granite and then incorporated into the enclave magma. This indicates that the magma chamber must have been active for a time sufficiently long for the alkali feldspars to grow, subsequently resorbed and rounded, and acquire plagioclase rims, before being mixed into the enclave magma.

6.6. Evolution of the Oak Point Granite

Fernandez and Barbarin (1991) discuss the rheological evolution a magma chamber that can be applied to the evolution of the OPG. They propose two significant thresholds during crystallization (Figure 6.2). The first coincides with the point when the

crystal content reaches about 30%. Prior to this point, the magma behaves as a Newtonian fluid, such that there exists a linear relationship between applied stress and resultant strain. Early in this stage, the viscosity of the felsic magma is low enough to permit distribution of the enclaves. As crystallization proceeds and the second threshold is reached, viscosity increases such that the magma evolves into a visco-plastic fluid, which has a yield stress. The second threshold is reached at a crystallinity of about 60%. At this point the magma body becomes more rigid, nearly solid. Now, enclaves and large crystals are unable to sink and their relative position becomes fixed. The granite may fracture and dikes of replenishment felsic magma may be intruded.

The model infers that calc-alkaline granites are the product of early hybridization with a mafic magma (Fernandez and Barbarin, 1991). This occurs when the felsic host has a low percentage (<30%) of crystals, before threshold one. The low viscosity enables convection currents to transport early crystals into different parts of the chamber and expose them to different magmatic environments. At this time the alkali feldspars in the OPG would have been resorbed and mantled as they migrated to hotter regions of the magma chamber. The common occurrence and wide distribution of micro-enclaves, as well as different morphologies and crystallization histories of adjacent feldspars reflect this early, almost complete mixing stage.

As crystallization proceeds and viscosity increases, the formation of discrete enclaves is more likely. The increased viscosity contrast would promote mingling rather than mixing. Enclave magmas are able to remain intact due to quenching of their outer portions. During this stage, the enclaves would be distributed throughout the OPG pluton (Fernandez and Barbarin, 1991).
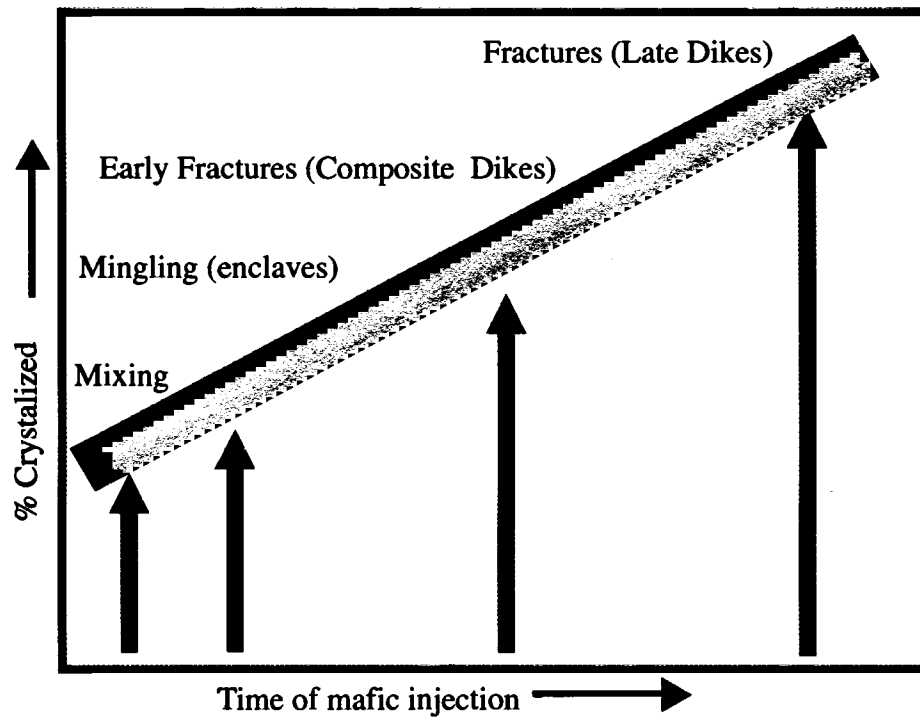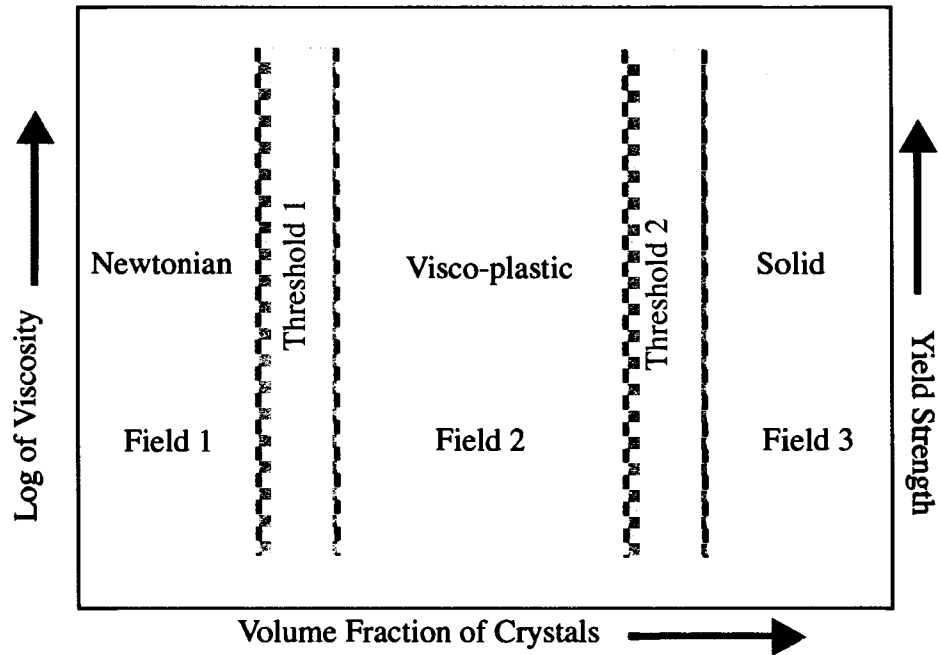
Figure 6.2: Evolution of a crystallizing magma (after Fernandez and Barbarin, 1991). Top figure shows rheological evolution and lower figure shows interaction of injected magmas in a crystallizing body.

The intrusion of late dikes could occur after the second threshold was reached. These dikes could replenish the chamber with fresh granitic magma, following the paths of early fractures. The composite dikes on Brooklin are the result of mafic and felsic magma migrating into these fractures. The numerous occurrences of the aplite dikes, a feature not observed in other MASLI type plutons, may reflect the level of exposure. Mafic dikes may be more common at lower levels, near the MASLI layers, whereas higher levels may have more granitic dikes.

Chapter 7

CONCLUSIONS

The magmatic enclaves in the Oak Point Granite, Deer Isle, Maine, provide evidence for the evolution of the pluton. Results show that the enclaves and the host granite formed from two different contemporaneous magmas. Furthermore, chemical analysis shows that mixing between mafic and felsic magmas explain the chemical variation in the enclaves and the Oak Point Granite.

The fine-grain size and micro-textures of the enclaves indicate rapid cooling in the host granite. Furthermore the presence of rapakivi feldspar inclusions, similar in texture, size, and color as those in the OPG support a magmatic origin for the enclaves. Variations in feldspar zoning and textures, as well as clinopyroxene cores in hornblende grains are indicative of hybridization.

The similarity of planar enclave orientations and feldspar foliation in the host granite is thought to reflect either magmatic flow or setting. Both seem plausible but available data does not permit a conclusion to be made. In either case, this alignment suggests a low viscosity magma. The wide distribution of the enclaves throughout the pluton supports convection currents.

Geochemical data show linear relationships for most major and several trace element Harker diagrams indicating magma mixing during petrogenesis. The composition of the MCCD best represents a mafic injection into the active Oak Point Granite magma chamber. This magma subsequently evolved into a residual magma that represents the

mafic end member for mixing. The felsic group (the FCCD, felsic enclave and aplite dikes) represents the felsic end member.

The enclave chemistry suggests that they derived from the residual magma produced by fractionation of the mafic injection. Depletion of compatible elements in early crystallizing mafic minerals, and enrichment of incompatible elements in the most mafic enclaves, with respect to the MCCD, reflects fractionation processes. The depleted nature of these elements in the other samples analyzed suggests that limited exchange occurred between the enclaves and the host granite after hybridization.

The common occurrence of aplite dikes is interpreted to be the result of late felsic replenishments, filling cracks formed in the crystallizing granite. The composite dikes presumably began as aplite dikes, but were later intruded by the parental mafic magma. The presence of resorbed xenocrysts across the irregular contact between the two components shows that both were contemporaneously liquid and exchange was possible. However, the chemical differences between the two components shows that exchange was, in part limited, probably due to quenching of the MCCD.

The position of the OPG, dioritic and felsic enclaves on linear trends suggests that they were produced by magma mixing. The presence of resorbed rapakivi cores, complex plagioclase zoning, and wide distribution of micro-enclaves suggests that the OPG had an mixing event before the formation and distribution of the enclaves. Further petrographic and chemical studies are required to determine the validity of this hypothesis.

REFERENCES

Barbarin, B., 1988. Field evidence for successive mixing and mingling between the Piolard Diorite and the Saint-Julien-la-Vetre Monzogranite (Nord-Forez, Massif Central, France). Canadian Journal of Earth Science, 25, p. 49-59.

Barbarin, B., 1991. Enclaves of the Mesozoic calc-alkaline granitoids of the Sierra Nevada batholith, California. In: Enclaves and Granite Petrology. Developments in Petrology 13: Didier, J. and Barbarin, B. (eds.) Elsevier, Amsterdam, p. 135-154.

Barbey, P., 1991. Restites in migmatites and autochthonous granites: Their main features and their genesis. In: Enclaves and Granite Petrology. Developments in Petrology 13: Didier, J. and Barbarin, B. (eds.) Elsevier, Amsterdam, p. 479-492.

Campbell, I. H. and Turner, J. S., 1985. Turbulent mixing between fluids with different viscosities. Nature, 313, p. 39-42.

Chapman, M. and Rhodes, J. M., 1992. Composite layering in the Isle au Haut complex, Maine: evidence for periodic invasion of a mafic magma into an evolving magma reservoir. Journal of Volcanology and Geothermal Research, 51, p. 41-60.

Chen, Y. D., Price, R. C., and White, A. J. R., 1989. Inclusions in three S-type granites from southeastern Australia. Journal of Petrology, 30, p. 1181-1218.

Cox, K. G., Bell, J. D., and Pankhurst, R. J., 1979. The interpretation of igneous rocks. London: George Allen & Unwin, 450p.

D'Lemos, R. S., 1996. Mixing between granitic and dioritic crystal mushes, Guernsey, Channel Islands, UK. Lithos, 38, p. 233-257.

Deer, W. A., Howie, R. A., and Zussman, J., 1992. An introduction to the rock forming minerals. Longman Scientific and Technical, England, 696p.

Didier, J., 1991. The main types of enclaves in the Hercynian granitoids of the Massif Central, France. In: Enclaves and Granite Petrology. Developments in Petrology 13: Didier, J. and Barbarin, B. (eds.) Elsevier, Amsterdam, p. 47-61.

Didier, J. and Barbarin, B., 1991. The different types of enclaves in granites-Nomenclature. In: Enclaves and Granite Petrology. Developments in Petrology 13: Didier, J. and Barbarin, B. (eds.) Elsevier, Amsterdam, p. 19-23.

Fernandez, A.N. and Barbarin, B., 1991. Relative rheology of coeval mafic and felsic magmas: nature of resulting interaction process. Shape and mineral fabrics of mafic microgranular enclaves. In: Enclaves and Granite Petrology. Developments in Petrology 13: Didier, J. and Barbarin, B. (eds.) Elsevier, Amsterdam, p. 263-276.

Foster, D. A. and Hyndman, D. W., 1990. Magma mixing and mingling between synplutonic mafic dikes and granite in Idaho-Bitterroot Batholith. In: The nature and origin of Cordilleran Magmatism: Anderson, J. L. (ed.), Geological Society of America Memoir 174, Boulder, CO, p. 347-358.

Gourgard, A., 1991. Comagmatic enclaves in lavas from the Mont-Dore composite volcano, Massif Central, France. In: Enclaves and Granite Petrology. Developments in Petrology 13: Didier, J. and Barbarin, B. (eds.) Elsevier, Amsterdam, p. 221-234.

Hibbard, M. J., 1991. Textural anatomy of twelve magma-mixed granitoid systems. In: Enclaves and Granite Petrology. Developments in Petrology 13: Didier, J. and Barbarin, B. (eds.) Elsevier, Amsterdam, p. 431-444.

Hildreth, W., 1981. Gradients in silicic magma chambers: Implications for lithospheric magmatism. Journal of Geophysical Research, 86, p. 10153-10192.

Hodge, D. S., Abbey, D. A., Harbin, M. A., Patterson, J. L., Ring, M. J., and Sweeney, J. F., 1982. Gravity studies of subsurface mass distributions of granitic rocks in Maine and New Hampshire. American Journal of Science, 282, p. 1289-1324.

Hogan, J. P. and Sinha, A. K., 1989. Compositional variation of plutonism in the Coastal Maine Magmatic Province; mode of origin and tectonic setting. In: Studies in Maine Geology, v. 4: Igneous and Metamorphic Geology: Tucker, R.D. and Marvinney, R.G., (eds.), p. 1-33.

Huppert, H. E. and Turner, J. S., 1981. A laboratory model of a replenished magma chamber. Earth and Planetary Science Letters, 54, p. 144-152.

Huppert, H. E., Turner, J. S., and Sparks, R. S. J., 1982. Replenished magma chambers: Effects of compositional zonation and input rates. Earth and Planetary Science Letters, 57, p. 345-357.

Huppert, H. E., Sparks, R. S., and Turner, J. S., 1984. Some effects of viscosity on the dynamics of replenished magma chambers. Journal of Geophysical Research, 89, p. 6857-6877.

Knesel, K. M., Davidson, J. P., and Duffield, W. A., 1999. Evolution of silicic magma through assimilation and subsequent recharge: Evidence from Sr isotopes in sanidine phenocrysts, Taylor Creek Rhyolite, New Mexico. Journal of Petrology, 40, p. 773-786.

Koyaguchi, T., 1991. Enclaves in volcanic rocks from Japan. In: Enclaves and Granite Petrology. Developments in Petrology 13: Didier, J. and Barbarin, B. (eds.) Elsevier, Amsterdam, p. 235-252.

LeFort, P., 1991. Enclaves of the Miocene Himalayan leucogranites. In: Enclaves and Granite Petrology. Developments in Petrology 13: Didier, J. and Barbarin, B. (eds.) Elsevier, Amsterdam, p. 35-46.

Marsh, B. D., 1989. Magma Chambers. Annual Review of Earth and Planetary Sciences, 17, p. 439-474.

Mason, B., and Moore, C. B., 1966. Principles of Geochemistry. John Wiley & Sons, New York, 344p.

Maury, R. C. and Didier, J., 1991. Xenoliths and the role of assimilation. In: Enclaves and Granite Petrology. Developments in Petrology 13: Didier, J. and Barbarin, B. (eds.) Elsevier, Amsterdam, p. 529-542.

Montel, J., Didier, J., and Pichavant, M., 1991. Origin of surmicaceous enclaves in intrusive granites. In: Enclaves and Granite Petrology. Developments in Petrology 13: Didier, J. and Barbarin, B. (eds.) Elsevier, Amsterdam, p. 509-528.

Orisini, J., Cocirta, C., and Zorpi, M., 1991. Genesis of mafic microgranular enclaves through differentiation of basic magmas, mingling and chemical exchanges with their host granitoid magmas. In: Enclaves and Granite Petrology. Developments in Petrology 13: Didier, J. and Barbarin, B. (eds.) Elsevier, Amsterdam, p. 445-464.

Paterson, S. R., Vernon, R. H., and Tobisch, O. T., 1989. A review of criteria for identification of magmatic and tectonic foliations in granitoids. Journal of Structural Geology, 11, p. 349-363.

Philpotts, A. R., 1991. Principles of igneous and metamorphic petrology. Prentice Hall, New Jersey, 498p.

Pitcher, W., 1991. Synplutonic dykes and mafic enclaves. In: Enclaves and Granite Petrology. Developments in Petrology 13: Didier, J. and Barbarin, B. (eds.) Elsevier, Amsterdam, p. 383-391.

Platevoet, B. and Bonin, B., 1991. Enclaves and mafic-felsic association in the Permian alkaline province of Corsica, France: Physical and chemical interactions between coeval magmas. In: Enclaves and Granite Petrology. Developments in Petrology 13: Didier, J. and Barbarin, B. (eds.) Elsevier, Amsterdam, p. 191-204.

Singer, B. S., Duncan, M. A., and Layne, G. D., 1995. Textures and Sr, Ba, Fe, K, and Ti composition profiles in volcanic plagioclase: clues to the dynamics of calc-alkaline magma chambers. American Mineralogist, 80, p. 776-798.

Snyder, D. and Tait, S., 1995. Replenishment of magma chambers: composition of fluid mechanics experiments with field relations. Contributions to Mineralogy and Petrology, 122, p. 230-240.

Snyder, D. and Tait, S., 1998a. A flow front instability in viscous gravity currents. Journal of Fluid Mechanics, 369, p. 1-21.

Snyder, D. and Tait, S., 1998b. The imprint of basalt on the geochemistry of silicic magmas. Earth and Planetary Science Letters, 160, p. 433-445.

Snyder, D., Crambes, C., Tait, S., and Wiebe, R. A., 1997. Magma mingling in dikes and sills. Journal of Geology, 105, p. 75-86.

Sparks, R. S. J. and Huppert, H. E., 1984. Density changes during the fractional crystallization of basaltic magmas: fluid dynamic implications. Contributions of Mineralogy and Petrology, 85, p. 300-309.

Sparks, R. S. J. and Marshall, L. A., 1986. Thermal and mechanical constraints on mixing between mafic and silicic magmas. In: Kushiro, I. (ed.), Sakuyama, M. and Fukuyama, H. Memorial Volume. Journal of Volcanology and Geothermal Research, 29, p. 99-124.

Sparks, R. S. J. and Marsh, B. D., 1990. Crystal capture, sorting and retention in convecting magma: Discussion and reply. Geological Society of America Bulletin, 102, p. 847-850.

Spera, F. J., 2000. Physical properties of magmas. In: Encyclopedia of Volcanoes: Sigurdsson, H., Houghton, B. F., McNutt, S. R., Rymer, H., Stix, J., and Ballard, R. D. (eds.) Academic Press, San Diego, p. 171-190.

Stewart, D. B., 1956. Rapakivi granite of the Deer Isle region, Maine: Ph.D. dissertation, Harvard University, Cambridge, MA, 150p.

Stewart, D. B., 1998. Miscellaneous Investigations Series, Map I-2551. USGS.

Stewart, D. B., Unger, J.D., and Hutchinson, D.R., 1995. Silurian tectonic history of Penobscot Bay region, Maine. Atlantic Geology, 31, p. 67-79.

Taylor, T. R., Vogel, T. A., and Wilband, J. T., 1980. Composite dikes at Mount Desert Island, Maine: An example of coexisting acidic and basic magmas. Journal of Geology, 88, p. 433-444.

Tindle, A. G., 1991. Trace element behaviour in microgranular enclaves from granitic rocks. In: Enclaves and Granite Petrology. Developments in Petrology 13: Didier, J. and Barbarin, B. (eds.) Elsevier, Amsterdam, p. 313-332.

Vernon, R. H., 1984. Microgranitoid enclaves in granites-globules of hybrid magma quenched in a plutonic environment. Nature, 309, p. 438-439.

Vernon, R. H., 1990. Crystallization and hybridism in microgranitoid enclave magmas: Microstructural evidence. Journal of Geophysical Research, 95, p. 17,849-17,859.

Vernon, R. H., 1991. Interpretations of microstructures of microgranitoid enclaves. In: Enclaves and Granite Petrology. Developments in Petrology 13: Didier, J. and Barbarin, B. (eds.) Elsevier, Amsterdam, p. 277-292.

Vernon, R. H., 2000. Review of microstructure evidence of magmatic and solid state flow. Electronic Geosciences, 5:2.

Vogel, T. A. and Wilband, J. T., 1978. Coexisting acidic and basic melts: Geochemistry of a composite dike. Journal of Geology, 86, p. 353-371.

Wiebe, R. A., 1973. Relations between coexisting basaltic and granitic magmas in a composite dike. American Journal of Science, 273, p. 130-151.

Wiebe, R. A., 1991. Comingling of contrasted magmas and generation of mafic enclaves in granitic rocks. In: Enclaves and Granite Petrology. Developments in Petrology 13: Didier, J. and Barbarin, B. (eds.) Elsevier, Amsterdam, p. 393-402.

Wiebe, R. A., 1993. The Pleasant Bay layered gabbro-diorite, coastal Maine: Ponding and crystallization of basaltic injections into a silicic magma chamber. Journal of Petrology, 34, p. 461-489.

Wiebe, R. A., 1994. Silicic magma chambers as traps for basaltic magmas: the Cadillac Mountain Intrusive Complex. Journal of Geology, 102, p. 423-437.

Wiebe, R. A., 1996. Mafic-Silicic layered intrusions: the role of the basaltic injections on magmatic processes and the evolution of silicic magma chamber. Transactions of the Royal Society of Edinburgh: Earth Sciences, 87, p. 233-242.

Wiebe, R. A. and Adams, S. D., 1997. Felsic enclave swarms in the Gouldsboro Granite, coastal Maine: A record of eruption through the roof of a silicic magma chamber. Journal of Geology, 105, p. 617-627.

Wiebe, R. A. and Ulrich, R., 1997. Origin of composite dikes in the Gouldsboro Granite, coastal Maine. Lithos, 40, p. 157-178.

Wiebe, R. A. and Collins, W. J., 1998. Depositional features and stratigraphy sections in granitic plutons: implications for the emplacement and crystallization of granitic magma. Journal of Structural Geology, 20, p. 1273-1289.

Wiebe, R. A., Smith, D., Sturm, M., King, E. M., and Seckler, M. S., 1997. Enclaves in the Cadillac Mountain Granite (coastal Maine): Samples of hybrid magma from the base of the chamber. Journal of Petrology, 38, p. 393-423.

Wiebe, R. A., Snyder, D., and Hawkins, D., 2000. Geological Society of America Field Forum: Correlating volcanic and plutonic perceptions of silicic magma chamber processes: Evidence from Coastal Maine plutons.

Wyllie, P. J., Cox, K. G., and Biggar, G. M., 1962. The habit of apatite in synthetic systems and igneous rocks. Journal of Petrology, 3, p. 238-243.

Appendix A

Data Tables

Type	Latitude	Longitude	Strike	Dip	Direction
Aplite	44.214549	-68.635724	28	24	SE
Aplite	44.215309	-68.637586	130	25	NE
Aplite	44.215481	-68.638207	30	34	SW
Aplite	44.215447	-68.638732	40	70	SE
Aplite	44.215103	-68.641455	80	37	SW
Aplite	44.215138	-68.642935	115	40	SW
Aplite	44.215172	-68.643413	55	40	SE
Aplite	44.215104	-68.645275	160	45	SW
Aplite	44.218588	-68.642121	155	40	SW
Aplite	44.217171	-68.636247	175	65	SW
Aplite	44.217516	-68.635961	10	67	SE
Aplite	44.217896	-68.635913	5	55	NW
Aplite	44.218586	-68.635530	173	35	SW
Aplite	44.218689	-68.635864	0	67	W
Aplite	44.218793	-68.635243	15	85	SE
Aplite	44.218931	-68.634766	17	63	SE
Aplite	44.218654	-68.633524	10	25	NW
Aplite	44.218723	-68.631900	120	75	NE
Aplite	44.221137	-68.628268	20	75	SE
Aplite	44.222516	-68.626118	5	60	SE
Aplite	44.222620	-68.626309	30	20	NE
Aplite	44.224036	-68.631801	45	35	NW
Aplite	44.202217	-68.571300	175	65	NE
Aplite	44.202079	-68.571062	142	70	NE
Aplite	44.202562	-68.570871	140	72	NE
Aplite	44.202665	-68.571300	70	34	SE
Aplite	44.202734	-68.571729	145	70	NE
Aplite	44.203526	-68.572730	150	65	NE
Aplite	44.204043	-68.573206	65	62	SE
Aplite	44.204388	-68.574016	155	64	NE
Aplite	44.209281	-68.585597	85	40	SE
Aplite	44.209109	-68.585358	95	35	SW
Aplite	44.209316	-68.585120	153	55	NE
Aplite	44.214069	-68.583597	120	50	NE
Aplite	44.214724	-68.584502	130	65	NE
Aplite	44.225588	-68.630701	5	50	SE
Aplite	44.228244	-68.626161	30	56	SE
Aplite	44.228893	-68.622595	80	43	NW
Aplite	44.230787	-68.622168	5	30	SE

Table A.1: Aplite dike, enclave and feldspar foliation attitudes and coordinates.

112

Type	Latitude	Longitude	Strike	Dip	Direction
Aplite	44.231063	-68.622645	162	28	NE
Aplite	44.231201	-68.623122	130	35	NE
Aplite	44.231314	-68.625012	175	40	NE
Aplite	44.231418	-68.625538	150	27	NE
Aplite	44.231211	-68.626589	155	42	NE
Aplite	44.231004	-68.627019	12	25	SE
Aplite	44.232315	-68.625680	11	40	SE
Aplite	44.232717	-68.623981	130	40	NE
Aplite	44.233625	-68.625154	30	40	SE
Aplite	44.233833	-68.625822	0	35	E
Aplite	44.213696	-68.613717	109	21	SW
Aplite	44.213903	-68.613527	35	55	NE
Aplite	44.213937	-68.613241	21	86	NW
Aplite	44.213903	-68.613813	73	65	SE
Aplite	44.214041	-68.612478	108	45	NE
Aplite	44.214109	-68.612192	74	75	SE
Aplite	44.214178	-68.612050	30	88	NW
Aplite	44.214247	-68.611716	25	85	NW
Aplite	44.214006	-68.611668	67	54	SE
Aplite	44.214040	-68.611477	41	77	NW
Aplite	44.214316	-68.611430	56	62	SE
Aplite	44.214178	-68.609857	35	74	SE
Aplite	44.214419	-68.609619	35	90	
Aplite	44.215453	-68.609715	85	16	SW
Aplite	44.215522	-68.610001	150	15	SW
Aplite	44.215728	-68.610096	30	85	SE
Aplite	44.216417	-68.610049	35	80	SE
Aplite	44.216279	-68.609954	19	80	NW
Aplite	44.216107	-68.609667	33	24	NW
Aplite	44.216555	-68.609572	50	40	NW
Aplite	44.215416	-68.600134	34	65	NW
Aplite	44.215209	-68.599991	41	33	SE
Aplite	44.235835	-68.630406	125	21	NE
Aplite	44.236110	-68.625582	36	41	SE
Aplite	44.233095	-68.618260	7	38	SE
Aplite	44.233680	-68.615210	117	47	NE
Aplite	44.230784	-68.609725	103	22	SW
Aplite	44.229026	-68.605719	43	38	SE
Aplite	44.228991	-68.605338	25	37	SE

Table A.1: continued

Type	Latitude	Longitude	Strike	Dip	Direction
Aplite	44.229198	-68.605004	116	68	NE
Aplite	44.229784	-68.604719	118	60	NE
Aplite	44.230025	-68.604147	128	58	NE
Aplite	44.231058	-68.604243	145	44	NE
Aplite	44.257811	-68.624648	105	17	NE
Aplite	44.258052	-68.624886	68	11	NW
Aplite	44.234127	-68.612254	117	53	NE
Aplite	44.234368	-68.611921	121	72	NE
Aplite	44.233299	-68.610394	117	47	NE
Aplite	44.234160	-68.606581	22	52	SE
Aplite	44.233712	-68.605770	127	46	NE
Aplite	44.231389	-68.536564	163	73	NE
Aplite	44.231562	-68.537136	165	76	NE
Aplite	44.232906	-68.541760	160	90	
Aplite	44.233044	-68.542188	46	77	SE
Aplite	44.233388	-68.542760	152	90	
Aplite	44.233836	-68.543380	58	81	NW
Aplite	44.234215	-68.544047	62	72	NW
Aplite	44.234526	-68.545525	175	79	NE
Aplite	44.234664	-68.547241	15	70	SE
Aplite	44.235457	-68.549147	120	58	NE
Aplite	44.235319	-68.549910	132	75	NE
Aplite	44.235526	-68.550243	80	27	SW
Aplite	44.236146	-68.551292	67	45	SE
Aplite	44.236663	-68.551530	151	75	NE
Aplite	44.237111	-68.552150	172	64	NE
Aplite	44.237352	-68.552054	165	51	NE
Aplite	44.237662	-68.552007	145	85	NE
Aplite	44.229114	-68.530940	68	68	SE
Aplite	44.228977	-68.530702	157	67	NE
Aplite	44.228908	-68.531036	173	66	NE
Aplite	44.228942	-68.530368	157	62	NE
Aplite	44.228839	-68.530130	170	69	NE
Aplite	44.228873	-68.529796	50	63	SE
Aplite	44.228183	-68.525554	172	81	NE
Aplite	44.228183	-68.525268	10	83	SE
Aplite	44.228114	-68.524887	166	80	NE
Aplite	44.228596	-68.524315	168	75	NE
Aplite	44.228975	-68.523171	10	71	SE

Table A.1: continued

Type	Latitude	Longitude	Strike	Dip	Direction
Aplite	44.229078	-68.523504	28	82	SE
Aplite	44.231937	-68.522979	96	30	SW
Aplite	44.234142	-68.523122	70	42	SE
Aplite	44.234693	-68.523217	14	60	SE
Aplite	44.235485	-68.523312	10	55	SE
Aplite	44.236277	-68.523169	156	83	NW
Aplite	44.237621	-68.524169	173	58	NE
Aplite	44.252141	-68.531347	63	68	SE
Aplite	44.260037	-68.519124	33	45	NW
Aplite	44.270473	-68.546860	100	75	SW
Aplite	44.205562	-68.595698	50	90	
Aplite	44.211453	-68.591268	143	50	NE
Aplite	44.214897	-68.589649	135	45	NE
Aplite	44.215345	-68.586885	150	25	SW
Aplite	44.215620	-68.586647	60	90	
Aplite	44.192262	-68.576587	60	90	
Aplite	44.192159	-68.576349	160	35	SW
Aplite	44.189437	-68.572203	115	25	SW
Aplite	44.189471	-68.571965	135	23	SW
Aplite	44.189471	-68.571726	15	25	NW
Aplite	44.189471	-68.570583	40	30	SE
Aplite	44.189471	-68.569201	0	5	SE
Aplite	44.189367	-68.569392	20	7	SE
Aplite	44.189712	-68.569010	165	60	SW
Aplite	44.189781	-68.568867	55	90	
Aplite	44.189677	-68.568629	148	65	NE
Aplite	44.189367 .	-68.568153	50	75	NW
Aplite	44.189195	-68.568010	140	85	SW
Aplite	44.188885	-68.568010	35	75	NW
Aplite	44.188128	-68.572393	70	78	SE
Aplite	44.188265	-68.572822	10	15	NW
Aplite	44.187370	-68.572917	35	35	NW
Aplite	44.198051	-68.588548	87	53	SE
Aplite	44.195192	-68.587261	157	53	SW
Aplite	44.195295	-68.588404	160	55	SW
Aplite	44.195433	-68.589167	123	32	SW
Aplite	44.194641	-68.594265	45	50	NW
Aplite	44.193195	-68.600030	60	68	SE
Aplite	44.188886	-68.579445	55	70	NW

Table A.1: continued

Type	Latitude	Longitude	Strike	Dip	Direction
Aplite	44.187370	-68.575204	25	30	NW
Aplite	44.187198	-68.575347	20	46	SE
Aplite	44.186888	-68.575823	170	32	NW
Aplite	44.186371	-68.576776	35	60	NW
Aplite	44.192986	-68.576968	20	40	NW
Aplite	44.192296	-68.574395	60	90	
Aplite	44.192537	-68.573871	60	35	NW
Aplite	44.192364	-68.566819	15	90	
Aplite	44.196153	-68.565009	5	56	SE
Aplite	44.211523	-68.601610	70	43	SE
Aplite	44.211420	-68.601944	52	44	SE
Aplite	44.211386	-68.602563	42	63	SE
Aplite	44.210252	-68.617338	18	82	NW
Aplite	44.209461	-68.622342	71	21	SE
Aplite	44.209564	-68.622580	110	35	SW
Aplite	44.214731	-68.616673	27	67	NW
Aplite	44.215075	-68.616960	30	80	NW
Aplite	44.215455	-68.619153	20	73	NW
Aplite	44.215455	-68.620392	20	75	NW
Aplite	44.215283	-68.621011	20	75	SE
Aplite	44.215697	-68.622203	5	80	SE
Aplite	44.215731	-68.623109	20	90	
Aplite	44.215685	-68.624738	45	57	SE
Aplite	44.215133	-68.626506	163	60	NW
Aplite	44.215376	-68.630088	10	55	NW
Aplite	44.215272	-68.630279	18	80	NW
Aplite	44.215100	-68.630518	30	78	NW
Aplite	44.214962	-68.630852	15	70	SE
Aplite	44.214548	-68.630566	0	90	
Aplite	44.213134	-68.635199	100	10	NE
Aplite	44.213342	-68.635677	10	18	SE
Aplite	44.214860	-68.636010	110	40	SW
Aplite	44.227541	-68.588749	53	56	SE
Aplite	44.226850	-68.579312	164	34	NE
Aplite	44.227263	-68.578026	156	52	NE
Aplite	44.229261	-68.576215	153	54	NE
Aplite	44.229295	-68.575929	67	78	NW
Aplite	44.230432	-68.577884	104	50	SE
Aplite	44.230398	-68.578885	90	60	E

Table A.1: continued

116

Type	Latitude	Longitude	Strike	Dip	Direction
Aplite	44.232087	-68.581221	153	45	NE
Aplite	44.232328	-68.582412	148	60	NE
Aplite	44.230951	-68.588322	18	35	SE
Aplite	44.231158	-68.588560	60	49	SE
Aplite	44.230400	-68.589037	12	43	SE
Aplite	44.229333	-68.590609	100	46	NE
Enclave	44.217553	-68.643602	125	35	SW
Enclave	44.218208	-68.642647	135	40	SW
Enclave	44.218137	-68.635817	127	47	SW
Enclave	44.218379	-68.635817	125	53	SW
Enclave	44.219067	-68.628652	120	35	SW
Enclave	44.221309	-68.628077	115	45	SW
Enclave	44.221447	-68.627982	125	30	SW
Enclave	44.202183	-68.570824	177	47	SW
Enclave	44.202217	-68.570585	120	27	SW
Enclave	44.202630	-68.570538	164	54	SW
Enclave	44.202596	-68.572015	135	37	SW
Enclave	44.204526	-68.574255	126	30	SW
Enclave	44.204836	-68.576971	133	24	SW
Enclave	44.205215	-68.578972	135	29	SW
Enclave	44.205250	-68.579401	165	44	SW
Enclave	44.209040	-68.585025	125	40	SW
Enclave	44.210211	-68.584406	145	62	SW
Enclave	44.211176	-68.584454	145	73	SW
Enclave	44.225105	-68.629746	108	54	SW
Enclave	44.225381	-68.630080	98	52	SW
Enclave	44.225899	-68.630605	117	35	SW
Enclave	44.233073	-68.624151	144	23	SW
Enclave	44.233280	-68.624676	129	33	SW
Enclave	44.213972	-68.612955	95	38	SW
Enclave	44.214213	-68.611192	99	57	SW
Enclave	44.216107	-68.610621	75	65	SW
Enclave	44.216314	-68.610716	103	46	SW
Enclave	44.216486	-68.610716	121	61	SW
Enclave	44.216521	-68.610430	93	44	SW
Enclave	44.216624	-68.609286	146	40	SW
Enclave	44.216934	-68.609144	130	37	SW
Enclave	44.217140	-68.606951	130	59	SW
Enclave	44.214761	-68.598609	140	58	SW

Table A.1: continued

117

Type	Latitude	Longitude	Strike	Dip	Direction
Enclave	44.214520	-68.598466	150	50	SW
Enclave	44.232749	-68.613683	118	50	NE
Enclave	44.229440	-68.608199	125	23	SW
Enclave	44.229233	-68.605338	138	23	SW
Enclave	44.229508	-68.604814	109	24	SW
Enclave	44.230197	-68.604052	146	25	SW
Enclave	44.230404	-68.604147	134	31	SW
Enclave	44.230542	-68.604100	155	24	SW
Enclave	44.231300	-68.604291	145	28	SW
Enclave	44.231196	-68.604005	155	38	SW
Enclave	44.231162	-68.604481	132	37	SW
Enclave	44.252669	-68.620085	103	27	SW
Enclave	44.257845	-68.624982	46	49	SE
Enclave	44.233953	-68.608106	140	25	SW
Enclave	44.234022	-68.607820	156	48	SW
Enclave	44.233539	-68.605627	135	38	SW
Enclave	44.233595	-68.542999	137	21	SW
Enclave	44.234940	-68.548766	3	20	NW
Enclave	44.235215	-68.548813	24	18	NW
Enclave	44.235560	-68.549910	157	19	SW
Enclave	44.235801	-68.550672	33	24	NW
Enclave	44.236215	-68.551625	35	36	NW
Enclave	44.236387	-68.551387	20	21	NW
Enclave	44.236732	-68.551911	5	20	NW
Enclave	44.236835	-68.552245	31	18	NW
Enclave	44.238420	-68.551864	45	14	NW
Enclave	44.238592	-68.551292	20	17	NW
Enclave	44.238695	-68.550196	11	20	NW
Enclave	44.229011	-68.529606	22	18	NW
Enclave	44.228804	-68.529463	170	24	SW
Enclave	44.228942	-68.528843	12	17	NW
Enclave	44.228907	-68.528509	28	23	NW
Enclave	44.228252	-68.527127	20	28	NW
Enclave	44.228390	-68.527175	41	33	NW
Enclave	44.228528	-68.527032	161	16	SW
Enclave	44.228218	-68.526651	4	22	NW
Enclave	44.228149	-68.526460	46	5	NW
Enclave	44.227942	-68.524839	16	18	NW
Enclave	44.227873	-68.524601	6	16	NW

Table A.1: continued

Type	Latitude	Longitude	Strike	Dip	Direction
Enclave	44.228734	-68.523743	42	23	NW
Enclave	44.228631	-68.523457	30	36	NW
Enclave	44.228665	-68.523266	27	15	NW
Enclave	44.228837	-68.523171	50	11	NW
Enclave	44.229319	-68.523552	52	34	NW
Enclave	44.236518	-68.523455	153	14	NW
Enclave	44.237001	-68.523931	13	17	NW
Enclave	44.237242	-68.524026	12	28	NW
Enclave	44.261140	-68.519123	145	19	SW
Enclave	44.263173	-68.519885	171	32	SW
Enclave	44.263380	-68.519837	12	23	NW
Enclave	44.264138	-68.519837	136	26	SW
Enclave	44.265103	-68.519550	157	52	SW
Enclave	44.264931	-68.519455	167	45	SW
Enclave	44.259830	-68.518885	14	27	NW
Enclave	44.213313	-68.590697	175	30	SW
Enclave	44.215414	-68.587362	155	25	SW
Enclave	44.215414	-68.586695	125	35	SW
Enclave	44.215586	-68.586361	145	27	SW
Enclave	44.189574	-68.571440	40	35	NW
Enclave	44.189333	-68.571440	10	27	NW
Enclave	44.189574	-68.569535	5	30	NW
Enclave	44.189608	-68.569249	170	28	SW
Enclave	44.189540	-68.568772	150	25	SW
Enclave	44.189850	-68.569201	40	35	NW
Enclave	44.189023	-68.567962	10	30	NW
Enclave	44.188782	-68.567771	7	34	NW
Enclave	44.188334	-68.571107	175	40	SW
Enclave	44.188196	-68.571917	140	45	SW
Enclave	44.193195	-68.597219	55	75	NW
Enclave	44.192296	-68.574014	130	56	SW
Enclave	44.191779	-68.571155	140	32	SW
Enclave	44.192364	-68.567296	26	55	NW
Enclave	44.192398	-68.565961	5	45	NW
Enclave	44.191985	-68.565056	75	27	NW
Enclave	44.191881	-68.564627	17	26	NW
Enclave	44.191916	-68.564389	33	35	NW
Enclave	44.192433	-68.563865	30	38	NW
Enclave	44.192880	-68.563770	31	30	NW

Table A.1: continued

Type	Latitude	Longitude	Strike	Dip	Direction
Enclave	44.194121	-68.564389	28	25	NW
Enclave	44.197325	-68.568488	25	47	NW
Enclave	44.197532	-68.569060	155	34	SW
Enclave	44.199185	-68.569775	170	20	SW
Enclave	44.211455	-68.605089	125	57	SW
Enclave	44.209323	-68.621484	130	40	SW
Enclave	44.214214	-68.615291	85	31	SE
Enclave	44.214662	-68.615958	115	40	SW
Enclave	44.215650	-68.625073	140	42	SW
Enclave	44.226575	-68.581933	12	40	NW
Enclave	44.226919	-68.578931	157	21	SW
Enclave	44.227435	-68.577787	141	26	SW
Enclave	44.227745	-68.577359	130	31	SW
Enclave	44.228675	-68.576358	168	28	SW
Enclave	44.229123	-68.575929	166	22	SW
Enclave	44.229054	-68.576215	171	26	SW
Enclave	44.230605	-68.578980	149	35	SW
Enclave	44.232294	-68.582889	155	37	SW
Enclave	44.229264	-68.590323	154	51	SW
Feldspar	44.215207	-68.645705	0	34	W
Feldspar	44.219239	-68.628843	145	35	SW
Feldspar	44.223138	-68.626834	130	40	SW
Feldspar	44.202389	-68.570585	152	55	SW
Feldspar	44.202768	-68.572348	135	46	SW
Feldspar	44.203733	-68.573063	154	42	SW
Feldspar	44.204491	-68.574541	110	50	SW
Feldspar	44.230236	-68.621834	5	40	NE
Feldspar	44.231314	-68.626063	110	20	SW
Feldspar	44.213971	-68.610953	117	40	SW
Feldspar	44.216968	-68.608858	147	34	SW
Feldspar	44.217003	-68.608143	147	53	SW
Feldspar	44.215761	-68.600754	124	51	SW
Feldspar	44.215002	-68.599086	138	35	SW
Feldspar	44.230748	-68.604100	157	32	SW
Feldspar	44.234056	-68.606295	170	42	SW
Feldspar	44.235560	-68.550481	84	40	NW
Feldspar	44.236525	-68.551816	65	30	NW
Feldspar	44.228907	-68.528176	36	25	NW
Feldspar	44.228183	-68.526031	10	27	NW

Table A.1: continued

Type	Latitude	Longitude	Strike	Dip	Direction
Feldspar	44.229457	-68.523695	2	30	NW
Feldspar	44.234899	-68.523264	150	38	SW
Feldspar	44.265206	-68.519741	170	41	SW
Feldspar	44.198120	-68.588834	170	40	SW
Feldspar	44.214828	-68.589030	125	30	SW
Feldspar	44.215551	-68.587028	95	20	SW
Feldspar	44.189299	-68.571202	170	35	SW
Feldspar	44.188747	-68.568010	35	45	NW
Feldspar	44.188747	-68.568438	5	35	NW
Feldspar	44.187026	-68.575585	125	40	SW
Feldspar	44.191917	-68.571441	155	47	SW
Feldspar	44.191848	-68.569821	170	35	SW
Feldspar	44.191917	-68.569535	170	45	SW
Feldspar	44.193328	-68.563913	10	33	NW
Feldspar	44.197222	-68.567964	150	30	SW
Feldspar	44.227917	-68.577168	155	40	SW
Feldspar	44.230501	-68.579171	152	37	SW
Feldspar	44.232156	-68.581602	173	30	SW

Table A.1: concluded

Sample	Total Count	Quartz	Microcline	Plagioclase	Mafic Total
GRANITE					
FLYPT	1997	13.6	39.4	27.6	19.4
GRNLW	1802	20.0	33.9	29.7	16.5
NASKG	1141	13.6	36.2	33.7	16.5
OAKPT	1172	19.4	41.0	27.4	12.2
PRSN	2182	17.6	37.0	28.9	16.5
ENCLAVE					
Fine-grained dioritic					
CI 1	600	0.3	14.0	66.5	19.2
ESC 1	655	0.0	0.0	65.6	34.4
FYPT 4	448	10.5	27.2	49.6	12.7
FYPT 7	549	3.3	20.8	58.1	17.9
GL1	670	0.6	28.1	57.6	13.7
OPE 1	525	2.3	14.3	64.0	19.4
OPE 10	618	0.0	21.2	59.7	19.1
OPE 2	729	0.4	23.9	60.6	15.1
NKG 3	635	1.3	14.5	65.5	18.7
NKPT1	700	0.3	14.9	64.6	20.3
NKG 19	676	1.2	30.0	49.3	19.5
NKG 20	434	0.9	21.7	55.3	22.1
SNCC 2	647	2.0	0.0	64.0	34.0
SNPF 2	555	0.2	19.6	59.5	20.7
SNS 1	648	4.6	23.5	59.6	12.3
Medium-grained dioritic					
SNS 23	458	5.9	0.0	69.9	24.2
SNS 24	624	4.0	7.7	59.5	28.8
SNS 27	664	2.4	0.0	68.1	29.5
Felsic Enclave					
SNS 7	537	24.8	44.9	26.1	4.3

Table A.2: Modal percents from granite and enclave samples.

	Granites GRNLW	FLYE	FLYEa	OAKPTa	OAKPT	NASKG
Wt%						
L.O.I.	0.87	0.51	0.48	0.48	0.19	0.56
SiO_2	66.06	67	66.89	66.24	66.54	63.63
TiO_2	0.575	0.577	0.58	0.62	0.632	0.782
Al_2O_3	16.29	15.32	15.31	15.31	15.42	16.33
Fe_2O_3	3.33	3.36	3.36	3.68	3.67	4.37
MnO	0.061	0.056	0.056	0.059	0.061	0.074
MgO	1.06	0.77	0.8	0.99	0.99	1.06
CaO	2.73	1.92	1.94	2.32	2.33	2.49
Na_2O	4.17	4.17	4.18	3.95	3.93	4.25
K_2O	4.64	4.94	4.95	4.83	4.86	5.03
P_2O_5	0.202	0.166	0.169	0.193	0.195	0.238
ppm						
V	72	68	68	76	78	89
Cr	17	18	16	21	23	19
Co	8	7	5	7	7	9
Zr	323	384	376	359	341	487
Ba	961	888	946	949	1004	1121
La	47	58	62	50	54	63
Nd	31	42	45	39	35	54
Ni	9	5	<3	3	11	7
Cu	10	7	5	10	10	9
Zn	51	48	46	61	51	58
Ga	21	20	19	19	18	21
Rb	119	127	127	114	113	96
Sr	337	223	225	273	275	281
Y	27	38	38	34	34	44
Nb	19	22	21	19	20	26
Pb	27	22	21	22	12	21
Th	10	13	12	12	12	9
U	4	5	4	4	4	4
Total	100.3	99.00	98.93	98.94	99.08	99.08

Table A.3: Whole rock chemistry. "a" denotes a duplicate sample.

	Granites		Enclaves				
	NASKGa	PRSN	PRSNa	FYPT 4	FYPT 7	GL 1	NKG 3
Wt%							
L.O.I.	0.71	0.56	0.68	0.67	0.77	0.65	0.44
SiO_2	63.77	65.12	64.75	64.4	59.96	62.94	57.6
TiO_2	0.785	0.683	0.682	0.892	1.068	0.798	1.234
Al_2O_3	16.33	16.02	16.02	16.03	16.61	17.26	18.68
Fe_2O_3	4.38	3.79	3.81	4.12	5.01	4.18	6.32
MnO	0.073	0.06	0.06	0.088	0.12	0.088	0.126
MgO	1.08	0.95	0.94	1.01	1.42	1.1	1.84
CaO	2.5	2.28	2.27	2.03	2.61	2.57	3.79
Na_2O	4.24	4.23	4.19	3.76	3.9	4.59	5.44
K_2O	5.05	4.91	4.93	6.46	6.89	4.9	3.49
P_2O_5	0.239	0.202	0.2	0.249	0.316	0.189	0.387
ppm							
V	89	79	80	97	114	89	128
Cr	19	20	25	15	13	10	8
Co	9	8	9	7	11	7	15
Zr	477	426	410	612	737	795	1079
Ba	1149	1025	1065	1028	833	1030	620
La	53	47	53	62	53	57	58
Nd	41	34	40	46	48	43	42
Ni	<3	283	<3	6	7	<3	<3
Cu	8	8	8	12	7	7	4
Zn	63	54	53	61	69	58	94
Ga	21	21	21	19	21	20	25
Rb	96	102	102	166	170	104	93
Sr	286	259	262	213	193	329	279
Y	43	37	37	56	59	52	39
Nb	24	21	21	36	39	27	28
Pb	20	24	23	28	25	22	20
Th	10	6	6	14	6	7	9
U	4	4	4	5	6	3	5
Total	99.43	99.05	98.78	99.91	98.92	99.54	99.77

Table A.3: continued

	Enclaves						
	NKPT 1	OPE 2	OPE 9	OPE 10	SNPF 2	SNS 3	SNS 7
Wt%							
L.O.I.	0.09	0.29	0.37	0.36	1.4	0.78	0.25
SiO_2	56.83	57.33	55.88	56.99	55.97	61.27	75.31
TiO_2	1.404	1.281	1.309	1.271	1.278	0.906	0.265
Al_2O_3	18.12	18.3	18.64	18.68	18.42	17.06	12.81
Fe_2O_3	6.12	6.17	7.26	6.2	6.08	4.83	1.61
MnO	0.116	0.103	0.128	0.114	0.11	0.082	0.024
MgO	1.75	1.33	1.94	1.72	1.84	1.25	0.36
CaO	3.87	2.73	4.59	3.71	3.54	2.27	0.71
Na_2O	5.06	4.55	5.65	5.01	4.79	4.64	2.53
K_2O	4.76	6.3	2.99	4.96	5.02	5.16	6.49
P_2O_5	0.38	0.324	0.405	0.368	0.382	0.254	0.073
ppm							
V	152	130	141	138	142	101	39
Cr	9	19	41	11	11	16	16
Co	13	11	17	13	15	10	<5
Zr	886	867	803	760	651	804	132
Ba	1733	1359	538	1135	854	712	967
La	77	57	55	46	83	75	26
Nd	74	47	47	41	53	47	23
Ni	<3	6	68	4	<3	6	4
Cu	27	5	8	13	22	<4	7
Zn	99	80	94	80	79	73	28
Ga	24	22	24	22	25	22	14
Rb	71	116	86	97	132	164	186
Sr	619	367	324	381	366	238	203
Y	45	32	46	38	39	39	14
Nb	32	29	32	32	33	35	8
Pb	11	14	7	9	11	39	30
Th	3	2	6	3	12	20	3
U	1	2	3	2	3	5	5
Total	98.89	98.96	99.69	99.76	99.19	98.73	100.51

Table A.3: continued

	Aplite Dikes		Composite Dike		Mafic Dikes	
	SNS 21	SNS 25A	FCCD	MCCD	FYPT 1	NKG 9
Wt%						
L.O.I.	0.38	0.28	0.28	0.81	1.73	3.11
SiO$_2$	75.45	76.63	74.27	51.76	41.51	44.78
TiO$_2$	0.074	0.077	0.083	1.43	3.486	3.095
Al$_2$O$_3$	13.13	12.57	13.25	16.58	8.24	10.03
Fe$_2$O$_3$	1.17	0.72	1.17	9.55	14.13	12.51
MnO	0.005	0.003	0.016	0.167	0.187	0.158
MgO	0.11	0.05	0.12	5.07	13.95	11.7
CaO	0.45	0.55	0.63	7.65	10.66	8.51
Na$_2$O	3.3	2.98	3.32	3.92	2.35	2.42
K$_2$O	5.52	5.49	5.63	1.63	2.13	2.16
P$_2$O$_5$	0.032	0.019	0.046	0.435	0.886	0.734
ppm						
V	18	19	19	185	375	319
Cr	23	18	17	49	322	317
Co	<5	<5	<5	38	65	61
Zr	75	46	61	308	269	261
Ba	274	199	276	429	242	251
La	16	19	12	43	45	48
Nd	10	15	9	36	52	48
Ni	26	<3	3	45	384	352
Cu	6	22	4	20	67	44
Zn	16	14	17	95	127	122
Ga	19	16	18	19	17	19
Rb	185	155	242	90	32	72
Sr	53	64	50	635	872	818
Y	44	6	44	28	20	19
Nb	20	6	16	15	71	56
Pb	28	25	38	10	4	3
Th	32	46	19	5	7	4
U	9	10	10	<1	<1	<1
Total	99.67	99.43	98.89	100.38	101.64	101.07

Table A.3: concluded

	SNCC2 pl1	SNCC2 pl2	SNCC2 pl6	SNCC2 pl6r	SNCC2 mc7
SiO_2	61.92	62.92	62.44	62.02	64.40
TiO_2	0.01	0.01	0.00	0.00	0.00
Al_2O_3	24.17	23.32	24.07	24.24	18.93
FeO	0.25	0.23	0.13	0.12	0.09
MnO	0.01	0.01	0.02	0.02	0.01
MgO	0.00	0.01	0.01	0.00	0.01
CaO	4.99	4.19	4.55	4.84	0.51
Cr_2O_3	0.00	0.01	0.01	0.00	0.00
Na_2O	8.50	8.61	8.68	8.90	1.27
K_2O	0.16	0.22	0.17	0.16	14.22
Total	100.01	99.51	100.07	100.31	99.43

Formula Units (recalculated for 8 O)

	SNCC2 pl1	SNCC2 pl2	SNCC2 pl6	SNCC2 pl6r	SNCC2 mc7
Si	2.74	2.79	2.76	2.74	2.97
Al	1.26	1.22	1.25	1.26	1.03
Fe	0.01	0.01	0.00	0.00	0.00
Ti	0.00	0.00	0.00	0.00	0.00
Mg	0.00	0.00	0.00	0.00	0.00
Mn	0.00	0.00	0.00	0.00	0.00
Cr	0.00	0.00	0.00	0.00	0.00
Na	0.73	0.74	0.74	0.76	0.11
Ca	0.24	0.20	0.22	0.23	0.03
K	0.01	0.01	0.01	0.01	0.84
Total	4.99	4.97	4.98	5.00	4.98

Mol. Percent

	SNCC2 pl1	SNCC2 pl2	SNCC2 pl6	SNCC2 pl6r	SNCC2 mc7
Ab	74.79	77.77	76.78	76.22	11.6
An	24.27	20.91	22.25	22.88	2.59
Or	0.93	1.32	0.97	0.90	85.81

Table A.4: Plagioclase microprobe analysis. Calculations and table format are after Deer, Howie and Zussman, 1992. "r" denotes analysis on the grain rim. Samples SNCC2 mc7 and NKPT1 mc3 are microcline grains.

	SNCC2 pl7r	NKG3 pl1	NKG3 pl1r	NKG3 pl2	NKG3 pl2r
SiO_2	61.92	60.38	63.00	61.66	62.56
TiO_2	0.00	0.00	0.00	0.01	0.01
Al_2O_3	23.46	24.75	22.78	23.64	23.16
FeO	0.14	0.08	0.15	0.09	0.21
MnO	0.00	0.00	0.00	0.01	0.01
MgO	0.01	0.00	0.00	0.01	0.00
CaO	4.56	6.11	3.78	4.78	4.29
Cr_2O_3	0.01	0.00	0.01	0.01	0.00
Na_2O	8.80	8.05	9.44	8.85	9.22
K_2O	0.26	0.17	0.15	0.18	0.14
Total	99.15	99.54	99.31	99.25	99.60

Formula Units (recalculated for 8 O)

	SNCC2 pl7r	NKG3 pl1	NKG3 pl1r	NKG3 pl2	NKG3 pl2r
Si	2.77	2.70	2.80	2.75	2.78
Al	1.24	1.30	1.20	1.24	1.21
Fe	0.01	0.00	0.01	0.00	0.01
Ti	0.00	0.00	0.00	0.00	0.00
Mg	0.00	0.00	0.00	0.00	0.00
Mn	0.00	0.00	0.00	0.00	0.00
Cr	0.00	0.00	0.00	0.00	0.00
Na	0.76	0.70	0.82	0.77	0.79
Ca	0.22	0.29	0.18	0.23	0.20
K	0.01	0.01	0.01	0.01	0.01
Total	5.01	5.00	5.02	5.00	5.00

Mol. Percent

	SNCC2 pl7r	NKG3 pl1	NKG3 pl1r	NKG3 pl2	NKG3 pl2r
Ab	76.58	69.77	81.18	76.22	78.92
An	21.91	29.25	17.96	22.74	20.31
Or	1.51	0.97	0.86	1.04	0.76

Table A.4: continued

	NKG3 pl3	NKG3 pl3r	NKG3 pl4	NKG3 pl4r	NKPT1 mc3
SiO_2	61.34	63.34	60.92	62.33	63.48
TiO_2	0.01	0.01	0.01	0.01	0.01
Al_2O_3	24.07	22.95	24.12	23.32	19.45
FeO	0.10	0.15	0.09	0.18	0.08
MnO	0.02	0.01	0.01	0.01	0.02
MgO	0.00	0.01	0.00	0.00	0.00
CaO	5.30	3.95	5.45	4.44	0.05
Cr_2O_3	0.01	0.00	0.00	0.00	0.01
Na_2O	8.59	9.19	8.35	8.95	1.04
K_2O	0.14	0.16	0.14	0.16	14.48
Total	99.57	99.76	99.10	99.41	98.63

Formula Units (recalculated for 8 O)

	NKG3 pl3	NKG3 pl3r	NKG3 pl4	NKG3 pl4r	NKPT1 mc3
Si	2.73	2.81	2.73	2.78	2.96
Al	1.26	1.20	1.27	1.22	1.07
Fe	0.00	0.01	0.00	0.01	0.00
Ti	0.00	0.00	0.00	0.00	0.00
Mg	0.00	0.00	0.00	0.00	0.00
Mn	0.00	0.00	0.00	0.00	0.00
Cr	0.00	0.00	0.00	0.00	0.00
Na	0.74	0.79	0.73	0.77	0.09
Ca	0.25	0.19	0.26	0.21	0.00
K	0.01	0.01	0.01	0.01	0.86
Total	4.99	5.01	5.00	5.00	4.98

Mol. Percent

	NKG3 pl3	NKG3 pl3r	NKG3 pl4	NKG3 pl4r	NKPT1 mc3
Ab	73.94	80.06	72.91	77.74	9.85
An	25.24	19.01	26.31	21.32	0.27
Or	0.82	0.93	0.79	0.94	89.88

Table A.4: continued

129

	NKPT1 pl2	NKPT1 pl2r	SNS7 ab12	SNS7 pl12r	SNS7 pl13
SiO_2	61.51	61.05	68.37	63.78	62.30
TiO_2	0.01	0.01	0.00	0.00	0.00
Al_2O_3	24.67	24.53	19.69	22.86	23.16
FeO	0.12	0.09	0.03	0.07	0.18
MnO	0.01	0.02	0.02	0.01	0.02
MgO	0.00	0.00	0.00	0.01	0.01
CaO	4.34	4.28	0.10	3.63	4.65
Cr_2O_3	0.00	0.00	0.00	0.01	0.01
Na_2O	7.99	8.42	11.60	9.37	8.54
K_2O	0.19	0.14	0.07	0.09	0.47
Total	98.85	98.53	99.88	99.84	99.35

Formula Units (recalculated for 8 O)

	NKPT1 pl2	NKPT1 pl2r	SNS7 ab12	SNS7 pl12r	SNS7 pl13
Si	2.74	2.74	2.99	2.82	2.78
Al	1.30	1.30	1.01	1.19	1.22
Fe	0.00	0.00	0.00	0.00	0.01
Ti	0.00	0.00	0.00	0.00	0.00
Mg	0.00	0.00	0.00	0.00	0.00
Mn	0.00	0.00	0.00	0.00	0.00
Cr	0.00	0.00	0.00	0.00	0.00
Na	0.69	0.73	0.98	0.80	0.74
Ca	0.21	0.21	0.00	0.17	0.22
K	0.01	0.01	0.00	0.01	0.03
Total	4.95	4.99	4.98	4.99	5.00

Mol. Percent

	NKPT1 pl2	NKPT1 pl2r	SNS7 ab12	SNS7 pl12r	SNS7 pl13
Ab	75.98	77.43	99.15	81.91	74.79
An	22.83	21.75	0.47	17.56	22.49
Or	1.19	0.82	0.39	0.53	2.72

Table A.4: continued

	SNS7 pl13r	SNS7 pl14	SNS7 pl14r	SNS7 pl15	SNS7 pl15r
SiO_2	61.46	61.93	63.61	61.00	62.04
TiO_2	0.01	0.00	0.00	0.01	0.01
Al_2O_3	23.93	23.32	22.63	23.99	23.37
FeO	0.19	0.16	0.07	0.13	0.11
MnO	0.01	0.01	0.01	0.00	0.01
MgO	0.00	0.01	0.01	0.00	0.00
CaO	5.37	4.85	3.72	5.43	4.62
Cr_2O_3	0.01	0.01	0.00	0.01	0.01
Na_2O	8.09	8.61	9.23	8.40	8.90
K_2O	0.43	0.25	0.18	0.18	0.20
Total	99.49	99.14	99.45	99.15	99.27

Formula Units (recalculated for 8 O)

	SNS7 pl13r	SNS7 pl14	SNS7 pl14r	SNS7 pl15	SNS7 pl15r
Si	2.74	2.77	2.82	2.73	2.77
Al	1.26	1.23	1.18	1.27	1.23
Fe	0.01	0.01	0.00	0.00	0.00
Ti	0.00	0.00	0.00	0.00	0.00
Mg	0.00	0.00	0.00	0.00	0.00
Mn	0.00	0.00	0.00	0.00	0.00
Cr	0.00	0.00	0.00	0.00	0.00
Na	0.70	0.75	0.79	0.73	0.77
Ca	0.26	0.23	0.18	0.26	0.22
K	0.02	0.01	0.01	0.01	0.01
Total	4.99	5.00	4.98	5.00	5.00

Mol. Percent

	SNS7 pl13r	SNS7 pl14	SNS7 pl14r	SNS7 pl15	SNS7 pl15r
Ab	71.32	75.17	80.94	72.91	76.82
An	26.16	23.41	18.05	26.04	22.04
Or	2.52	1.42	1.01	1.05	1.15

Table A.4: continued

	SNS7 pl16	SNS7 pl16m	SNS7 pl16r	FLYE pl1	FLYE pl1r
SiO_2	62.20	61.28	62.86	62.34	64.90
TiO_2	0.01	0.01	0.01	0.01	0.00
Al_2O_3	23.73	23.72	23.08	23.61	22.51
FeO	0.24	0.22	0.18	0.07	0.12
MnO	0.01	0.01	0.01	0.01	0.02
MgO	0.00	0.00	0.01	0.00	0.00
CaO	4.93	5.15	4.02	4.35	2.76
Cr_2O_3	0.00	0.01	0.01	0.00	0.00
Na_2O	7.89	8.43	9.02	8.90	8.93
K_2O	0.38	0.32	0.25	0.15	0.27
Total	99.40	99.14	99.45	99.45	99.53

Formula Units (recalculated for 8 O)

	SNS7 pl16	SNS7 pl16m	SNS7 pl16r	FLYE pl1	FLYE pl1r
Si	2.77	2.74	2.79	2.77	2.86
Al	1.24	1.25	1.21	1.24	1.17
Fe	0.01	0.01	0.01	0.00	0.00
Ti	0.00	0.00	0.00	0.00	0.00
Mg	0.00	0.00	0.00	0.00	0.00
Mn	0.00	0.00	0.00	0.00	0.00
Cr	0.00	0.00	0.00	0.00	0.00
Na	0.68	0.73	0.78	0.77	0.76
Ca	0.24	0.25	0.19	0.21	0.13
K	0.02	0.02	0.01	0.01	0.02
Total	4.96	5.00	4.99	5.00	4.94

Mol. Percent

	SNS7 pl16	SNS7 pl16m	SNS7 pl16r	FLYE pl1	FLYE pl1r
Ab	72.61	73.39	79.05	78.07	83.94
An	25.08	24.78	19.50	21.07	14.36
Or	2.31	1.83	1.46	0.86	1.70

Table A.4: continued

132

	FLYE pl2	FLYE pl2r	FLYE pl3	FLYE pl3r	FLYE pl4
SiO_2	62.97	64.28	62.14	62.80	60.92
TiO_2	0.00	0.01	0.01	0.01	0.01
Al_2O_3	22.94	22.53	23.24	22.82	23.18
FeO	0.13	0.10	0.17	0.13	0.22
MnO	0.01	0.02	0.00	0.00	0.01
MgO	0.00	0.00	0.01	0.01	0.00
CaO	3.50	2.88	4.12	3.40	4.48
Cr_2O_3	0.00	0.00	0.00	0.00	0.01
Na_2O	9.10	9.20	8.49	9.32	8.49
K_2O	0.49	0.28	0.50	0.36	0.71
Total	99.14	99.30	98.68	98.84	98.03

Formula Units (recalculated for 8 O)

	FLYE pl2	FLYE pl2r	FLYE pl3	FLYE pl3r	FLYE pl4
Si	2.81	2.85	2.78	2.81	2.76
Al	1.21	1.18	1.23	1.20	1.24
Fe	0.00	0.00	0.01	0.00	0.01
Ti	0.00	0.00	0.00	0.00	0.00
Mg	0.00	0.00	0.00	0.00	0.00
Mn	0.00	0.00	0.00	0.00	0.00
Cr	0.00	0.00	0.00	0.00	0.00
Na	0.79	0.79	0.74	0.81	0.75
Ca	0.17	0.14	0.20	0.16	0.22
K	0.03	0.02	0.03	0.02	0.04
Total	5.01	4.98	4.99	5.00	5.02

Mol. Percent

	FLYE pl2	FLYE pl2r	FLYE pl3	FLYE pl3r	FLYE pl4
Ab	80.13	83.82	76.55	81.54	74.28
An	17.03	14.49	20.52	16.41	21.65
Or	2.84	1.69	2.94	2.05	4.07

Table A.4: continued

	FLYE pl4r	GRNLW pl4	GRNLW pl4r	GRNLW pl1
SiO_2	60.77	61.43	62.91	63.20
TiO_2	0.00	0.01	0.00	0.00
Al_2O_3	22.89	23.91	23.36	23.77
FeO	0.17	0.22	0.14	0.19
MnO	0.01	0.00	0.01	0.01
MgO	0.01	0.00	0.00	0.01
CaO	4.31	4.91	4.06	3.99
Cr_2O_3	0.00	0.00	0.00	0.00
Na_2O	8.74	8.46	9.03	8.73
K_2O	0.61	0.48	0.43	0.22
Total	97.49	99.42	99.95	100.12

Formula Units (recalculated for 8 O)

	FLYE pl4r	GRNLW pl4	GRNLW pl4r	GRNLW pl1
Si	2.77	2.74	2.79	2.79
Al	1.23	1.26	1.22	1.24
Fe	0.01	0.01	0.01	0.01
Ti	0.00	0.00	0.00	0.00
Mg	0.00	0.00	0.00	0.00
Mn	0.00	0.00	0.00	0.00
Cr	0.00	0.00	0.00	0.00
Na	0.77	0.73	0.78	0.75
Ca	0.21	0.23	0.19	0.19
K	0.04	0.03	0.02	0.01
Total	5.03	5.00	5.01	4.99

Mol. Percent

	FLYE pl4r	GRNLW pl4	GRNLW pl4r	GRNLW pl1
Ab	75.87	73.63	78.11	78.79
An	20.67	23.60	19.43	19.90
Or	3.46	2.77	2.46	1.32

Table A.4: continued

	GRNLW pl1r	GRNLW pl2	GRNLW pl2r
SiO_2	63.93	61.97	64.18
TiO_2	0.00	0.01	0.00
Al_2O_3	23.66	24.25	23.31
FeO	0.63	0.19	0.14
MnO	0.01	0.01	0.01
MgO	0.01	0.00	0.00
CaO	3.85	4.71	3.48
Cr_2O_3	0.00	0.00	0.00
Na_2O	7.78	8.54	8.31
K_2O	0.19	0.55	0.43
Total	100.06	100.23	99.86

Formula Units (recalculated for 8 O)

	GRNLW pl1r	GRNLW pl2	GRNLW pl2r
Si	2.81	2.74	2.82
Al	1.23	1.27	1.21
Fe	0.02	0.01	0.01
Ti	0.00	0.00	0.00
Mg	0.00	0.00	0.00
Mn	0.00	0.00	0.00
Cr	0.00	0.00	0.00
Na	0.66	0.73	0.71
Ca	0.18	0.22	0.16
K	0.01	0.03	0.02
Total	5.01	4.98	4.99

Mol. Percent

	GRNLW pl1r	GRNLW pl2	GRNLW pl2r
Ab	77.54	74.22	79.03
An	21.20	22.63	18.31
Or	1.26	3.15	2.67

Table A.4: concluded

	SNCC2 hb5	SNCC2 hb1	SNCC2 hb2	SNCC2 hb3
SiO_2	45.39	45.66	45.17	49.03
TiO_2	1.51	1.19	1.46	2.38
Al_2O_3	7.48	7.63	7.39	6.95
FeOt	17.70	17.71	17.81	18.97
MnO	0.71	0.63	0.67	1.69
MgO	10.76	10.70	10.64	11.72
CaO	11.33	11.49	11.46	12.28
Cr_2O_3	0.01	0.01	0.01	1.04
Na_2O	1.54	1.30	1.44	2.41
K_2O	0.84	0.78	0.85	1.86
H_2O	1.68	1.68	1.60	2.63
F	0.64	0.62	0.77	1.80
Total	99.59	99.41	99.26	101.73
O=F,Cl	0.27	0.26	0.32	0.32
Total	99.32	99.15	98.94	101.41

Formula Units (recalculated for 24 O)

Si	6.87	6.91	6.87	7.18
Al (iv)	1.13	1.09	1.13	0.82
Sum	*8.00*	*8.00*	*8.00*	*8.00*
Al (vi)	0.21	0.27	0.20	0.21
Ti	0.17	0.14	0.17	0.14
Fe	2.24	2.24	2.27	2.20
Mn	0.09	0.08	0.09	0.10
Mg	2.43	2.41	2.41	2.44
Cr	0.00	0.00	0.00	0.00
Sum	*5.15*	*5.14*	*5.13*	*5.09*
Ca	1.84	1.86	1.87	1.82
Na	0.45	0.38	0.42	0.37
K	0.16	0.15	0.16	0.15
Sum	*2.45*	*2.40*	*2.46*	*2.33*
OH	1.70	1.70	1.63	1.64
F	0.30	0.30	0.37	0.36
Sum	*2.00*	*2.00*	*2.00*	*2.00*

Mg/(Mg+Fe)

	0.52	0.52	0.51	0.53

Table A.5: Hornblende microprobe analysis. Calculations and table format are after Deer, Howie and Zussman, 1992. Sample FLYE S-px2 is a suspect clinopyroxene core in a hornblende grain.

136

	NKG3 hb1	NKG3 hb2	NKG3 hb3	NKPT1 hb1
SiO_2	45.20	45.05	45.93	45.28
TiO_2	1.51	1.48	1.33	1.39
Al_2O_3	7.26	7.05	6.57	7.66
FeOt	18.32	17.76	17.65	17.89
MnO	0.77	0.73	0.76	0.43
MgO	10.41	10.50	10.70	10.65
CaO	10.83	11.10	11.15	11.29
Cr_2O_3	0.00	0.00	0.00	0.01
Na_2O	1.67	1.58	1.41	1.44
K_2O	0.86	0.85	0.78	0.93
H_2O	1.58	1.50	1.59	1.61
F	0.81	0.95	0.79	0.77
Total	99.22	98.55	98.67	99.33
O=F,Cl	0.34	0.40	0.33	0.32
Total	98.88	98.15	98.34	99.01

Formula Units (recalculated for 24 O)

	NKG3 hb1	NKG3 hb2	NKG3 hb3	NKPT1 hb1
Si	6.90	6.91	7.01	6.87
Al (iv)	1.10	1.09	0.99	1.13
Sum	*8.00*	*8.00*	*8.00*	*8.00*
Al (vi)	0.20	0.19	0.19	0.25
Ti	0.17	0.17	0.15	0.16
Fe	2.34	2.28	2.25	2.27
Mn	0.10	0.10	0.10	0.06
Mg	2.37	2.40	2.44	2.41
Cr	0.00	0.00	0.00	0.00
Sum	*5.18*	*5.14*	*5.13*	*5.14*
Ca	1.77	1.82	1.82	1.84
Na	0.49	0.47	0.42	0.42
K	0.17	0.17	0.15	0.18
Sum	*2.43*	*2.46*	*2.40*	*2.44*
OH	1.61	1.54	1.62	1.63
F	0.39	0.46	0.38	0.37
Sum	*2.00*	*2.00*	*2.00*	*2.00*

Mg/(Mg+Fe)

	NKG3 hb1	NKG3 hb2	NKG3 hb3	NKPT1 hb1
	0.50	0.51	0.52	0.51

Table A.5: Continued

	NKPT1 hb2	FLYE hb1	FLYE hb2	FLYE hb3
SiO_2	44.91	44.84	44.12	44.01
TiO_2	1.34	1.58	1.22	1.59
Al_2O_3	7.56	6.92	7.19	7.08
FeOt	18.70	18.92	19.22	16.59
MnO	0.51	0.85	0.93	0.58
MgO	10.31	10.23	9.87	11.77
CaO	10.93	10.93	11.03	10.80
Cr_2O_3	0.01	0.01	0.01	0.01
Na_2O	1.29	1.63	1.55	1.82
K_2O	0.90	0.84	0.86	0.86
H_2O	1.62	1.48	1.45	1.34
F	0.71	1.01	1.01	1.26
Total	98.81	99.23	98.46	97.72
O=F,Cl	0.30	0.42	0.42	0.53
Total	98.51	98.81	98.04	97.19

Formula Units (recalculated for 24 O)

	NKPT1 hb2	FLYE hb1	FLYE hb2	FLYE hb3
Si	6.88	6.88	6.85	6.80
Al (iv)	1.12	1.12	1.15	1.20
Sum	*8.00*	*8.00*	*8.00*	*8.00*
Al (vi)	0.24	0.13	0.16	0.10
Ti	0.15	0.18	0.14	0.18
Fe	2.40	2.43	2.49	2.15
Mn	0.07	0.11	0.12	0.08
Mg	2.35	2.34	2.28	2.71
Cr	0.00	0.00	0.00	0.00
Sum	*5.21*	*5.19*	*5.20*	*5.22*
Ca	1.79	1.80	1.83	1.79
Na	0.38	0.49	0.47	0.54
K	0.18	0.16	0.17	0.17
Sum	*2.35*	*2.45*	*2.47*	*2.50*
OH	1.66	1.51	1.51	1.38
F	0.34	0.49	0.49	0.62
Sum	*2.00*	*2.00*	*2.00*	*2.00*

Mg/(Mg+Fe)

	NKPT1 hb2	FLYE hb1	FLYE hb2	FLYE hb3
	0.49	0.49	0.48	0.56

Table A.5: Continued

	FLYE hb4	GRNLW hb2	GRNLW hb1	FLYE S-px2
SiO_2	44.45	47.38	47.04	45.08
TiO_2	1.73	1.31	1.31	1.07
Al_2O_3	7.09	6.49	6.64	7.90
FeOt	17.05	13.72	14.64	18.19
MnO	0.60	0.65	0.73	0.84
MgO	11.34	13.90	13.11	10.49
CaO	10.77	11.56	11.33	11.11
Cr_2O_3	0.02	0.00	0.00	0.05
Na_2O	1.85	1.32	1.33	1.24
K_2O	0.86	0.64	0.71	0.75
H_2O	1.37	1.70	1.70	1.48
F	1.22	0.68	0.65	1.02
Total	98.36	101.18	99.18	99.22
O=F,Cl	0.51	0.29	0.27	0.43
Total	97.85	100.89	98.91	98.79

Formula Units (recalculated for 24 O)

	FLYE hb4	GRNLW hb2	GRNLW hb1	FLYE S-px2
Si	6.83	7.03	7.02	6.87
Al (iv)	1.17	0.97	0.98	1.13
Sum	8.00	8.00	8.00	8.00
Al (vi)	0.12	0.16	0.19	0.29
Ti	0.20	0.15	0.15	0.12
Fe	2.19	1.70	1.83	2.32
Mn	0.08	0.08	0.09	0.11
Mg	2.60	3.07	2.92	2.38
Cr	0.00	0.00	0.00	0.01
Sum	5.19	5.17	5.18	5.23
Ca	1.77	1.84	1.81	1.81
Na	0.55	0.38	0.38	0.37
K	0.17	0.12	0.14	0.15
Sum	2.49	2.34	2.33	2.33
OH	1.41	1.68	1.69	1.51
F	0.59	0.32	0.31	0.49
Sum	2.00	2.00	2.00	2.00

Mg/(Mg+Fe)

	FLYE hb4	GRNLW hb2	GRNLW hb1	FLYE S-px2
	0.54	0.64	0.61	0.51

Table A.5: Concluded

	SNCC2 bt2	SNCC2 bt3	SNCC2 bt7	NKG3 bt3	NKG3 bt4
SiO_2	36.45	37.55	36.39	36.68	36.40
TiO_2	4.11	3.94	3.49	3.91	4.04
Al_2O_3	13.60	12.77	13.21	13.08	13.46
FeOt	20.34	20.90	20.83	21.18	21.17
MnO	0.36	0.42	0.31	0.39	0.37
MgO	11.03	11.02	11.08	10.37	10.39
CaO	0.06	0.04	0.04	0.01	0.10
Cr_2O_3	0.01	0.01	0.02	0.01	0.00
K_2O	0.08	0.07	0.08	0.09	0.15
Na_2O	9.15	10.34	9.45	9.32	8.63
H_2O	1.35	1.33	1.12	1.31	1.34
F	3.25	3.31	3.33	3.24	3.23
Total	99.81	101.70	99.34	99.59	99.28
O=F,Cl	0.57	0.56	0.47	0.55	0.56
Total	99.24	101.14	98.87	99.04	98.71

Formula units (recalculated for 24 O)

	SNCC2 bt2	SNCC2 bt3	SNCC2 bt7	NKG3 bt3	NKG3 bt4
Si	5.61	5.71	5.65	5.69	5.64
Al (iv)	2.47	2.29	2.42	2.39	2.46
Sum	*8.00*	*8.00*	*8.00*	*8.00*	*8.00*
Al (vi)	0.08	0.00	0.06	0.07	0.10
Ti	0.48	0.45	0.41	0.46	0.47
Fe	2.62	2.66	2.70	2.75	2.74
Mn	0.05	0.05	0.04	0.05	0.05
Mg	2.53	2.50	2.56	2.40	2.40
Cr	0.00	0.00	0.00	0.00	0.00
Sum	*5.76*	*5.67*	*5.78*	*5.73*	*5.77*
Ca	0.01	0.01	0.01	0.00	0.02
Na	0.02	0.02	0.02	0.03	0.04
K	1.80	2.01	1.87	1.84	1.71
Sum	*1.83*	*2.04*	*1.90*	*1.87*	*1.77*
OH	3.34	3.36	3.45	3.36	3.35
F	0.66	0.64	0.55	0.64	0.65
Sum	*4.00*	*4.00*	*4.00*	*4.00*	*4.00*

Mg/(Mg+Fe)

	SNCC2 bt2	SNCC2 bt3	SNCC2 bt7	NKG3 bt3	NKG3 bt4
	0.49	0.48	0.49	0.47	0.47

Table A.6: Biotite microprobe analysis. Calculations and table format are after Deer, Howie and Zussman, 1992.

	NKPT1 bt3	SNS7 bt14	SNS7 bt15	SNS7 bt17	SNS7 bt16
SiO_2	36.04	36.89	36.75	37.12	37.29
TiO_2	3.90	4.10	3.55	3.56	3.35
Al_2O_3	13.62	13.02	13.32	13.17	12.97
FeOt	21.26	18.37	17.87	18.15	18.18
MnO	0.24	0.52	0.53	0.52	0.51
MgO	11.07	11.94	12.33	12.29	12.55
CaO	0.06	0.01	0.04	0.01	0.01
Cr_2O_3	0.01	0.01	0.00	0.00	0.01
K_2O	0.13	0.07	0.08	0.09	0.09
Na_2O	9.14	9.77	9.73	9.74	9.74
H_2O	1.26	1.16	1.25	1.26	1.28
F	3.29	3.34	3.29	3.30	3.29
Total	100.03	99.21	98.73	99.22	99.28
O=F,Cl	0.53	0.49	0.53	0.53	0.54
Total	99.50	98.72	98.21	98.69	98.74

Formula units (recalculated for 24 O)

	NKPT1 bt3	SNS7 bt14	SNS7 bt15	SNS7 bt17	SNS7 bt16
Si	5.56	5.68	5.67	5.70	5.73
Al (iv)	2.48	2.36	2.42	2.39	2.35
Sum	*8.00*	*8.00*	*8.00*	*8.00*	*8.00*
Al (vi)	0.04	0.04	0.10	0.09	0.08
Ti	0.45	0.48	0.41	0.41	0.39
Fe	2.74	2.37	2.31	2.33	2.34
Mn	0.03	0.07	0.07	0.07	0.07
Mg	2.55	2.74	2.84	2.82	2.87
Cr	0.00	0.00	0.00	0.00	0.00
Sum	*5.82*	*5.69*	*5.73*	*5.72*	*5.74*
Ca	0.01	0.00	0.01	0.00	0.00
Na	0.04	0.02	0.02	0.03	0.03
K	1.80	1.92	1.92	1.91	1.91
Sum	*1.85*	*1.94*	*1.95*	*1.94*	*1.94*
OH	3.39	3.44	3.39	3.39	3.38
F	0.61	0.56	0.61	0.61	0.62
Sum	*4.00*	*4.00*	*4.00*	*4.00*	*4.00*

Mg/(Mg+Fe)

	NKPT1 bt3	SNS7 bt14	SNS7 bt15	SNS7 bt17	SNS7 bt16
	0.48	0.54	0.55	0.55	0.55

Table A.6: Continued

141

	FLYE bt1	GRNLW bt1	GRNLW bt2
SiO_2	36.43	37.32	36.99
TiO_2	4.01	3.52	3.61
Al_2O_3	12.89	14.10	14.46
FeOt	20.63	17.90	18.04
MnO	0.45	0.61	0.48
MgO	10.95	12.78	11.97
CaO	0.02	0.01	0.03
Cr_2O_3	0.01	0.01	0.01
K_2O	0.09	0.09	0.08
Na_2O	9.48	9.14	8.82
H_2O	1.60	1.05	0.98
F	3.10	3.46	3.46
Total	99.65	99.99	98.93
O=F,Cl	0.67	0.44	0.41
Total	98.98	99.55	98.52

Formula units (recalculated for 24 O)

Si	5.65	5.65	5.65
Al (iv)	2.36	2.52	2.60
Sum	*8.00*	*8.00*	*8.00*
Al (vi)	0.01	0.17	0.25
Ti	0.47	0.40	0.41
Fe	2.68	2.27	2.30
Mn	0.06	0.08	0.06
Mg	2.53	2.88	2.72
Cr	0.00	0.00	0.00
Sum	*5.75*	*5.79*	*5.76*
Ca	0.00	0.00	0.01
Na	0.03	0.03	0.02
K	1.88	1.76	1.72
Sum	*1.91*	*1.79*	*1.75*
OH	3.22	3.50	3.53
F	0.78	0.50	0.47
Sum	*4.00*	*4.00*	*4.00*

Mg/(Mg+Fe)

	0.49	0.56	0.54

Table A.6: Concluded

	NKPT1 px1	NKPT1 px3
SiO_2	51.91	52.12
TiO_2	0.13	0.16
Al_2O_3	0.68	0.77
Cr_2O_3	0.00	0.01
FeOt	11.66	11.19
MnO	0.76	0.88
MgO	11.90	12.57
CaO	21.05	20.11
Na_2O	0.46	0.40
K_2O	0.01	0.00
Total	98.56	98.22

Formula Units (recalculated for 6 O)

	NKPT1 px1	NKPT1 px3
Si	1.99	2.00
Al	0.01	0.00
Sum	*2.00*	*2.00*
Al	0.02	0.03
Cr	0.00	0.00
Fe	0.37	0.36
Ti	0.00	0.00
Mg	0.68	0.72
Mn	0.02	0.03
Ca	0.87	0.83
Na	0.03	0.03
K	0.00	0.00
Sum	*2.00*	*2.00*

Mg/(Mg+Fe)

	NKPT1 px1	NKPT1 px3
	0.65	0.67

Table A.7: Pyroxene microprobe analysis. Calculations and table format are after Deer, Howie and Zussman, 1992.

Generalized Field Maps

LEGEND FOR APPENDIX B

Lithologies (after Stewart, 1998)

TG	Stonington Granite (Devonian)
PG	Oak Point Granite (Devonian)
RP	Serpentinite (Ordovician?)
V	Castine Volcanics (Late Cambrian)
SW	Ellsworth Schist (Middle Cambrian)

Planar Features

Enclave

Feldspar Foliation

Aplite Dike

Other features

Poor to no exposure

Sample Locations

▲ Enclave

● Granite

■ Aplite Dike

✗ Mafic Dike

╅ Composite Dike

℥ Section not surveyed
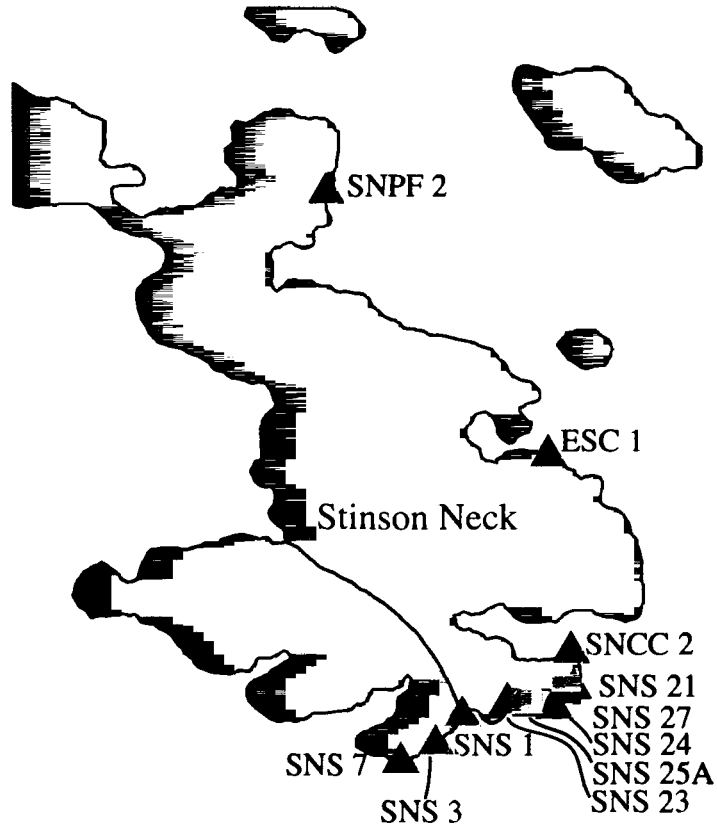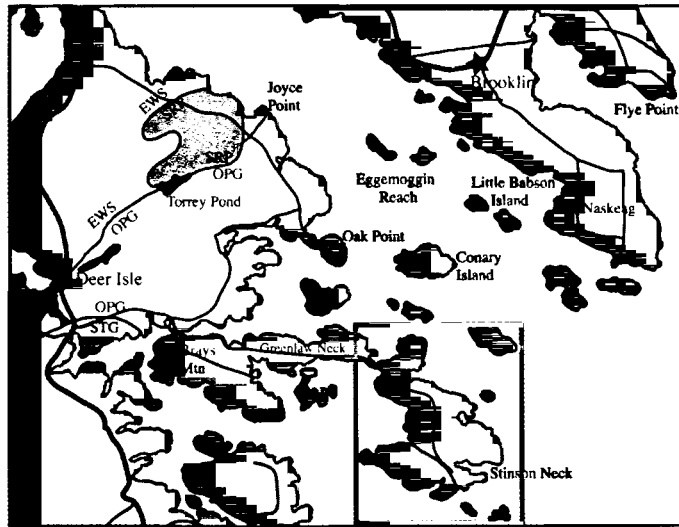
Figure B.1: Sample location maps.
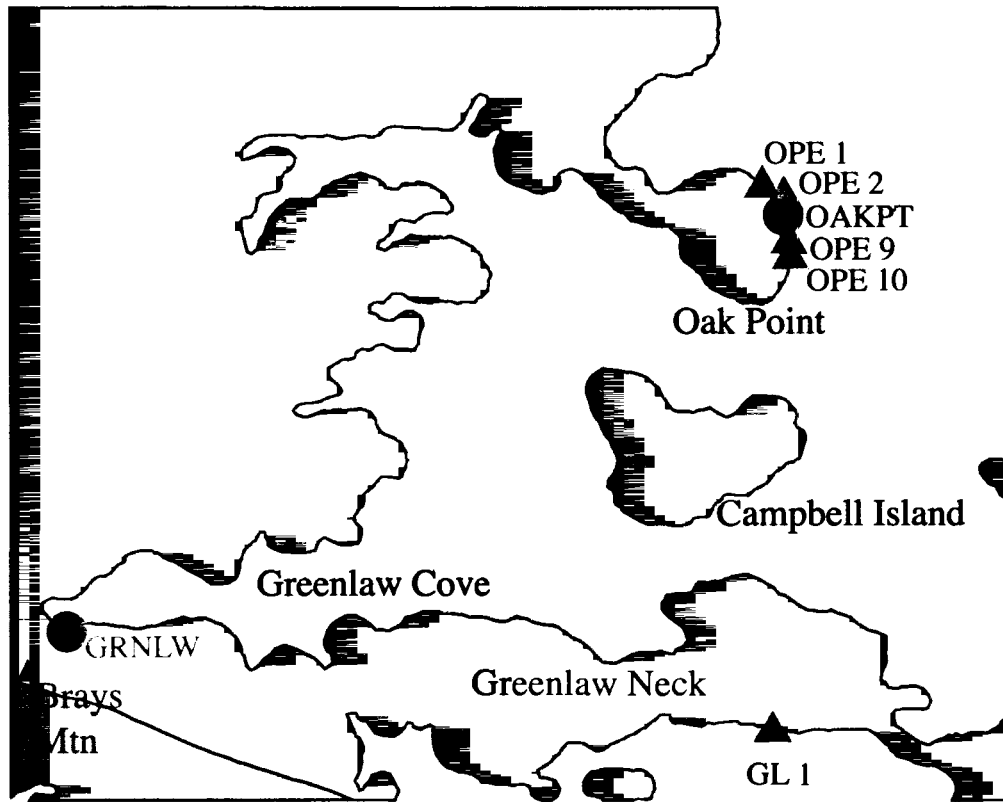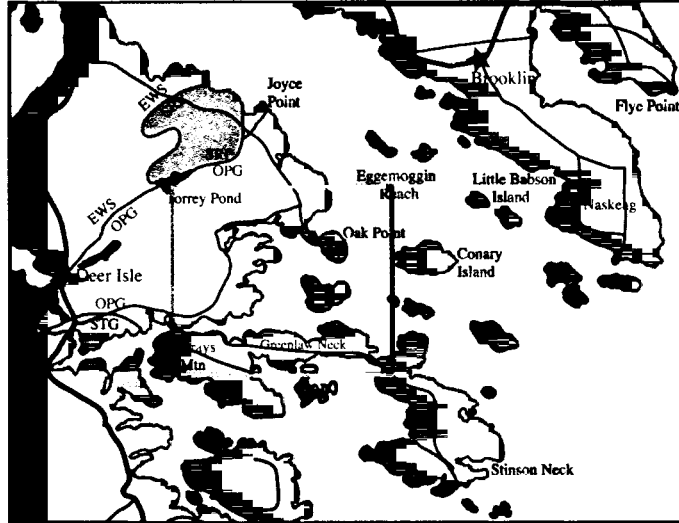
Figure B.1: Continued
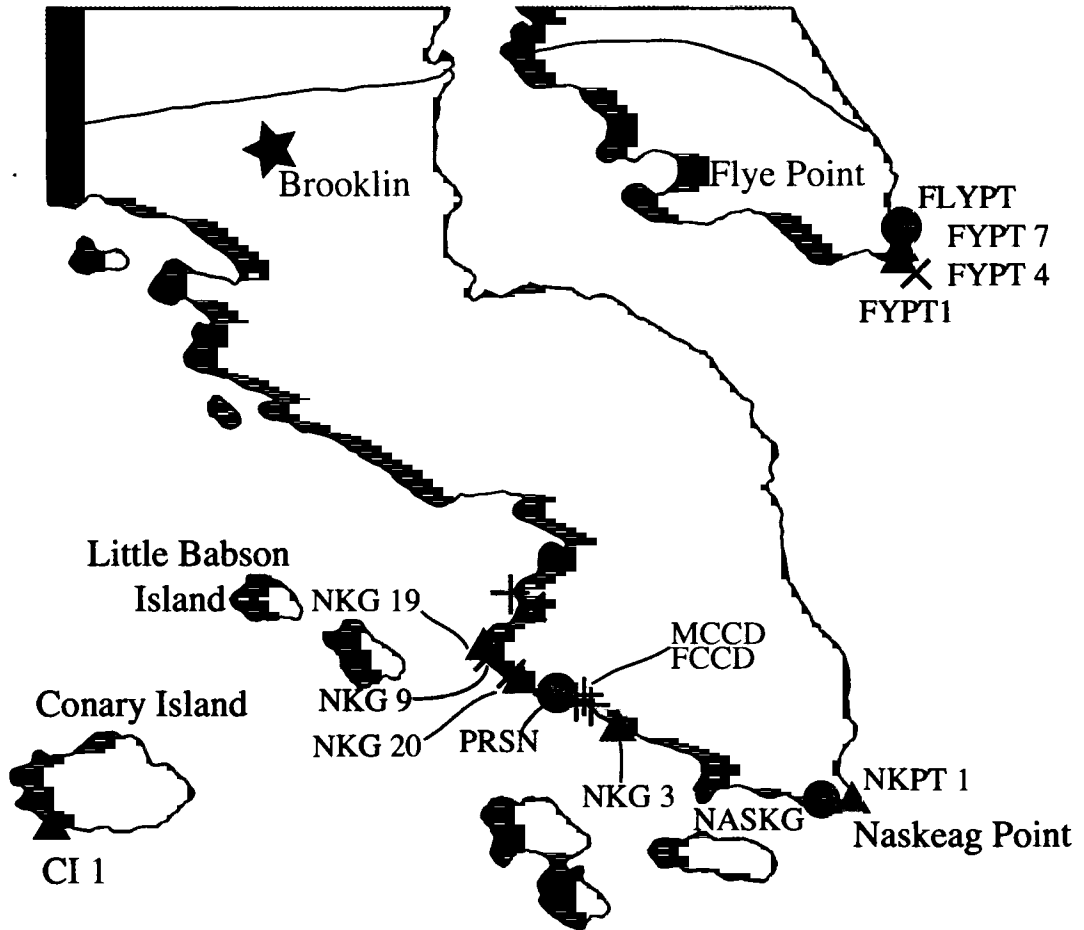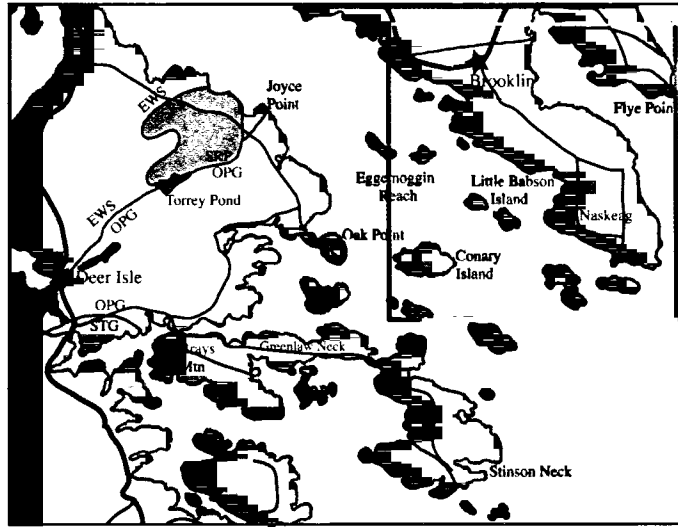
Figure B.1: Concluded
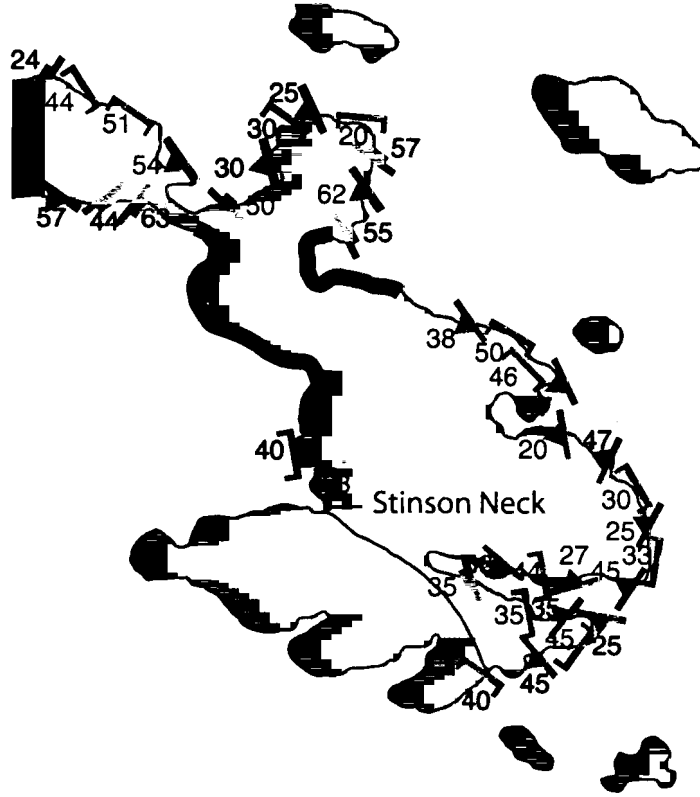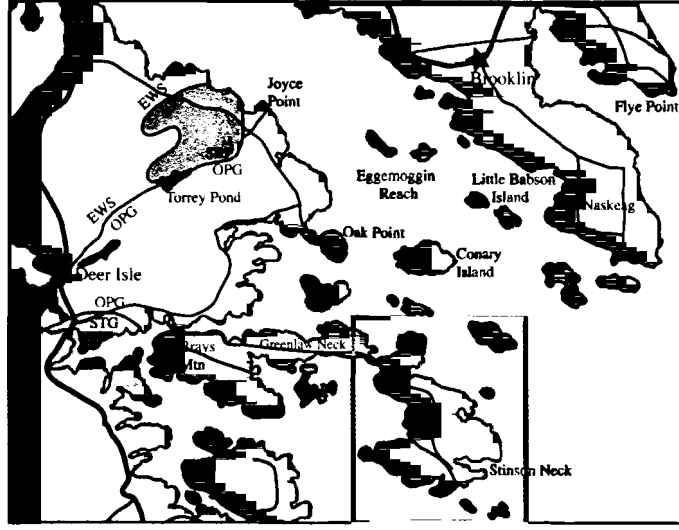
Figure B.2: Structural maps.
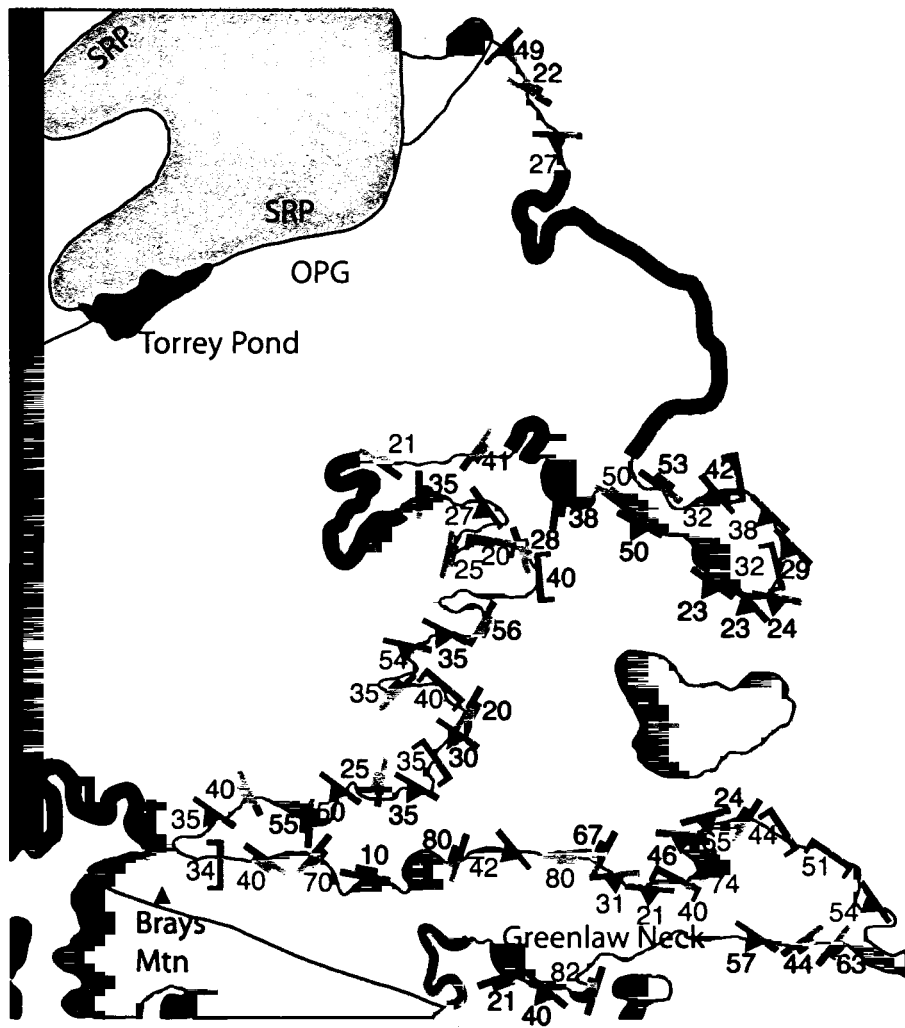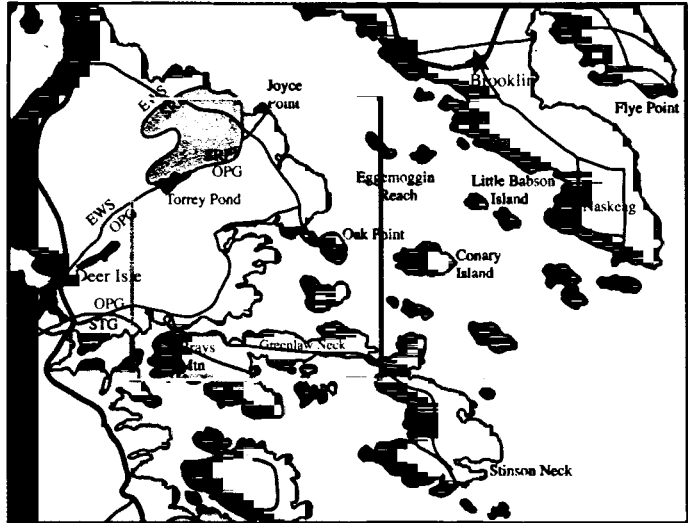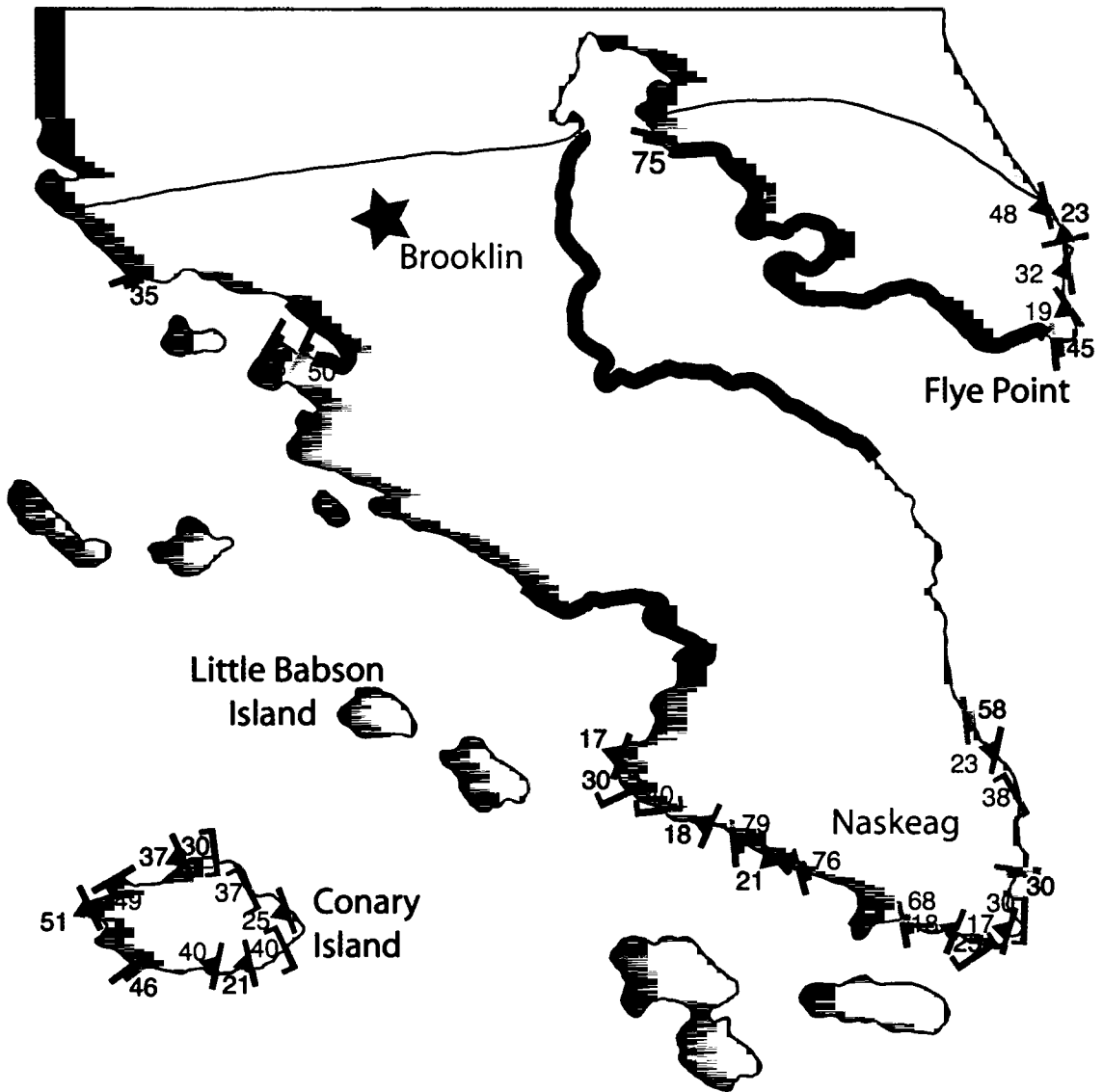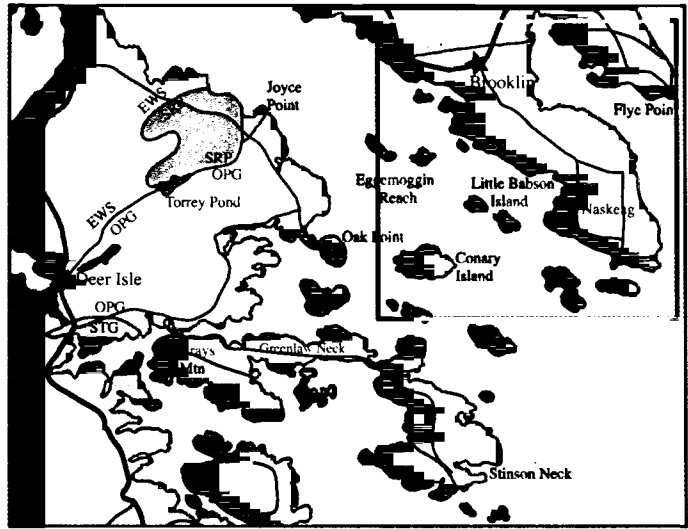
Figure B.2: Continued

Figure B.2: Concluded

150

BIOGRAPHY OF THE AUTHOR

Ben Johnston was born in Cincinnati, OH. He graduated from Purcell Marian High School in 1991. Ben attended the University of Cincinnati and graduated in 1998 with a Bachelor's degree in Geology. Ben entered the Geological Sciences graduate program at The University of Maine in the fall of 1999.

After receiving his degree, Ben will be joining Gina's Pies are Square, a restaurant, in Wilton, Wisconsin. Ben is a candidate for the Master of Science degree in Geological Sciences from the University of Maine in December, 2001.